The Role of ID2 in Intestinal Homeostasis and Tumorigenesis

Dissertation
Zur Erlangung des Grades
Doktor der Naturwissenschaften

Am Fachbereich Biologie
Der Johannes Gutenberg-Universität in Mainz

Valeriya Zinina

geb. am 29.10.1994 in Samara (Russland)

Mainz, 2024

Dekan: Prof. Dr. Eckhard Thines

1.Berichterstatter: Prof. Dr. Miguel Andrade

2.Berichterstatter: Dr. Natalia Soshnikova

Tag der mündlichen Prüfung: 30.09.2024

TABLE OF CONTENTS

LIST OF FIGURES

ABBREVIATIONS

bHLH – Basic helix-loop-helix

bp – Base pair

CBC – Crypt Base Columnar

CNV – Copy number variation analysis

EC – Enterochromaffin cell

EE – Enteroendocrine

EEC – Enteroendocrine Cell

FACS – Fluorescence-activated cell sorting

FAP – Familial adenomatous polyposis

FDR – False Discovery Rate

GAP – Goblet cell-associated antigen passage

GSEA – Gene Set Enrichment Analysis

HLH – Helix-loop-helix

ISC – Intestinal stem cells

KO – Knockout

LOH – loss of heterozygosity

MCR – Mutation cluster region

Min –Multiple intestinal neoplasia

NES – Normalized Enrichment Score

PBS – Phosphate-buffered saline

PCR – Polymerase chain reaction

PFA – Paraformaldehyde

qRT-PCR – Quantitative real-time reverse transcription polymerase chain reaction

Sc – Single-cell

Scr – Scramble

SSC – Saline-sodium citrate

TA – Transit amplifying

TBS – Tris-buffered saline

TBSX – Tris-buffered saline with Triton X-100 0.1%

UEA – Ulex europaeus agglutinin

WT – Wild type

ABSTRACT

The small intestinal epithelium is a dynamic system comprising various specialized cell types. Intestinal stem cells located at the crypt base differentiate into absorptive enterocytes and secretory goblet, Paneth, tuft, and enteroendocrine cells (EECs). The differentiation process along the secretory lineage is regulated by basic Helix-Loop-Helix (bHLH) transcription factors in progenitor cells. However, the precise mechanisms of differentiation into distinct secretory cell types remain unclear.

In this study, I explored the role of Inhibitor of Differentiation 2 (ID2), a negative regulator of bHLH-containing factors, in regulating secretory lineage differentiation. Previous research by the group highlighted ID2's functions in gut development. Here, lineage tracing analyses demonstrated that *Id2* is activated in fully differentiated EECs in the adult small intestine. Functionally, ID2 promotes differentiation along the enteroendocrine N-cell lineage by mediating BMP signaling. Additionally, ID2 operates in common secretory progenitors to suppress tuft cell fate.

Id2 is also known to be activated in various cancers. In my research, I performed RNA *in situ* hybridization analysis and confirmed *Id2* expression in small intestinal adenomas of the $Apc^{min/+}$ mouse model of colorectal cancer. As shown in the current study, the absence of *Id2* in the gut epithelium during early embryonic stages significantly reduced tumor numbers in all parts of the small intestine in these mice. Experiments with an inducible *Id2* knockout mouse model and tumoroid cultures revealed that *Id2* depletion lowers tumor grade *in vivo* and reduces the clonogenic capacity of cultured tumoroids. Furthermore, using CRISPR/Cas9 technology on intestinal organoids, I demonstrated ID2's necessity in tumorigenesis and maintaining the undifferentiated state of cancer stem cells. Collectively, these results indicate that ID2 is crucial for both tumorigenesis and the progression of small intestinal tumors.

ZUSAMMENFASSUNG

Das Dünndarmepithel ist ein dynamisches System, das aus verschiedenen spezialisierten Zelltypen besteht. Intestinale Stammzellen am Kryptengrund differenzieren sich zu absorptiven Enterozyten sowie zu sekretorischen Becher-, Paneth-, Tuft- und enteroendokrinen Zellen. Der Differenzierungsprozess entlang der sekretorischen Linie wird durch basic Helix-Loop-Helix (bHLH)-Transkriptionsfaktoren in Vorläuferzellen reguliert. Die genauen Mechanismen der Differenzierung in verschiedene sekretorische Zelltypen bleiben jedoch unklar.

In dieser Studie untersuchte ich die Rolle des Inhibitors der Differenzierung 2 (ID2), eines negativen Regulators von bHLH-enthaltenden Faktoren, bei der Regulierung der sekretorischen Liniendifferenzierung. Frühere Forschungen der Gruppe haben die Funktionen von ID2 in der Darmentwicklung näher beleuchtet. Hier zeigten Abstammungsanalysen, dass *Id2* in vollständig differenzierten enteroendokrinen Zellen im erwachsenen Dünndarm aktiviert wird. Funktionell fördert ID2 die Differenzierung entlang der enteroendokrinen N-Zell-Linie durch Vermittlung des BMP-Signalwegs. Zusätzlich wirkt ID2 in gemeinsamen sekretorischen Vorläufern, um das Tuft-Zell-Schicksal zu unterdrücken.

Id2 ist auch dafür bekannt, in verschiedenen Krebsarten aktiviert zu sein. In meiner Forschung führte ich RNA-*in-situ*-Hybridisierungsanalysen durch und bestätigte die *Id2*-Expression in Dünndarmadenomen des $Apc^{min/+}$ Mausmodells für kolorektalen Krebs. Wie in der aktuellen Studie gezeigt, reduzierte das Fehlen von *Id2* im Darmepithel während der frühen embryonalen Stadien signifikant die Tumoranzahl in allen Teilen des Dünndarms bei diesen Mäusen. Experimente mit einem induzierbaren *Id2*-Knockout-Mausmodell und Tumoroid-Kulturen zeigten, dass die *Id2*-Depletion den Tumorgrad *in vivo* senkt und die klonogene Kapazität der kultivierten Tumoroide reduziert. Darüber hinaus demonstrierte ich mithilfe der CRISPR/Cas9-Technologie an Darmorganoiden die Notwendigkeit von ID2 bei der Tumorentstehung und der Aufrechterhaltung des undifferenzierten Zustands von Krebsstammzellen. Zusammengenommen zeigen diese Ergebnisse, dass ID2 sowohl für die Tumorentstehung als auch das Fortschreiten des Dünndarms dieser Mäuse entscheidend ist.

1. INTRODUCTION

1.1 Small Intestinal Epithelium Structure and Homeostasis.

The small intestinal epithelium is a dynamic system with specialized cell types. Constant mechanical and chemical actions from the lumen are leading to the frequent death of epithelial cells, and therefore, rapid replenishment is needed. As a result, the small intestinal epithelium is the most highly regenerative organ, fully renewing every 4-7 days (Liu *et al.*, 2020). Epithelial homeostasis requires a balance between cell proliferation, differentiation and shedding. The monolayer small intestinal epithelium has a compartmentalized crypt-villus architecture, which successfully maintains this balance and ensures efficient reparation in response to injury. Crypts of Lieberkühn represent invaginations in the epithelial surface. At least six crypts encircled each villus (Barker, 2014). Intestinal stem cells (ISC) are located at the bottom of the crypt, where they are protected from the luminal damaging factors, and differentiate into distinct cell populations when moving up toward the villus tip. Intestinal stem cell differentiation involves complex coordination between signaling pathways, the most important of which are Wnt, BMP, and Notch. Wnt signaling maintains an undifferentiated state of stem cells and has a decreasing crypt-villus gradient, while BMP promotes differentiation and shows a counter gradient (Spit *et al.*, 2018). Notch signaling is regulated using a lateral inhibition mechanism and thus mediates binary cell fate decisions between absorptive and secretory lineage in common progenitor cells. The absorptive lineage consists of the largest population of enterocytes (comprising more than 80% of all intestinal epithelial cells) and M cells, which are responsible for sensing luminal bacteria. The secretory lineage includes chemo-sensing tuft cells, mucus-producing goblet cells, Paneth cells that form the stem cell niche, and enteroendocrine cells that produce hormones. The small intestinal stem cell differentiation is reviewed in Figure 1.1.

The small intestine of a mouse is comprised of three main regions: the duodenum, the jejunum, and the ileum. The duodenum is about 7 cm long and is connected to the antrum of the stomach at its proximal end. The jejunum is approximately 30 cm long, while the ileum is the final part of the small intestine, measuring around 4 cm and ending at the cecum (Collins *et al.*, 2023; Casteleyn *et al.*, 2010).

Our group follows a specific method to divide the small intestine into three equal parts for all our assays, which are the anterior, middle, and posterior parts. It is important to note that these parts do not correspond directly to the duodenum, jejunum, and ileum. The anterior part includes the duodenum and the proximal part of the jejunum, while the middle part includes most of the jejunum. Finally, the posterior part includes the distal jejunum and ileum. Since the lengths of the duodenum, jejunum and ileum can vary between mice (Casteleyn *et al.*, 2010) and the exact borders between them may not be easily defined, we use equal parts to ensure consistency in our measurements.

1.2 Intestinal Stem and Transit Amplifying Cells.

The clonal analysis of mouse intestinal epithelial progenitors revealed 4-6 stem cells per crypt (Bjerknes *et al.*, 1999). Despite earlier studies reporting the existence of cycling crypt-base columnar cells (Cheng *et al.*, 1974; Bjerknes *et al.*, 1981), they were not functionally described, and their unique markers needed to be identified. The selected Wnt target genes analysis identified *Lgr5* (leucine-rich-repeat-containing G-protein-coupled receptor 5, also known as Gpr49) as a marker of small intestinal and colonic stem cells by Barker *et al.*, 2007. The experiment conducted in

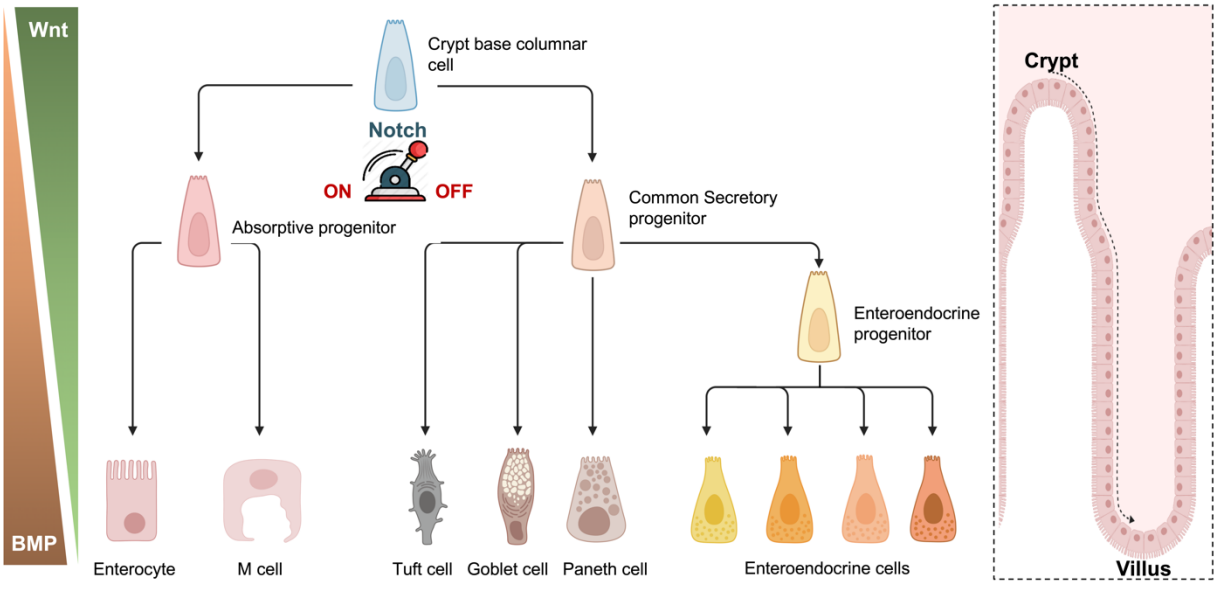

Figure 1.1. Small intestinal stem cell differentiation. Wnt and BMP signalings show opposite gradients in the crypt-villus axis. Stem cells are located at the crypt base. Notch signaling determines the absorptive or secretory fate of stem cell differentiation. Absorptive populations are enterocytes and M cells. Secretory populations are tuft, goblet, Paneth cells, and enteroendocrine cells. Created with BioRender.com.

this study traced the lineage of LGR5^{+} cells and demonstrated their ability to generate all cell lineages of the small intestinal epithelium. *Lgr5*-null mice exhibit neonatal lethality, characterized by the dilation of the gastrointestinal tract with air and the absence of milk in the stomach. This condition is caused by the fusion of the tongue to the floor of the oral cavity in *Lgr5*-null neonates, which hinders proper tongue movement and feeding (Morita *et al.*, 2004). When discussing the effect of LGR5 deficiency on the small intestinal epithelium, it has been observed that it does not have a significant effect on cell proliferation, as demonstrated by CldU staining. Additionally, it does not disrupt the differentiation of cell populations presented at embryonic day (E) 18.5. However, it does lead to precocious Paneth cell differentiation in the intestines of E18.5, whereas it typically occurs within the first two weeks after birth (Garcia *et al.*, 2009). In 2011, a study by de Lau and colleagues found that when *Lgr5* was conditionally deleted in the intestinal epithelium of adult mice, there were no visible changes and no confirmation of the Paneth cell phenotype observed in *Lgr5* null neonatal mice.

Further analysis of the proposed stem cells revealed the expression of other marker genes. The experiment was performed by van der Flier *et al*. in 2009, using *Lgr5*^{EGFPiresCreERT2} mice, which allowed for the sorting of LGR5^{+} cells based on the expression of the EGFP reporter. FACS analysis revealed two populations with higher and lower GFP, identified in the study as LGR5^{+} stem cells and their immediate transit-amplifying (TA) daughters, respectively. One of the identified genes, specifically expressed in stem cells but not in TA cells, was *Ascl2*, which encodes a basic helix-loop-helix (bHLH) transcription factor, previously identified as a direct Wnt target (van der Flier *et al.*, 2007; Hatzis *et al.*, 2008; Schuijers *et al.*, 2015). *Ascl2*$^{-/-}$ embryos die from placental failure by E10.5 (Guillemot *et al.*, 1994). Therefore, the effect of ASCL2 deficiency on stem cells was shown using *Ah*^{Cre}*:Ascl2*$^{floxed/floxed}$ mouse, which allows for conditional *Ascl2* knock-out in the gastrointestinal tract. The analysis of these mice showed that stem cells were absent; there was an increase in apoptotic cells in crypts and an increase in crypt fission, representing a repair process (van der Flier *et al*., 2009). On the other hand, transgenic expression of the *Ascl2* throughout the intestinal epithelium induces crypt hyperplasia and ectopic crypts on villi (van der Flier *et al*., 2009). These results suggest that ASCL2 is a master regulator of the crypt stemness program. In 2015, Schuijers and colleagues demonstrated how the expression of *Ascl2* is regulated. They demonstrated that ASCL2 functions as a bistable switch with

two states - "on" and "off". These states are defined by the initial amount of ASCL2 and correspond to the stem cell state ("on") and non-stem cell state ("off"). The switch between the "off" and "on" states of *Ascl2* is triggered by Wnt/R-spondin1 signaling. When in the "on" state, *Ascl2* is regulated through an autoactivation loop.

Another stem cell marker gene, *Olfm4*, encodes an olfactomedin domain-containing protein. Although its functions are not yet fully understood, it is known to play a role in host defence during gastric and colonic infections (Liu *et al.*, 2010; Liu *et al.*, 2016). While initial research found no impact of OLFM4 deficiency on mouse small intestinal architecture and homeostasis (Liu *et al.*, 2010), a later study demonstrated crypt hyperplasia in *Olfm4*$^{-/-}$ mice and robust inflammation in jejunum and ileum (Liu *et al.*, 2016). In 2009, van der Flier *et al.* identified *Olfm4* as a marker for intestinal stem cells in mice using *in situ* hybridization for *Olfm4* mRNA. However, a later study by Liu and Rodgers in 2022 cast doubt on its precision as a marker for small intestinal stem cells by identifying the presence of OLFM4 protein not only in the crypt base but also in the lower third to half of the crypts. Several studies confirmed that *Olfm4* is a direct target of Notch signaling (VanDussen *et al.*, 2012; Tsai *et al.*, 2014). Tsai and colleagues demonstrated in 2022 that increased Notch signaling and *Olfm4* expression are associated with stem cell maturation in human intestinal organoids.

In 2012, Muñoz and colleagues identified the SPARC-related modular calcium binding 2 (*Smoc2*) gene as a marker of small intestinal stem cells. The SMOC proteins are known as BMP antagonists, which have been shown by various researchers (Rainger *et al.*, 2011; Mommaerts *et al.*, 2014; Thomas *et al.*, 2009; Long *et al.*, 2021). As shown by Muñoz and colleagues, *Smoc2* null mice did not show any intestinal phenotype. Their lineage tracing experiment used LacZ-labeling induced in *Smoc2*-expressing cells to confirm *Smoc2* as a stem cell marker. The experiment showed labeling throughout the entire crypt-villus axis, similar to the *Lgr5* lineage tracing result.

Within the stem cell zone of the crypt, there are cells known as +4 cells. They are located above the crypt base columnar cells (CBC) and were first discovered by Potten *et al.* in 1978. They derive their name from their position in the crypt. While CBC cells occupy positions +1 to +3 from the crypt base and are protected by Paneth cells, +4 cells sit above the highest Paneth cell. While these cells are distinct from the *Lgr5*-expressing cells, they similarly contribute to all mature intestinal epithelial lineages. The identified markers of +4 cells are BMI1 (Sangiorgi and Capecchi, 2008; Yan *et al.*, 2012), TERT (Montgomery *et al.*, 2011), HOPX (Takeda *et al.*, 2011) and

LRIG1 (Powell *et al.*, 2012; Wong *et al.*, 2012). All four of them, however, show very significant expression in LGR5$^+$ cells as well (Barker *et al.*, 2012). Interestingly, +4 cells resist a higher radiation dose than LGR5$^+$ cells and have the potential to restore the stem cell zone after damage (Yan *et al.*, 2012). Thus, +4 cells demonstrate the potential of quiescent LGR5$^+$ stem cells that become active in response to an injury.

Transit amplifying (TA) cells can also revert to LGR5+ stem cells after damage (Barker *et al.*, 2012). They also express LGR5$^+$ stem cell signature genes like *Sox9* (van der Flier *et al.*, 2009) and *Olfm4* (Tsai *et al.*, 2022), albeit at a lower level. TA cells are a rapidly proliferating population that fills the crypts and gradually loses their progenitor identity as they move towards the intestinal lumen. Upon reaching the crypt-villus junction, TA cells differentiate into either absorptive or secretory epithelial lineage (Sancho *et al.*, 2015).

1.3 Secretory Lineage of the Small Intestinal Epithelium.

Paneth cells are the only mature cells located at the bottom of the crypt, intercalated between ISCs. They were first identified by Gustav Schwalbe in 1872 and named by Josef Paneth in 1887. When Paneth cells differentiate from the secretory progenitor, they move downward to the crypt bottom, while other cells move upwards towards the villus tip (Cui *et al.*, 2023). This positioning is regulated by ephrin type-B receptor 3 (*EphB3*), a receptor tyrosine kinase enriched in Paneth cells. Homozygous *EphB3*-null mice exhibit a disordered distribution of Paneth cells across the crypt (Batlle *et al.*, 2002). Each crypt contains 5 to 16 Paneth cells, higher in the distal small intestine, corresponding with increased bactericidal activity (Nakamura *et al.*, 2020). Paneth cells appear in mice approximately 7 to 10 days after birth (Cui *et al.*, 2023). They can be distinguished from other cell types by granules in the cytoplasm. These granules contain various antimicrobial peptides (AMPs), such as lysozyme, α-defensins (termed cryptdins in mice), secretory phospholipase A2, and lipopolysaccharide (LPS)-binding protein (LBP), among others (Hansen *et al.*, 2009; Ouellette, 2010). Lysozyme (LYZ1) is the first discovered antimicrobial peptide (AMP), and it is used as a Paneth cell marker (Wallaeys *et al.*, 2023). Paneth cells secrete lysozyme into the intestinal lumen (Bel *et al.*, 2017), where it hydrolyses β-(1,4)-glycosidic bonds in peptidoglycan, a major structural component of the bacterial cell wall (Nawaz *et al.*, 2022). *Lyz1*-deficiency reduces immune response to bacterial

molecular patterns, leading to the growth of lysozyme-sensitive mucolytic bacteria like *Ruminococcus gnavus*, which is a pathobiont associated with Crohn's disease (Yu *et al.*, 2020). Another class of AMPs, α-defensins, represent 70% of secreted peptides from Paneth cells (Ayabe *et al.*, 2000) and are released within minutes into the crypt lumen in response to bacterial antigens. α-defensins (cryptdins) are synthesized as inactive precursors (procryptdins) and activated by matrix metalloproteinase 7 (MMP-7 or matrilysin) through proteolytic processing (Ayabe *et al.*, 2002). Certain α-defensins create channels in the bacterial membranes. These channels cause depolarization and, ultimately, the death of the bacterial cell (Ganz, 2003). Others can form channels in enterocytes, which can lead to the flushing of the intestinal crypt and the resulting symptom of diarrhea (Markel *et al.*, 2007). Finally, defensins can activate the NF-κB and MAPK pathways in enterocytes, leading to the production of inflammatory cytokines (Lin *et al.*, 2004).

In addition to their defensive function supported by AMPs, Paneth cells also play an essential role in forming the niche for intestinal stem cells. Paneth cells maintain stem cells by providing EGF, Wnt and Notch ligands (Kim *et al.*, 2012; Sato *et al.*, 2011a). Paneth cells primarily produce Wnt3, which is transferred to nearby $LGR5^+$ stem cells through direct contact. Wnt3 has low solubility and cannot diffuse freely but is tethered to the membrane of the receiving stem cell by Frizzled receptors. The Frizzled-bound Wnt spreads through stem cell division, creating a crypt-villus gradient of Wnt (Farin *et al.*, 2016). In addition to Wnt signaling, stem cells also require activation of Notch signaling. This activation also involves direct contact between signal-sending and signal-receiving cells (del Álamo *et al.*, 2011). Notch signaling is initiated by Notch ligands DLL1 or DLL4 on Paneth cells that bind to Notch receptors (Notch1 or Notch2) on stem cells (Barreto E Barreto *et al.*, 2021).

Paneth cell differentiation depends on the presence of Wnt signals. Therefore, in a Wnt-rich environment, if a cell does not receive Notch signals, it will be differentiated into a Paneth cell. As a result, differentiation along the Paneth cell lineage becomes the default path for all stem cells. (Gehart and Clevers, 2019).

Goblet cells were named by Schulze in 1866 due to their cup-like shape on top (Gustafsson and Johansson, 2022). The primary function of goblet cells is to produce mucus, which acts as a protective barrier for the intestinal epithelium. The key component of the small intestinal mucus is mucin 2 (MUC2), a large, highly

glycosylated polymer (Johansson *et al.*, 2011). The C-terminus of MUC2 forms dimers, and the N-terminus forms trimers, creating a net-like structure densely packed in goblet cell secretory granules (Ambort *et al.*, 2012). Another important goblet cell marker, anterior gradient homolog 2 (AGR2), presents within the endoplasmic reticulum of goblet cells and plays a role in mucin processing (Park *et al.*, 2009). *Muc2*$^{-/-}$ mice lack identifiable goblet cells along the entire length of the intestine (Velcich *et al.*, 2002). Proteomic analysis of the small and large intestinal mucus performed by Rodríguez-Piñeiro *et al.* in 2013 revealed other proteins associated with MUC2, specifically CLCA1, FCGBP, and ZG16. Calcium-activated chloride channel regulator 1 (CLCA1) was shown to facilitate the processing and removal of mucus (Nyström *et al.*, 2018). IgGFc-binding protein (FCGBP) is a mucin-like protein that maintains mucosal structure and regulates early immune response to microbial infection (Liu *et al.*, 2022). Zymogen granule membrane protein 16 (ZG16) binds to gram-positive bacterial peptidoglycan, forming aggregates that prevent bacterial penetration of mucus, which helps keep the commensal bacteria at a distance from the host's epithelium (Bergstrom *et al.*, 2016). Goblet cells are responsible not only for producing mucus but also for creating Goblet Cell-Associated Antigen Passages (GAPs). These passages play a crucial role in detecting and transporting luminal antigens to the innate immune cells present in the lamina propria, thereby supporting gut immunity (Gustafsson and Johansson, 2022; McDole *et al.*, 2012).

Tuft cells, rare chemosensory cells, are found in the gastrointestinal and respiratory tracts (Chang *et al.*, 1986). In the small intestine of mice, tuft cells comprise only 0.4% of the total epithelial cell population (McKinley *et al.*, 2017). They are characterized by blunt and long surface microvilli and numerous vesicles in the apical cytoplasm (Sato, 2007). Intestinal tuft cells are critical sentinels in the gut epithelium that promote type 2 immunity in response to intestinal parasites (Howitt *et al.*, 2016). They use various receptors on their apical surface to monitor the intestinal lumen. These receptors include taste receptors, similar to those on the tongue and soft palate (Hendel *et al.*, 2022). There are three types of taste receptors: type 1 responds to sweet and umami flavors, type 2 to bitter flavors, and type 3 to sour flavors (Bachmanov *et al.*, 2014). Tuft cells express type 1 and type 2 receptors (Howitt *et al.*, 2016; Luo *et al.*, 2019; Howitt *et al.*, 2020). Another important receptor is the succinate

receptor 1 (SUCNR1), which responds to succinate, a metabolite secreted by certain symbiotic bacteria, protists, and helminths (Nadjsombati *et al.*, 2018).

For years, researchers have faced a challenging task in defining the markers of tuft cells. In 2008, Bezençon and colleagues used transgenic mice to isolate cells from the small intestinal epithelium that expressed *Trpm5*. This gene encodes for a cation channel responsible for transducing bitter, sweet, and umami tastes (Liman *et al.*, 2007). The researchers found that these cells were almost exclusively tuft cells (in this study, Bezençon and colleagues used the term "brush cells" as an alternative name for "tuft cells"), which were observed earlier but not defined as a separate cell population. Genes involved in inflammation, such as the IL-17 receptor B, were highly and specifically expressed in $TRPM5^{+}$ cells, indicating an important role in controlling intestinal inflammation. In 2011, Gerbe and colleagues conducted a study on the transcriptional regulation of tuft cell differentiation. They demonstrated that ATOH1, a transcription factor that defines the secretory lineage, is crucial for tuft cell differentiation. At the same time, transcription factors that define other secretory lineages were dispensable. These results finally established tuft cells as a separate population along the secretory lineage. Additionally, this study revealed the doublecortin-like kinase 1 protein (DCLK1) as a marker of tuft cells. Previously, DCLK1 was believed to be produced in quiescent stem cells, but Gerbe and colleagues demonstrated that DCLK1-expressing cells are post-mitotic and continuously renewed. Further studies have identified POU2F3 as a master regulator of tuft cell differentiation, which is currently used alongside DCLK1 and TRPM5 as another tuft cell marker (Yamashita *et al.*, 2017; Gerbe *et al.*, 2016).

Enteroendocrine cells (EECs) represent a rare population of hormone-producing cells, accounting for only 1% of the total epithelial cells. Although hormone-producing cells are rare compared to other cell populations, the gut is still considered the body's largest endocrine organ (Ahlman and Nilsson, 2001). EECs are most frequent in the proximal small intestine and decrease towards the colon (Gunawardene *et al.*, 2011). There are two types of EECs: open type, which have a bottle-neck shape and a prolongation with microvilli in direct contact with the intestinal lumen, and closed type, which are strictly linked to the basal membrane and do not reach the intestinal lumen or possess microvilli (Rezzani *et al.*, 2022). One of the unique characteristics of EECs is the presence of hormone-storing secretory granules.

These granules accumulate and release their contents upon stimulation through exocytosis at the basolateral membrane. The secreted hormones can then act locally or be transported through the bloodstream to affect distant targets (Sternini *et al.*, 2008). Chromogranin A (CHGA) is an acidic glycoprotein and one of the major components of secretory granules. It is crucial for granulogenesis and acts as a chaperone for prohormone sorting to the regulated secretory pathway (Kim *et al.*, 2001, Koshimizu *et al.*, 2010). CHGA is widely used as a pan-marker of EECs (Beumer *et al.*, 2020a). There are currently seven known subtypes of EEC that are classified based on the hormones they secrete: enterochromaffin (EC) cells (producing serotonin, 5-HT), D cells (producing somatostatin, SST), L cells (producing glucagon-like peptide 1, GLP-1), I cells (producing cholecystokinin, CCK), N cells (producing neurotensin, NTS), K cells (producing gastric inhibitory peptide, GIP), X cells (producing ghrelin, GHRL) (Atanga *et al.*, 2023). However, recent research on epithelial plasticity indicates that these subtypes have the ability to switch and secrete different hormones and peptides (Beumer *et al.*, 2020b).

Enterochromaffin (EC) cells are the most abundant EECs in the gastrointestinal tract (Yang *et al.*, 2021). Their primary secretory product is serotonin (5-HT), synthesized by hydroxylating and decarboxylating tryptophan (Ahlman and Nilsson, 2001). Ninety-five percent of the body's serotonin is located in the gastrointestinal tract, primarily in the secretory granules of EC cells (Gunawardene *et al.*, 2011). EC cells are scattered throughout the small intestine, with a slightly higher frequency in the anterior region compared to the posterior. Small intestinal EC cells have a pyramid shape with a large basolateral surface and an apical process that extends to the luminal surface and thus refer to the open type EECs (Modlin *et al.*, 2006; Wang, Y. *et al.*, 2020; Wei *et al.*, 2022). Tryptophan 5-hydroxylase, the enzyme responsible for synthesizing 5-HT, was found in the cytoplasm of EC cells using immunofluorescent staining (Modlin *et al.*, 2006) and is currently used as an EC cell marker. Studies in both animals and humans have demonstrated that 5-HT promotes gut motility processes, such as peristalsis and migrating complexes in both the small and large intestines (Chen *et al.*, 2001*;* Coleman *et al.,* 2003; Heredia *et al.*, 2009). Consequently, drugs that target 5-HT receptors, particularly 5-HT_3 and 5-HT_4 receptors, have been clinically used to treat motility disorders (Kendig and Grider, 2015). EC cells also produce tachykinin 1 (TAC1, substance P), a peptide involved in muscle contraction and inflammation (O'Connor *et al.*, 2004). In 2018, Beumer and

colleagues discovered that EC cells express different hormones depending on whether they originate from the crypt or the villus. Crypt EC cells express *Tac1* and *Tph1*, while villus EC cells express secretin (*Sct*) instead of *Tac1* and even higher levels of *Tph1*. *Sct* is expressed not only in villus EC cells but also in virtually all mature enteroendocrine cells to a moderate extent (Fazio Coles *et al.*, 2020; Haber *et al.*, 2017). SCT is a hormone that helps to stimulate the secretion of a fluid in the pancreas that is rich in bicarbonate. When secretin enters the bloodstream or the intestinal lumen, it interacts with the pancreatic ductal cells and stimulates bicarbonate secretion. This bicarbonate secretion helps to neutralize the pH of the gastric chyme as it enters the small intestine.

D cells, like EC cells, are found throughout the small intestine, but they are slightly more abundant in the duodenum than in other regions (Penman *et al.*, 1983). Additionally, they tend to be located more frequently in the lower third of the crypt (Low, 2004). D cells are open-type and have a spindle-like shape with slender apical processes (Gunawardene *et al.*, 2011). Their main secretory product is somatostatin (SST) - a hormone that inhibits the release or action of many gut hormones that regulate gastrointestinal function (Dharmsathaphorn, 1985). Mechanistically, somatostatin stimulates the contraction of EECs, translocating the secretory vesicles from the cell periphery to the perinuclear region, thus inhibiting their release, as demonstrated by Saras *et al.* in 2007.

L cells are mainly found in the posterior small intestine and are primarily located in the basal part of the crypts (Beumer *et al.*, 2020b; Gunawardene *et al.*, 2011). These are open-type endocrine cells with a cone-shaped appearance located on the basal lamina of the intestinal epithelial lining; they have microvilli that protrude into the intestinal lumen (Kuhre *et al.*, 2021). L cells are classified based on their production of proglucagon, which is a hormone precursor. It is encoded by the proglucagon gene *Gcg* and consists of a 160 amino acid pro-peptide (Xiong *et al.*, 2012). After translation, proglucagon undergoes cell-specific processing through site-specific cleavage to yield proglucagon-derived peptides (PGDPs). In the pancreatic α-cells, it is converted to glucagon by prohormone convertase 2 (PC2). Conversely, in the intestinal L cells, proglucagon is cleaved by PC1 to produce glucagon-like peptide (GLP)-1 and GLP-2 (Whalley *et al.*, 2011). Tucker *et al.* (1996) demonstrated that tissue-specific processing is due to the differential expression of PC1 and PC2 in intestinal and islet cell lines, respectively. The primary role of GLP-1 is to enhance

insulin secretion in response to food intake, commonly referred to as its incretin effect. GLP-1 stimulates insulin secretion from pancreatic β-cells in a blood-glucose-dependent manner (Drucker, 2013; Marathe *et al.*, 2013). Another secretory product of L cells is Peptide YY, first identified by Böttcher *et al*. in 1984. PYY is released together with GLP-1 following a meal to mediate postprandial satiety (De Silva and Bloom, 2012). According to Ballantyne (2006), PYY has several additional effects, including reducing intestinal and colonic transit, gastric emptying, gastric acid secretion, pancreatic exocrine and insulin secretion.

I cells represent a lineage differentiated from L cells when they move towards the villus tip and get exposed to a higher level of BMP signaling, as per the study conducted by Beumer *et al.* in 2018. As I cells move closer to the villus tip, they are exposed to higher BMP signaling, leading to their differentiation into N cells. Therefore, L cells are mostly found in the lower part of the crypt, I cells are located around the intervillus region, and N cells are mostly found around the villus tip. The main hormone secreted by I cells is cholecystokinin (CCK). However, other populations of peptidergic EECs (non-EC) also produce CCK, but at a lower level. The physiological actions of CCK include stimulating pancreatic secretion and gallbladder contraction in response to fat and protein intake, regulating gastric emptying, and inducing satiety (Liddle, 1997).

N cells are classified based on their neurotensin (NTS) expression. Additionally, among the L/I/N cell lineage, N cells exhibit the highest expression of PYY. NTS functions include stimulating pancreatic and biliary secretions, inhibiting gastric acid secretion and motility, inhibiting jejunum-ileum motility, and stimulating colon motility (Rostène and Alexander, 1997; Vincent *et al.*, 1999). It also promotes the proliferation of normal gastrointestinal epithelium (Rock *et al.*, 2022).

K cells are predominantly present in the duodenum, unlike L cells (Gutierrez-Aguilar and Woods, 2011). Their primary secretory product is Glucose-dependent insulinotropic peptide (GIP), which, together with GLP-1, is a known incretin hormone, albeit less potent (Pacini *et al.*, 2010). Furthermore, GIP suppresses the secretion of gastric acid, gastrin, and peristalsis in the stomach and intestines (Villar *et al.*, 1976).

X cells are classified based on their production of ghrelin (GHRL). They exist in both open and closed types (Sakata *et al.*, 2002). There is a higher concentration of X cells in the stomach and anterior part of the small intestine (Wierup *et al.*, 2007). Ghrelin is a hormone that is released during periods of fasting and suppressed post-

feeding (Tschöp *et al.*, 2000). Furthermore, ghrelin stimulates gastric emptying and intestinal motility (Dornonville de la Cour *et al.*, 2004; Tack *et al.*, 2006).

1.4 Development of Mouse Small Intestine.

The process of gastrulation leads to the formation of three primary germ layers: ectoderm, mesoderm, and endoderm. Gastrulation in mice occurs mainly over three days from embryonic day (E) 6.25 to E9.5 (Bardot *et al.*, 2020). The gastrointestinal tract develops from two embryonic layers: the endoderm, which forms the epithelium, and the mesoderm, which forms the smooth muscle layer, mesenchyme, and other cell types (McLin *et al.*, 2009). The anterior-posterior (AP) axis is patterned just before gastrulation, with continued lineage diversification. Thus, during the early somite-stage embryo (E8.5), the endoderm divides into three main parts. The foregut forms the liver, lungs, airways, thymus, thyroid, stomach, pancreas, esophagus and proximal duodenum. The midgut becomes the distal duodenum, jejunum, ileum, cecum, and the ascending and proximal transverse colon. Lastly, the hindgut endoderm forms the transverse colon, descending colon, sigmoid, and anorectum (Spence *et al.*, 2011; Bayer *et al.*, 2021).

After the establishment of the primary germ layers, the endoderm undergoes a complex series of changes that give rise to the gut tube. The process of gut tube formation can be visualized as the endoderm resembling a flat sheet of paper that folds into a tube and seals in the middle when the two sides meet. In the mouse, gut tube closure is completed by E9.0 (Chin *et al.*, 2017). The process is mainly regulated by transcription factors GATA4 and SOX17. Mice, mutant for *Gata4* and *Sox17*, display incomplete gut tube closure (Kuo *et al.*, 1997; Kanai-Azuma *et al.*, 2002). On embryonic day 9.5 the gut tube represents a simple, pseudostratified epithelium. Various transcription factors precisely regulate gut organogenesis. SOX2 activates the foregut transcriptional program, regulating the differentiation of the stomach, liver, pancreas and esophagus, while CDX2, produced by the hindgut endoderm, is considered a master regulator of intestinal identity (Chin *et al.*, 2017). Inducing *Sox2* expression in the embryonic intestinal epithelium leads to anteriorization of the intestine. This causes intestinal epithelial cells to take on the morphology and gene expression profile of immature gastric cells (Raghoebir *et al.*, 2012), while ectopic expression of *Cdx2* in the gastric epithelium induces intestinal metaplasia (Silberg *et*

al., 2002). Stomach-like tissue formation in the intestine is observed when *Cdx2* is conditionally deleted around E13.5 (Grainger *et al.*, 2010), while deletion of *Cdx2* during earlier embryogenesis transforms intestinal epithelium into esophagal-like squamous epithelium (Gao *et al.*, 2009). PDX1 and NEUROD1 regulate the formation of the pancreas, caudal stomach, and duodenum (Wells *et al.*, 2000). The paired box (Pax) transcription factors 4 and 6 play a critical role in the development of pancreatic endocrine cells (Sosa-Pineda *et al.*, 1997; St-Onge *et al.*, 1997) as well as endocrine cells of the proximal intestines and distal stomach (Larsson *et al.*, 1998). NKX2.2 and ISL-1 are crucial for regulating the proper development and cell specification of the pancreas (Sussel *et al.*, 1998; Ahlgren *et al.*, 1997) and intestinal enteroendocrine cell specification (Desai *et al.*, 2008; Terry *et al.*, 2014).

From E9.5 to E14.5, the gut tube rapidly elongates due to the proliferation of the epithelium and mesenchyme. The process is controlled by noncanonical Wnt and Hh signallings (Chin *et al.*, 2017; Cervantes *et al.*, 2009; Mao *et al.*, 2010). Starting at E14.5, the pseudostratified epithelium undergoes significant restructuring, resulting in villi formation. The process begins in the duodenum and gradually extends towards the ileum, taking approximately 36 hours to complete (Walton *et al.*, 2012).

Mesenchymal cells expressing the platelet-derived growth factor receptor α (PDGFRa) form clusters below the sites of future epithelial villi (Figure 1.2). These clusters signal the overlying epithelium to stop proliferation in the nascent villi and initiate epithelial folding (Karlsson *et al.*, 2000). Additionally, the epithelium-derived Hedgehog signaling is necessary for this process. Blocking Hedgehog signaling

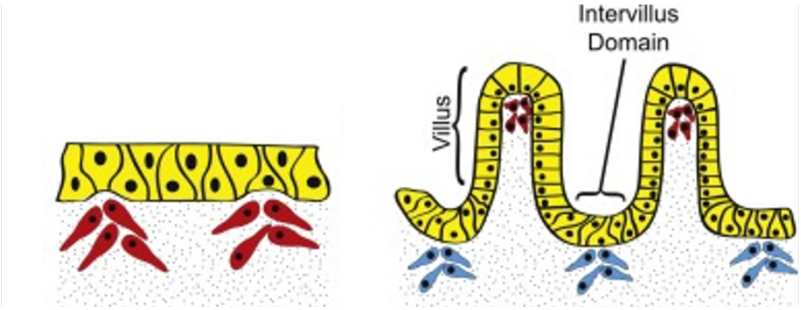

Figure 1.2. Villi formation in the developing mouse gut. From E14.5 onwards, mesenchymal clusters (red) form near the nascent villus, causing epithelial deformation. Clusters form below the villi, creating the intervillus domain. Villus morphogenesis will repeat multiple times, forming new clusters (blue) next to the intervillus domain after the previous round (red). The figure is taken from Chin *et al.*, 2017.

disrupts mesenchymal cell clustering and villus formation (Madison *et al.*, 2005; Walton *et al.*, 2012).

After villus formation, epithelial proliferation is limited to the base of the villi for the remainder of development (Kolev *et al.*, 2023). At around E16.5 the epithelium differentiates into the functional cell types of the small intestine, including mucus-producing goblet cells, hormone-producing enteroendocrine cells and absorptive enterocytes (Chin *et al.*, 2017). The timing of tuft cell development is still being discussed. However, a study in 2011 by Saqui-Salces *et al.* detected tuft cells in mice at E18.5. Paneth cells are absent during fetal development in mice and only emerge after birth, typically at 7-10 days old (Cui *et al.*, 2023).

1.5 Canonical WNT Signaling and Its Role in Small Intestinal Homeostasis.

Wnt is one of the key signaling pathways regulating embryonic gut development and adult gut homeostasis. Most of the Wnt signaling target genes are associated with cell proliferation, making it essential for the intestinal stem cell niche. It is activated by Wnt ligands (Wnts) - secreted proteins, which act at a short distance. Because of the poor solubility, most Wnts require direct cell-cell contact between secreting and receiving cells. An essential core for Wnt secretion is formed by a porcupine (PORCN) and Wntless (WLS) (Valenta *et al.*, 2016). PORCN is an acyltransferase which palmitoylates Wnts and enables their binding to a transmembrane protein WLS, which in turn conveys them to the plasma membrane for secretion (Clevers *et al*., 2014). The main intestinal Wnt ligand is Wnt3a, secreted by Paneth cells, which produce a niche for stem cells and physically contact them (Sato *et al.*, 2011a). However, not only Paneth cells serve as a source for Wnts. The study by Valenta *et al.* in 2016 demonstrated that selectively ablating Wnt secretion in the mouse intestinal epithelium did not impact stem cells. However, organoids derived from these mice only survived when adding Wnt3a ligand to the culture medium. At the same time, mice with fully ablated Wnt secretion died within 2 weeks. These results indicate a non-epithelial Wnt ligand source, which allows overcoming the epithelial-specific ablation of Wnt secretion. Valenta *et al.* identified subepithelial mesenchymal cells as the source of Wnt2b production, the first indication of an extra-epithelial Wnt source.

Wnt ligands bind to a two-part receptor: a seven-transmembrane Frizzled (Fzd) and LRP5/6, on a Wnt-responsive cell. The Fzd family represents a group of cell surface receptors in mammals with 10 members. They share a common structure, including a conserved extracellular cysteine-rich domain and a domain with seven transmembrane segments (Wang *et al.*, 2016). The expression of different Fzds in the small intestinal epithelium differs in different cell types: CBC cells have an enriched expression of Fzd2 and Fzd7, while Fzd9 expression is highest in the Paneth cells (Flanagan *et al.*, 2015). Low density lipoprotein receptor-related proteins 5 and 6 (LRP5 and LRP6) are the single-pass transmembrane proteins, which act as coreceptors of Wnt ligands (Ren *et al.*, 2021). The binding of Wnt ligands to Fzd and

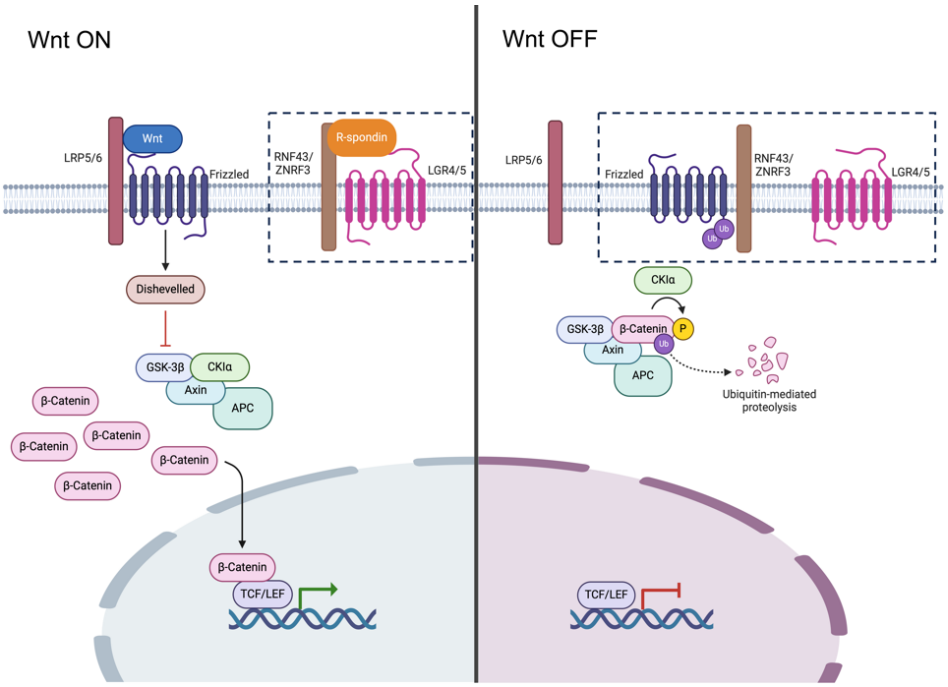

Figure 1.3 Wnt signaling activation. Wnt ligands bind to a two-part receptor: a Frizzled (Fzd) and LRP5/6, on a Wnt-responsive cell. LRP5 and LRP6 act as coreceptors of Wnt ligands. The binding of Wnt ligands to Fzd and LRP5/6 dimerizes them on the cell surface and recruits AXIN protein. The destruction complex comprises of AXIN, adenomatous polyposis coli (APC) protein, glycogen synthase kinase 3β (GSK3β), and casein kinase 1 (CK1) to target β-catenin for degradation. Binding the destruction complex to the cytoplasmic domain of the Wnt receptor turns off the destruction of β-catenin. Stabilized β-catenin accumulates in the cytoplasm, translocates into the nucleus, and drives transcription by binding to TCF/LEF family factors (Wnt signaling "on" state). In the absence of Wnt ligands, the destruction complex remains active, and β-catenin gets degraded (Wnt signaling "off" state). In dotted squares: RNF43/ZNRF3 are E3 ubiquitin ligases that regulate the amount of FZD receptors in the Wnt signaling pathway. They bind to the FZD receptor, leading to its destruction in lysosomes. R-Spondins inhibit RNF43/ZNRF3 and increase the amount of available FZD receptors by sequestering RNF43/ZNRF3 via RSPO/LGR binding. Created with BioRender.com.

LRP5/6 leads to their dimerization on the cell surface and induces conformational changes. The protein Dishevelled (DVL), bound to the FZD cytoplasmic domain, creates a platform for the interaction between the LRP5/6 tail and AXIN protein. This interaction happens through the DIX domains on DVL and AXIN (Schwarz-Romond *et al.*, 2007; Fiedler *et al.*, 2011). AXIN is a part of the destruction complex with adenomatous polyposis coli (APC) protein, glycogen synthase kinase 3β (GSK3β), and casein kinase 1 (CK1) (McCartney and Näthke, 2008; Moon *et al.*, 2002; Polakis, 2007; Reya and Clevers, 2005). AXIN and APC are carcase proteins that hold the whole complex together, GSK3β and CK1 protein kinases phosphorylate the cytoplasmic tail of LRP5/6, which subsequently recruits AXIN. The function of the destruction complex is to target β-catenin, a transcriptional coactivator of Wnt target gene expression, for degradation by the proteasome. However, binding the destruction complex to the cytoplasmic domain of the Wnt receptor turns off the destruction of β-catenin. Stabilized β-catenin accumulates in the cytoplasm, translocates into the nucleus, and drives transcription by binding to TCF/LEF family factors and displacing transcriptional co-repressor GROUCHO (Wnt signaling “on” state). In the absence of Wnt ligands, the destruction complex remains active. Being phosphorylated by GSK3β and CK1 protein kinases from the complex, β-catenin gets degraded in the cytoplasm by the proteasome and is thus unable to translocate into the nucleus and activate transcription of Wnt target genes (Wnt signaling “off” state; Stamos and Weis, 2013; Nusse and Clevers, 2017). Two transmembrane E3 ubiquitin ligases, RNF43 or ZNRF3, are another module of Wnt signaling regulation. These two enzymes are responsible for controlling the amount of available FZD receptors. The binding of the FZD receptor to RNF43/ZNRF3 leads to its ubiquitination, endocytosis and destruction in lysosomes (Koo *et al.*, 2012; Hao *et al.*, 2012). However, RNF43/ZNRF3 are inhibited by R-Spondins (RSPO), secreted soluble agonists of the canonical Wnt signaling (de Lau *et al.*, 2012). The binding of R-spondins to LGR family receptors (expressed by stem cells LGR4 and LGR5) leads to the sequestration of RNF43/ZNRF3 by RSPO/LGR. This results in an increase in the amount of FZD available for Wnt ligands (de Lau *et al.*, 2014; Gehart and Clevers, 2019). Wnt signaling activation is reviewed in Figure 1.3.

There are several known secreted inhibitors of Wnt signaling: (1) Dickkopf (DKK) family members, which bind to the extracellular domain Lrp5/6 and thus block Wnt binding (Jiang *et al.*, 2022); (2) Wnt inhibitory factor 1 (WIF1) and secreted

Frizzled receptor proteins (Sfrp), which sequester Wnt proteins (Niehrs, 2012); (3) NOTUM, which deacylates Wnt proteins, thus preventing them from binding to their receptors (Janda *et al.*, 2012; Kakugawa *et al.*, 2015)

The Wnt signaling is characterized by a decreasing gradient from the crypt to the villus tip. This is because the sources of Wnt ligands are located at the bottom of the crypt. Due to their poor solubility, Wnts mainly propagate from their source in a cell-bound manner through cell division rather than through diffusion (Farin *et al.*, 2016).

The Wnt signaling pathway induces the transcription of Wnt-target genes through the interaction of β-catenin with TCF/LEF transcription factors. The mammalian TCF/LEF family consists of four nuclear factors: TCF7, LEF1, TCF7L1, and TCF7L2 (also known as TCF1, LEF1, TCF3, and TCF4, respectively; Hrckulak *et al.*, 2016). TCF7L2 is the main effector of canonical Wnt signalling. The gut analysis of *Tcf7l2* knock-out mouse showed the crucial role of Wnt signaling for intestinal stem cells, as the stem cell compartment was completely lost (Korinek *et al.*, 1998). LEF1 is the only member of the TCF/LEF family that is not expressed in healthy intestinal stem cell crypts but is induced during intestinal tumorigenesis (Hovanes *et al.*, 2001).

1.6 *Apc*$^{min/+}$ Mouse Model of Familial Adenomatous Polyposis. Intestinal Cancer Initiation and Progression.

The accurate modulation of Wnt signaling pathway is indispensable, given its significant involvement in cell proliferation. As such, any dysregulation of Wnt signaling can lead to the acquisition of malignant traits in intestinal stem cells. Common mechanisms by which the Wnt/β-catenin pathway is dysregulated in cancer are reviewed by White *et al.*, 2012. The most common of them are loss-of-function mutations in *Apc* gene, which lead to a breakdown of the destruction complex and constitutive activation of the signaling. Humans with germline *Apc* mutation develop hundreds to thousands of colon tumours in their first few decades of life. This inherited syndrome is called Familial Adenomatous Polyposis (FAP). Germline and somatic *Apc* mutations typically group between codons 1250 and 1464, a region termed “mutation cluster region”, MCR (Kohler *et al.*, 2008). In addition, there is a correlation between the localization of mutation in the gene and the number of developing polyps (intestinal polyposis phenotype) (Nieuwenhuis and Vasen, 2007). Mutations in the MCR are

associated with the most severe intestinal phenotypes, while mutations outside the MCR lead to reduced polyp multiplicity (Zeineldin and Neufeld, 2013). However, the germline mutation(s) within one *Apc* allele is insufficient to drive adenoma formation in both FAP patients and rodent models. Loss of function in both alleles is required for tumorigenesis (Luongo *et al.*, 1994). Therefore, additional somatic mutations within the second *Apc* allele or loss of heterozygosity (LOH) at the second allele occur within colorectal tumours of FAP patients (Luongo *et al.*, 1994).

APC is well-conserved between humans and rodents, with 92% similarity at the amino acid level. The Multiple intestinal neoplasia (Min) mouse is a classical model for FAP (Su *et al.*, 1992). The autosomal dominant mutation in this rodent model was generated by *N*-ethyl-*N*-nitrosourea mutagenesis. The mutagen caused a nonsense mutation in codon 850 of the *Apc* gene on chromosome 18, resulting in the production of a truncated APC protein. Spontaneous LOH of the other *Apc* allele occurs, and mice develop multiple intestinal adenomas (Figure 1.4 A) and colonic polyps (Moser *et al.*, 1990). A major difference between the $Apc^{min/+}$ mouse model and the human disease is that human FAP patients predominantly develop colonic lesions, whereas the mice develop more polyps in the small intestine. The mechanism of LOH of the other *Apc* allele remains a question of discussion. My copy number variation (CNV) analysis of cultured tumoroids and previously published results of Haigis *et al.*, 2002 indicate tumours carry two mutant copies of chromosome 18, which, according to Haigis and colleagues, results from somatic recombination between homologs. The Sanger sequencing result in Figure 1.4B illustrates that wild-type small intestinal organoids exhibit a homogenous sequence of a normal *Apc* allele. In contrast, Sanger sequencing of the DNA extracted from the ear biopsy of $Apc^{min/+}$ detected heterozygosity at a position of Min mutation: one mutant and one normal allele, which compensates for the APC function (Figure 1.4C). Finally, tumoroids, tumor cells selected in cell culture, possess a homogenous sequence of the mutant allele and, consequently, lack the functional full-length APC protein (Figure 1.4D). The timing and mechanisms that cause LOH in cancer-initiating cells are still being debated among researchers. Some prior studies have used chemical carcinogens or anti-inflammatory drugs (Shoemaker *et al.*, 1995; Sansom *et al.*, 2001) and have suggested that adenoma formation may occur during embryonic development. However, the exact stage of embryonic development at which this occurs remains to be identified.

In 2009, Barker *et al.* conducted a study where they found that depletion of *Apc* from LGR5⁺ stem cells resulted in their rapid transformation. These transformed cells remained at the bottom of crypts and powered the growth of a small tumor called microadenoma. The growth of these microadenomas was leading to the development of macroscopic adenomas within 3-5 weeks. Deletion of *Apc* in TA cells also induced microadenoma formation; however, they did not progress. These results suggest that LGR5⁺ stem cells are the cells of origin of intestinal cancer.

Cancer cells are able to promote tumor growth through additional mechanisms despite being stem cells with constitutively active Wnt signaling. Research conducted by Flanagan *et al.* in 2021 revealed that cells with *Apc* mutation secrete NOTUM and, in lesser amounts, other inhibitors such as DKK and WIF1. They work to inhibit the Wnt signalling in the neighbouring wild-type crypts, thereby restricting their proliferation. However, a study by van Neerven *et al.* in 2021 showed that this inhibition could be counteracted by lithium chloride, which is an agonist of the Wnt signaling pathway. These findings shed light on the mechanism of tumorigenesis and open up new therapeutic opportunities.

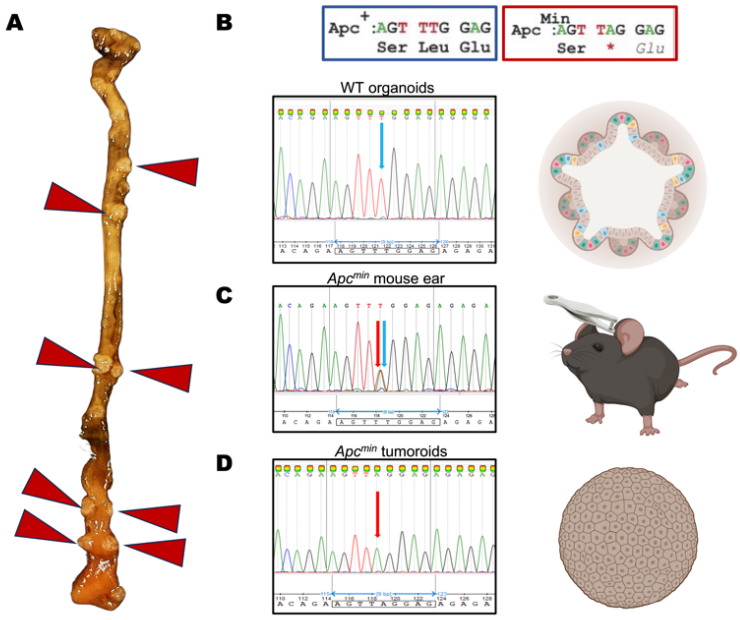

Figure 1.4 *Apc*$^{min/+}$ mouse model of familial adenomatous polyposis. A. Small intestine dissected from 20-week-old *Apc*$^{min/+}$ mouse; multiple intestinal adenomas are shown by red arrows. B. The Sanger sequence of wild-type small intestinal organoids shows the homogenic sequence of the normal *Apc* allele. C. The Sanger sequence of the gDNA from the ear biopsy of the *Apc*$^{min/+}$ mouse reveals a heterogeneous sequence with two peaks at the site of the Min mutation. D. The Sanger sequence of the tumoroid's gDNA reveals a homozygous sequence of a mutant allele. Created with BioRender.com.

1.7 The Role of Notch Signaling in Small Intestinal Homeostasis.

Notch signaling is essential for intestinal stem cells self-renewal. As mentioned earlier, activation of Notch signaling requires direct cell-to-cell contact, which allows binding of Notch receptor exposed on the membrane of the signal-receiving cell and juxtaposed ligand on the membrane of a neighboring cell. Paneth cells express Notch ligands DLL1, DLL4 and JAG1. DLL1 and DLL4 are essential, and inactivation of both causes loss of stem and progenitor cells; in contrast, JAG1 is not essential (Pellegrini *et al.*, 2011). Mammals have four single-span transmembrane receptors in the Notch family, namely Notch 1-4. Intestinal stem cells express only Notch1 and Notch2, while Notch3 and Notch4 are not expressed (Fre *et al*, 2011). The simultaneous deletion of Notch1 and Notch2 causes the complete loss of proliferative stem and progenitor cells in the intestinal epithelium (Riccio *et al.*, 2008). Inhibition of Notch1 alone has a severe effect on Notch signaling activation, whereas Notch2 inhibition has no significant effect (Wu *et al.*, 2010).

All Notch proteins have an extracellular domain followed by a negative regulatory region (NRR), including three cysteine-rich Lin12-Notch repeats (LNR) and a heterodimerization domain (HD). The extracellular domain is followed by the transmembrane domain and the intracellular domain (NICD). The last contains functionally important RAM (RBPjk association module), linked to seven ankyrin repeats (ANK domain), two nuclear localization signals on both sides of the ANK domain, and the C-terminal PEST domain (proline/ glutamic acid/ serine/threonine-rich motifs). RAM is responsible for interaction with transcription factors in the nucleus, and the PEST domain is important for the stability of the Notch intracellular domain (NICD). After the synthesis, Notch precursors undergo a series of glycosylations vital for their functional activity, first in the endoplasmic reticulum and then in the Golgi apparatus (Shi *et al.*, 2003; Moloney *et al.,* 2000). Glycosylated Notch precursor is subjected to the first S1 cleavage in Golgi apparatus. As a result of this cleavage, a heterodimer NECT-NTMIC (Notch extracellular domain – Notch transmembrane and intracellular domain) is formed. The next S2 cleavage is the only one that involves ligand binding, making it crucial for signal initiation. Once bound with ligands, the receptor extends the LNR domain and exposes the S2 site for cleavage. The product of S2 cleavage is composed of the transmembrane domain and the intracellular domain, also called Notch extracellular truncation (NEXT). NEXT is further cleaved at

the S3 site, releasing NICD. The enzyme responsible for S3 cleavage is γ-secretase (Kopan and Ilagan, 2009; Zhou *et al.*, 2022 provide a more detailed explanation of the Notch signalling induction process).

NICD can translocate into the nucleus and bind to the transcription factor RBP-J and co-A activators mastermind (Co-A MAM). Together, they form a transactivation complex that induces the transcription of target genes, including the hairy/enhancer of split (HES) (Kageyama *et al.*, 2000). In the absence of Notch, RBP-J is associated with a corepressor (Co-R) and inhibits gene expression. The mechanism of Notch signaling activation is reviewed in Figure 1.5.

HES1, 3 and 5 are basic helix-loop-helix transcriptional repressors. The best characterized of them, HES1, has been shown to be expressed by stem cells in the intestinal crypt (Kayahara *et al.*, 2003). It was demonstrated to repress the expression of the *Atoh1* gene, required for a progenitor cell to differentiate towards secretory lineage (Yang *et al.*, 2001; Shroyer *et al.*, 2007; van Es *et al.*, 2010). *Hes1* knockout mice were shown to display an excessive number of enteroendocrine and goblet cells (Jensen *et al.*, 2000). A later study by Ueo and colleagues in 2012 demonstrated that

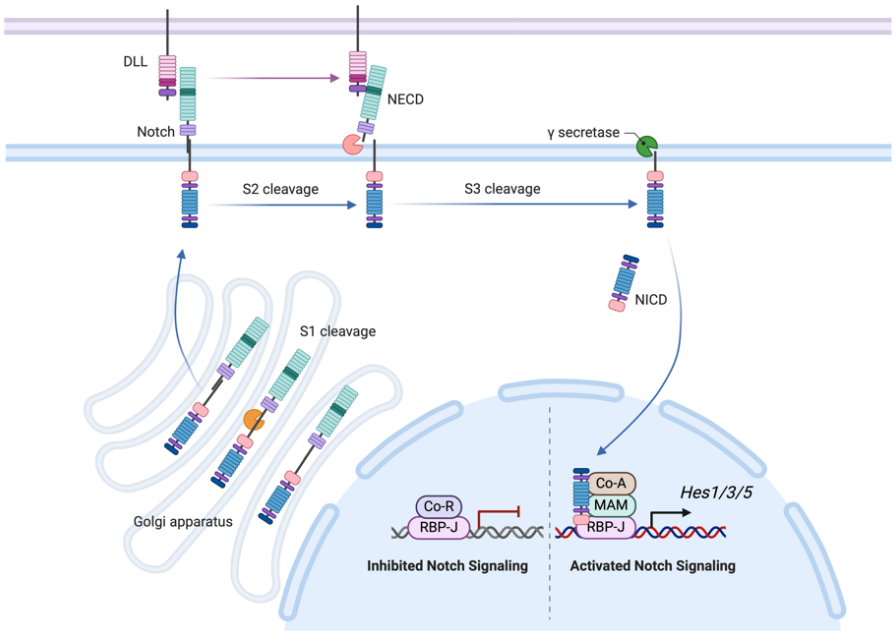

Figure 1.5 Notch signaling activation. In the Golgi apparatus, the NOTCH precursor undergoes an S1 cleavage, forming a heterodimer. The S2 cleavage, which is ligand-dependent, initiates the signal by cleaving the heterodimer to form NEXT. Finally, NEXT is cleaved at the S3 site by γ-secretase, releasing NICD. Once NICD is released, it enters the nucleus and forms a transactivation complex with RBP-J and co-A activators mastermind (Co-A MAM) that activates HES transcription. In the absence of NOTCH, RBP-J is associated with a corepressor (Co-R) and inhibits gene expression. Created with BioRender.com.

this effect was not observed anymore at the age of 2 months, suggesting the compensatory effect of HES3 and HES5 at the adult stage. Confirming this hypothesis, researchers demonstrated the remaining phenotype in *Hes1/3/5* knockout mice at postnatal and adult stages. Thus, Notch signaling activation has a repressive effect on *Atoh1* expression, which results in the differentiation of progenitor cells towards absorptive lineage. *Atoh1* de-repression drives progenitor cells to differentiate along the secretory lineage when Notch is inactivated. It is worth noting that Notch pathway is regulated through a principle of lateral inhibition. This means that when ligands are differentially expressed in adjacent cells, this induces Notch signaling in the cell with low ligand levels while inhibiting the pathway in the cell with high ligand levels (Lim *et al.*, 2015). This regulation mechanism highlights the importance of Notch signaling in determining cell fates, where the “on” and “off” states of Notch result in distinct cell specifications.

1.8 The Role of BMP Signaling in Small Intestinal Homeostasis.

Another essential signaling pathway controlling proper intestinal stem cell differentiation is BMP. It is conserved and regulates the development and homeostasis of the gut from *Drosophila* to vertebrates (Wang and Chen, 2018). Bone morphogenic proteins (BMPs) are secreted cytokines, members of the transforming growth factor β (TGF-β) family. Major BMPs of the intestine are BMP2 and BMP4 (Wang and Chen, 2018) secreted by intercrypt and intervillus mesenchymal cells (Hardwick *et al.*, 2004; Haramis *et al.*, 2004). BMPs bind with the type I and type II receptors. Ligand binding results in the formation of a receptor complex consisting of two type I and two type II components, which mediates signaling via a cytoplasmic Ser/Thr kinase domain (Massagué, 2012). When a Type II constitutively active kinase transphosphorylates the Type I receptor kinase, the Type I receptor kinase gets activated. This activation triggers intracellular signaling by phosphorylating downstream effector molecules such as Mothers Against Decapentaplegic Homologue 1 (SMAD1), SMAD5 or SMAD8, so-called receptor-regulated (R-)SMADs. These effector molecules then bind to the common SMAD (SMAD4 or cSMAD) and translocate to the nucleus, where they regulate gene expression (Sanchez-Duffhues *et al.*, 2020). The mechanism of BMP signaling activation is reviewed in Figure 1.6.

Two studies demonstrated the effect of epithelial-specific knockout of *Bmpr1a* gene, coding for BMP receptor Type I. He *et al*. in 2004 showed polyp formation in mice with *Bmpr1a* deletion. Auclair *et al.* in 2007 showed that *Bmpr1a*-mutant mice displayed hyperproliferation within the crypts, but did not develop tumors. Both studies confirm the importance of BMP signaling in maintaining intestinal homeostasis by promoting differentiation. It is crucial, however, to maintain precise regulation of BMP signaling levels along the crypt-villus axis. Facilitating the differentiation of progenitor cells exiting the stem cell zone, BMP must be inhibited in the crypts since it can induce the premature differentiation of stem cells. This is ensured by BMP inhibitors such as Gremlin 1, Gremlin 2, Chordin-like 1 or Noggin secreted by myofibroblasts and smooth muscle cells beneath crypts (Kosinski *et al.*, 2007). Ectopic expression of Gremlin 1 in intestinal epithelium causes ectopic crypt formation and initiation of intestinal neoplasia similar to *Bmpr1a* deletion (Davis *et al.*, 2015). These results again highlight the significance of maintaining the increasing crypt-villus gradient of BMP. Moreover, BMP gradient regulates hormonal plasticity in certain crypt-localised enteroendocrine cell types as they move towards the villus tip (Beumer *et al.*, 2018). Chapter 1.3 discusses the BMP-controlled hormonal plasticity of EC and L/I/N cell lineages.

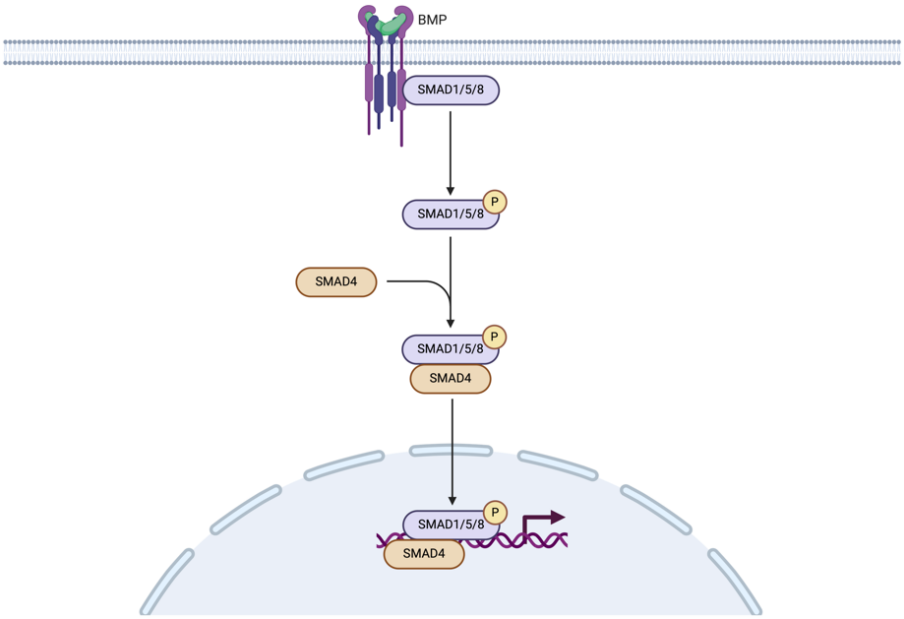

Figure 1.6 BMP signaling activation. BMPs bind to type I and type II receptors, forming a receptor complex that mediates signaling via a kinase domain. Activation of the Type I receptor kinase triggers intracellular signaling by phosphorylating downstream effector molecules like SMAD1, SMAD5 or SMAD8. These effector molecules bind to SMAD4 and regulate gene expression in the nucleus. Created with BioRender.com.

1.9 Organoid System as a Highly Effective Tool for Modeling *in vivo* Conditions.

In 2009, Sato *et al.* achieved the first successful culture of intestinal stem cells for an extended period. To ensure small intestinal stem cell self-renewal *in vitro*, they tested different combinations of growth factors. The minimal essential conditions to achieve this include epidermal growth factor (EGF), which activates KRAS signaling, Noggin, which represses BMP signaling, and R-spondin, which activates Wnt signaling. Small intestinal stem cells were cultured using Matrigel due to the enrichment of laminin in the crypt base (Sasaki *et al.*, 2002; Sato *et al.*, 2009). Intestinal stem cells were grown in a culture system with the entire crypt. This resulted in the formation of "organoids", which mimic the crypt-villus structures found in the gut. The organoids comprise budding structures similar to crypts surrounding a central cyst structure. The intestinal stem cells and Paneth cells are located at the base of these crypt-like structures. Post-mitotic cells move towards the central cyst structure and are shed into the lumen. When single $LGR5^{+}$ stem cells were grown in the same culture system, they also formed organoid structures. However, their outgrowth efficiency was lower, with only around 6% of the plated stem cells showing growth (Sato *et al.*, 2009). The outgrowth efficiency of the entire crypts is higher because Paneth cells are located alongside stem cells. A later study by Sato *et al.* demonstrated that doublets of stem and Paneth cells had an outgrowth efficiency of 60%. Wnt3A at 100 ng ml^{-1} for the first 3 days of culture overcomes the Paneth-cell dependence of single stem cells (Sato *et al.*, 2011a).

Sato *et al*. (2011b) also established the *in vitro* culture of small intestinal adenoma tumoroids. They generated adenomas in $Lgr5^{GFP\text{-}ires\text{-}CreERT2}:Apc^{fl/fl}$ mice by tamoxifen-induced Cre activation and *Apc* gene disruption. The adenomas were then dissected and placed into cell culture. As the loss of APC leads to constitutive activation of Wnt signaling, the researchers excluded R-spondin from the organoid culture medium. Tumoroids are cystic structures that differ from normal small intestinal organoids as they do not bud. Interestingly, Nogging is not required to grow tumoroids in cell culture. However, tumoroids also stop expressing *Lgr5* when Noggin is removed from the medium, similar to normal small intestinal organoids, as observed in a study by Sato *et al*. in 2009. This result highlights the importance of BMP inhibition in maintaining *Lgr5* expression in intestinal organoids and tumoroids, which is necessary

for their clonogenicity. According to a study by Sato *et al.*, LGR5^{+} cells with higher *Lgr5* expression sorted from tumoroids have a higher outgrowth efficiency than the ones with lower *Lgr5* expression (Sato *et al.*, 2011a).

Intestinal stem cells can be maintained in cell culture using a standard organoid medium containing EGF, Noggin, and R-spondin. Understanding the effect of signaling pathways on the regulation of differentiation allows for the manipulation of intestinal cell cultures and the enrichment of desired cell populations. Thus, to enrich secretory populations in cell culture, inhibitors of γ-secretase and, therefore, Notch signaling, such as RO4929097 or DAPT, can be added to the medium. Beumer and colleagues demonstrated enteroendocrine cell plasticity using a conditional organoid medium with removed Noggin and added BMP4 in their study. Measuring hormone expression in organoids grown in standard and BMP-high medium reveals induced/inhibited hormones after BMP treatment (Beumer *et al.*, 2018). Therefore, the organoid system is a powerful tool for modeling *in vivo* conditions and studying their effects on the differentiation of intestinal stem cells.

1.10 Transcriptional Regulation of Secretory Lineage Differentiation.

Intestinal stem cells (ISC) are located at the crypt bottom and, when moving up towards the villus, form a population of undifferentiated Transit-amplifying (TA) cells. At this stage, the precursor cells differentiate along absorptive or secretory lineage. ATOH1, as mentioned earlier, is expressed in common secretory progenitor and is required for differentiation of all secretory populations. It was confirmed by the study, where its mosaic intestine-specific deletion caused the loss of all secretory cells in mutant crypts and the generation of only absorptive enterocytes from them (Schroyer *et al*., 2007). However, the model in which ATOH1 is the only regulator of secretory differentiation was challenged by the study of Gracz *et al.*, 2018. The study demonstrated that the transcription factor SOX4 can promote differentiation towards enteroendocrine and tuft cell lineages independently of ATOH1.

The downstream lineage-specific differentiation involves a set of other transcription factors. Neurogenin3 (NEUROG3), a bHLH transcription factor, defines enteroendocrine lineage downstream ATOH1, and *Neurog3* deficient mice do not develop enteroendocrine cells and their progenitors (Jenny *et al.,* 2002). However, a recent study by Hayashi *et al.* in 2023 found that *Neurog3*-induced tdTomato labelled

not only enteroendocrine cells but also some Paneth, Goblet cells, and enterocytes. On the other hand, NEUROD1, a downstream target of NEUROG3, only traced enteroendocrine cells in the same study. A time-resolved transcriptome analysis conducted by Gehart *et al.* in 2019 revealed *Neurog3* expression in early/intermediate enteroendocrine progenitors, while Neurod1 marked intermediate/late progenitors. Among other pro-endocrine transcription factors stimulated by *Neurog3* and expressed in intermediate to late progenitors are *Nkx2.2*, *Pax4*, *Pax6*, and *Isl1* (López-Díaz *et al.*, 2007; Gehart *et al.* in 2019).

Neurog3 expression was shown to be repressed by the growth factor-independent 1 (GFI1) transcription factor, which is expressed in Paneth and goblet cells, thus defining their fate versus enteroendocrine progenitors (Bjerknes and Cheng, 2010). Indeed, mice with *Gfi1* deletion show an increased number of enteroendocrine cell populations while lacking Paneth cells and having fewer goblet cells (Shroyer *et al.*, 2005). Terminal differentiation of goblet cells also depends on

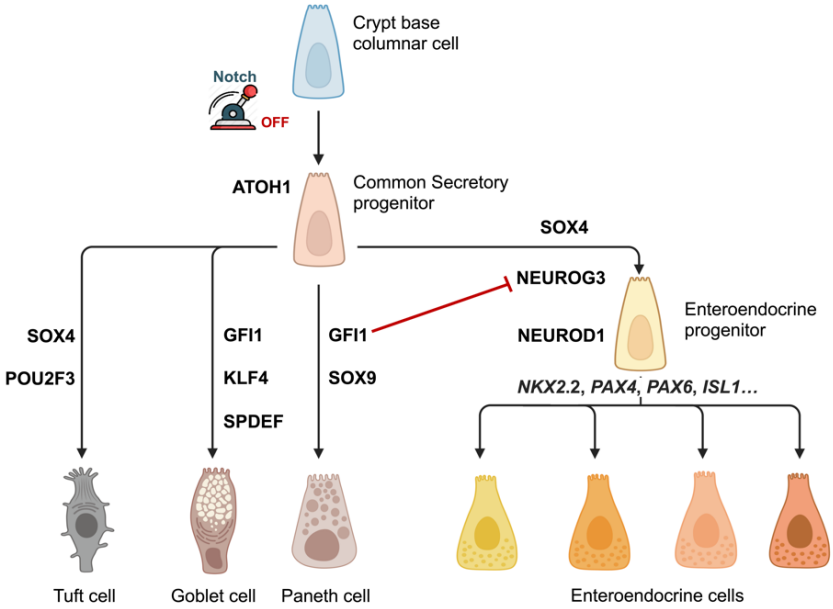

Figure 1.7 Transcriptional regulation of secretory lineage differentiation. ATOH1 is necessary for secretory differentiation, but SOX4 can promote differentiation towards enteroendocrine and tuft cell lineages independently of ATOH1. Neurogenin3 (NEUROG3) defines the enteroendocrine lineage downstream of ATOH1. NEUROG3 activates NEUROD1, which traces enteroendocrine cells. Other pro-endocrine transcription factors, including NKX2.2, PAX4, PAX6, and ISL1, are stimulated by NEUROG3 and expressed in intermediate to late progenitors. GFI1 transcription factor represses NEUROG3 and determines the fate of Paneth and goblet cells. The differentiation of goblet cells requires KLF4 and SPDEF, while Paneth cells depend on SOX9. POU2F3 is necessary for the differentiation of tuft cells. Created with BioRender.com.

Kruppel-like factor 4 (KLF4) and SAM pointed domain containing Ets transcription factor (SPDEF) (Katz *et al.*, 2002). Paneth cell differentiation, in turn, depends on the expression of a transcription factor called SRY-box containing gene 9 (SOX9) (Bastide et al., 2007; Mori-Akiyama et al., 2007). Tuft cells, as mentioned in Chapter 1.3, express POU2F3, which is required for their differentiation. Deletion of *Pou2f3* in mice results in the absence of tuft cells (Gerbe *et al.*, 2016). All transcriptional regulation of secretory lineage differentiation is reviewed in Figure 1.7.

1.11 Functions of ID2 in Intestinal Homeostasis and Tumorigenesis

Inhibitor of DNA binding/differentiation (ID2) is a transcription factor of the large family of the helix-loop-helix (HLH) transcription factors. The lack of a Basic domain prevents ID2 and other ID-family factors from binding DNA. However, they function as negative regulators of basic helix-loop-helix (bHLH) transcriptional factors that regulate gene expression during cell fate determination (Roschger and Cabrele, 2017). ID2 is crucial in mouse embryonic development and is responsible for proper and opportune bone formation, myogenesis, angiogenesis and neuronal system development. *Id2* knockout mice, although viable, show pronounced phenotypic features: they lack ILC2 (Yagi *et al.,* 2014) and Peyer's patches (Yokota *et al*., 1999), show a substantial reduction in the number of the CD4+ and CD8αβ+ T cell subsets of intestinal intraepithelial lymphocytes (Fujimoto *et al.*, 2007) as well as natural killer cells (Yokota *et al.*, 1999), also could exhibit reduced body weight and disrupted circadian rhythms (Duffield *et al.*, 2009).

In addition to the listed systems of organs and tissues, ID2 is also crucially important for gut development. In particular, previous group results showed a broad expression of *Id2* in the embryonic small intestine. They demonstrated that it restricts the number and controls the timing of $Lgr5^{+}$ intestinal stem cell progenitors and prevents their precocious commitment to adult intestinal stem cells (ISC). Additionally, ID2 is necessary to prevent premature Wnt activation in the embryonic intestinal epithelium (Nigmatullina *et al.*, 2017). In 1999, Hollnagel *et al.* conducted a study that demonstrated how BMP4 induces the expression of the *Id2* gene in embryonic stem cells, as well as in various other cell lines. The study concluded that *Id2* is a direct target of BMP induction in embryonic stem cells. Furthermore, Beumer *et al.* conducted a study in 2018 which analyzed BMP-controlled hormone expression and

detected the induction of *Id2* expression in enteroendocrine cells upon BMP treatment. Later, in 2019, Gehart *et al.* proposed ID2 as a common transient regulator of enteroendocrine lineage. An early study by Ghil *et al.* in 2002 showed that ID2 inhibits NEUROD1 binding to its target sequence, suggesting its inhibitory role in enteroendocrine lineage differentiation. Additionally, the study of Hua *et al.* in 2006 confirmed that BMP4 induce *Id2* expression in pancreatic epithelial progenitors. As per the proposed model, BMP4 stimulation promotes ID2 binding to NEUROD1, which prevents it from binding to the E-box elements of endocrine-specific genes. This binding blocks pancreatic epithelial progenitors from differentiating along the NEUROD-specific endocrine lineage but instead induces their expansion. Despite previous studies, the precise role of ID2 in regulating intestinal stem cell differentiation and defining specific fates was not elucidated. Single-cell RNA sequencing data from our group showed that *Id2*-positive cells are present in enteroendocrine cells (EECs), common progenitors for secretory and enterocyte lineages, enterocytes, and goblet cell clusters (Figure 1.8A, Zinina *et al.*, 2022). *Id2* expression strongly correlates with *Chromogranin B* (*ChgB*) and *Secretin* (*Sct*), which are highly expressed in EECs: 39% of *ChgB*$^{+}$ and 31% of *Sct*^{high} cells were *Id2*-positive, compared to only 10% of non-EEC lineage cells. *Id2* expression was also shown to correlate with enterochromaffin cell markers *Chromogranin A* (*ChgA*) and *Tachykinin Precursor 1* (*Tac1*), with 40% of *ChgA*$^{+}$ and 30% of *Tac1*$^{+}$ cells expressing *Id2*. Additionally, 44% of *Ghrelin*$^{+}$ (*Ghrl*$^{+}$, X cells), 39% of *Neurotensin*$^{+}$ (*Nts*$^{+}$, N cells), and 31% of *Cholecystokinin*$^{+}$ (*Cck*$^{+}$, I cells) were *Id2*-positive, whereas less than 10% of *Gastric Inhibitory Peptide*$^{+}$ (*Gip*$^{+}$, K cells) or *Somatostatin*$^{+}$ (*Sst*$^{+}$, D cells) showed *Id2* expression (Figure 1.8B).

Another topic of discussion is the role of ID2 in oncogenesis. Several research works have shown its oncogenic activity in different types of cancer (Vandeputte *et al.*, 2002; Fukuma *et al.*, 2003). In 2004, Russell *et al.* found an unexpected role of ID2 in intestinal oncogenesis. Their study revealed that ID2 has a tumor inhibitory function in the intestinal epithelium. They demonstrated that mice lacking ID2 develop tubulovillus adenoma with high proliferative activity and accumulation of β-catenin. The study further showed that ID2 is essential for the differentiation and cell cycle exit of the mouse intestinal epithelium. In 2015, Biyajima and colleagues conducted a study which produced important results. Firstly, the researchers showed that *Id2* expression was five times higher in adenomas of *Apc*$^{\Delta 716}$ mice (mice that had a truncation mutation at codon 716, which failed to produce a functional APC protein after LOH)

than in normal crypts. Secondly, using luciferase reporter assays, they demonstrated that *Id2* expression is stimulated by Wnt signaling in $Apc^{\Delta 716}$ adenomas. Commenting on the previous results of Russel *et al.*, Biyajima and colleagues distinguished tumors arising from *Id2* deficiency and *Apc* deficiency, stating that the former did not show nuclear β-catenin accumulation. Based on this, they estimated that 96% of tumors in $Apc^{\Delta 716}$:$Id2^{-/-}$ mice are *Apc*-deficient and display nuclear accumulation of β-catenin. Next, they demonstrated a reduced ileal tumor formation in $Apc^{\Delta 716}$:$Id2^{-/-}$ mice compared to $Apc^{\Delta 716}$. Finally, they proposed that ID2 increases c-Myc protein levels by decreasing the mRNA level of its antagonist Mxd1 in ileal crypt epithelium of $Apc^{\Delta 716}$ mice, exhibiting an oncogenic function. It is important to note that both studies conducted by Russel *et al.* in 2004 and Biyajima *et al.* in 2015 used mice with a constitutive *Id2* knockout, which makes it difficult to determine if the effect observed was due to the epithelial function of ID2.

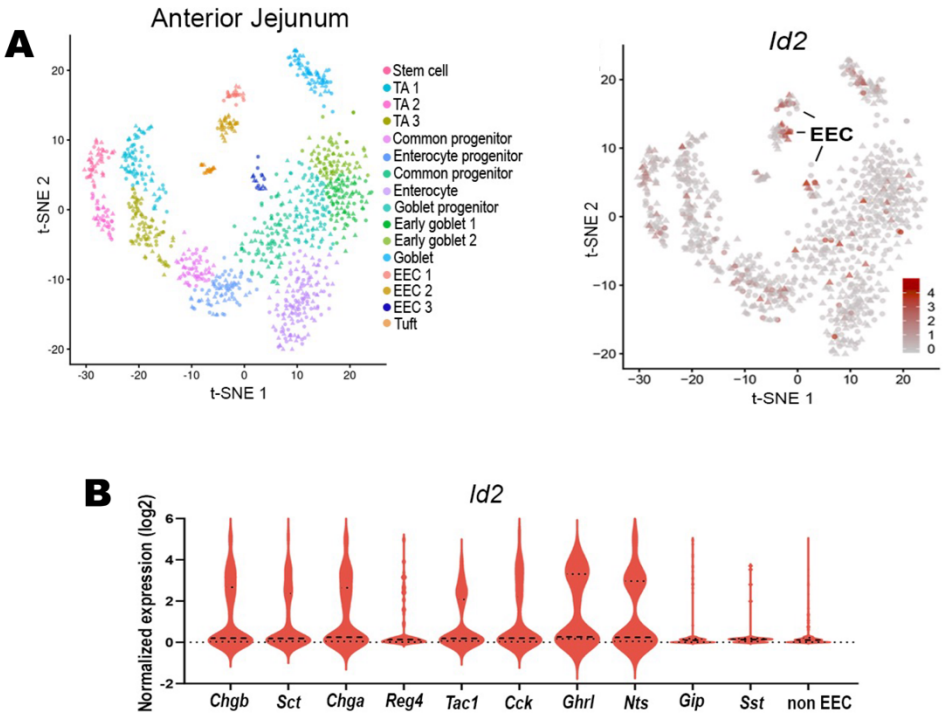

Figure 1.8 Single-cell transcriptome analysis of adult intestinal epithelium. A: T-stochastic neighbour embedding (t-SNE) plot of epithelial cells from adult anterior jejunum showing expression of *Id2* in enteroendocrine cells (EEC). B: Violin plots for *Id2* expression across various enteroendocrine cell types and the whole epithelium (non-EEC). The figure is adapted from Zinina *et al.*, 2022.

1.12 Aim of the Thesis

This thesis investigated the role of ID2 in the differentiation of intestinal stem cells and its impact on cell fate specification. The functions of ID2 in this context had not been fully elucidated. To address this, a mouse model with conditional depletion of *Id2* in the small intestinal epithelium was employed.

Additionally, the study examined the oncogenic potential of ID2 to determine its necessity in the intestinal epithelium for promoting tumorigenesis. Existing research on this topic was limited, and prior studies utilized suboptimal mouse models. Therefore, Apc^{min} mice with epithelium-specific *Id2* depletion were used to provide deeper insights into this aspect.

2. MATERIALS AND METHODS

2.1 Reagents.

Reagent	Company
10X Standard Taq Reaction Buffer	NEB
4-hydroxytamoxifen	Sigma-Aldrich
Transcription Optimized 5X Buffer	Promega
Accutase	Sigma-Aldrich
Acetic Anhydride	Carl Roth
Advanced DMEM/F12 media	Invitrogen
Ampicilin, sodium salt	Sigma-Aldrich
B27 supplement (50x)	Thermo Fisher Scientific
BCIP	Roche
BMP2	Peprotech
Boehringer blocking Reagent	Roche
Chir99021	StemCell Technologies
Citric acid	Sigma-Aldrich
Collagenase	Sigma-Aldrich
Denhardt's Solution (50X)	Thermo Fisher Scientific
Dextran sulfate	Sigma-Aldrich
DIG RNA Labeling Mix	Roche
dNTP Mix (10 mM each)	Thermo Fisher Scientific
DTT, Molecular Grade	Promega
Dulbecco's phosphate-buffered saline (DPBS) 10X, no calcium, no magnesium	Gibco
EDTA	Carl Roth
EGF (10 µg)	R&D systems
Eosin solution	Sigma-Aldrich
Ethanol >99.5%, purest	Carl Roth
Ethanol >99.8%, denatured	Carl Roth
Formamide	Carl Roth
Gill’s hematoxylin solution 2	Sigma-Aldrich

H_2O_2 30%	Carl Roth
Heparin, sodium salt	Sigma-Aldrich
HEPES	Sigma-Aldrich
Hygromycin B (50 mg/mL)	Gibco
KCl, Potassium chloride	Carl Roth
L-glutamine (200 mM)	Sigma-Aldrich
LB Agar	Sigma-Aldrich
LB-medium	Sigma-Aldrich
LDN193189	StemCell Technologies
Matrigel	Corning
MEM non-essential amino acids solution (100x)	Sigma-Aldrich
$MgCl_2$, Magnesium chloride	Carl Roth
Tri-Sodium citrate dihydrate	Carl Roth
NaCl, Sodium chloride	Carl Roth
NBT	Roche
Nicotinamide	Carl Roth
Noggin	R&D systems
Nonidet P 40	Carl Roth
Peanut oil	Sigma-Aldrich
Paraformaldehyde, granulated	Carl Roth
Polymerase SP6	New England Biolabs
Polymerase T7	New England Biolabs
Proteinase K	Sigma-Aldrich
Puromicin solution, 10 mg/mL	Gibco
R-spondin-1 (25 µg)	R&D systems
RNaseOUT™ Recombinant Ribonuclease Inhibitor	Invitrogen
RO4929097	Peprotech
ROTI Histokitt Mounting Medium	Carl Roth
ROTI Phenol/Chloroform/Isoamyl alcohol	Carl Roth

SDS	Carl Roth
Tamoxifen	Sigma-Aldrich
Tris Base	Carl Roth
Triton X-100	Thermo Fisher Scientific
Yeast tRNA	Thermo Fisher Scientific
Trypsin/EDTA solution, 1x	Sigma-Aldrich
Tween-20	Sigma-Aldrich
Vectashield Mounting Medium	Vector Laboratories
Xylol	Carl Roth
Y-27632 inhibitor (1M)	Tocris

2.2 Buffers.

Buffer	**Composition**
20xSSC pH 4.5-5.0 (for 1L)	175,3 g NaCl, 88,2 g NaCitrate, pH adjusted with citric acid
Hybridization buffer for RNA *in situ* hybridization	5xSSC, 50% Formamide, 10% Dextran sulfate, 1X Denhardt, 100ug/mL Heparin, 100ug/mL tRNA (boiled at 95°C for 5min), 5mM EDTA pH adjusted with citric acid
TBS	2mM KCl, 150 mM NaCl, 100mM Tris-Cl pH 7.5
TBSX	2mM KCl, 150 mM NaCl, 100mM Tris-Cl pH 7.5, 0,1% Triton X-100

Blocking solution for RNA *in situ* hybridization	1% Boehringer blocking Reagent, 10% goat serum in TBSX
NTMT	50mM $MgCl_2$, 100 mM NaCl, 100mM Tris-Cl pH 9.0-9.5, 0.1% Tween-20
Mouse tail lysis buffer	Tris-Cl (pH 8.5) 100 mM, EDTA 5 mM, NaCl 200 mM, SDS 0.2% (w/v)

2.3 Antibodies and Viability Dyes.

Name	**Company**	**Dilution**	**Application**
rabbit anti-CHGA	ImmunoStar	1:1000	FACS
rabbit anti-5-HT	Immunostar	1:2000	FACS
rabbit anti-DCLK	Cell Signaling Technology	1:500	FACS
UEA-FITC	Sigma-Aldrich	1:1000	FACS
rabbit anti-CCK	Immunostar	1:2000	FACS
rabbit anti-NTS	Immunostar	1:5000	FACS
rabbit anti-GCG-AlexaFluor488	Thermo Fisher Scientific	1:1000	FACS
rabbit anti-PYY	Cell Signaling Technology	1:500	FACS
EpCAM-APC	eBioscience	1:1000	FACS, IF
DAPI	Sigma-Aldrich	1:1000	FACS, IF
Viability Dye eFlour780	Thermo Fisher Scientific	1:1000	FACS
donkey anti-rabbit AlexaFluor488 plus	Thermo Fisher Scientific	1:2000 1:1000	FACS, IF
rabbit anti-phospho-histone H3 antibody	Cell Signaling	1:2000	IF
anti-DIG	Roche	1:3000	RNA *in situ* hybridization

2.4 Cell Culture Media.

Medium	Composition
Standard organoid medium	Advanced DMEM/F12, B-27® Supplement 1x, Penicillin-streptomycin cocktail 1x, MEM Non-Essential Amino Acid Solution 1x, L-glutamine 2mM, HEPES 15mM
ENR	Standard organoid medium, EGF 100 ng/mL Noggin 100 ng/mL R-spondin 250 ng/mL
ERo	Standard organoid medium, EGF 100 ng/mL RO4929097 1 µM
BERo	Standard organoid medium, BMP2 20 ng/mL EGF 100 ng/mL RO4929097 1 µM
ELR	Standard organoid medium, EGF 100 ng/mL LDN193189 0.2 µM R-spondin 250 ng/mL
EL	Standard organoid medium, EGF 100 ng/mL LDN193189 0.2 µM
ELRCNic	Standard organoid medium, EGF 100 ng/mL LDN193189 0.2 µM R-spondin 250 ng/mL Chir99021 10 µM Nicotinamide 10 mM

2.5 Kits.

Kit name	Company
Agilent High Sensitivity DNA Assay Kit	Agilent Technologies
Agilent RNA 6000 Nano Kit	Agilent Technologies
Click-iT EdU Cell Proliferation Kit for Imaging, AlexaFluor647 dye	Thermo Fisher Scientific
GeneJET Plasmid-Midiprep-Kit	Thermo Fisher Scientific
High-Capacity Reverse Transcription Kit	Applied Biosystems
Nextera XT Library Prep Kit	Illumina
NucleoSpin Gel and PCR Clean-up Kit	Macherey-Nagel
pGEM-T Easy Vector Systems Kit	Promega
SMARTer Ultra Low RNA Kit for Illumina Sequencing	Takara Bio
Microspin G-50 Columns	Sigma-Aldrich

2.6 Primers.

PCR primers were designed using Primer Blast (http://www.ncbi.nlm.nih.gov/tools/primer-blast/).

Primer name	Sequence
Mouse Genotyping PCR	
Apc_com	TTCCACTTTGGCATAAGGC
Apc_mut	TTCTGAGAAAGACAGAAGTTA
Shh_fwr	GGTGCGCTCCTGGACGTAGC
Shh_rev	GGGACAGCTCACAAGTCCTC
Id2_flox_fwd	GGATCTCTAACAGCCCGCTCAC
Id2_flox_rev	GATTTCTCTGGCTAGCTGAAGACGG
CreERT2_fwr	TACGGCGCTAAGGATGACTCT
CreERT2_rev	ATCATGTGAACCAGCTCCCTG
GFP_fwr	AGGACGACGGCAACTACAAG
GFP_rev	TGTTCTGCTGGTAGTGGTCG

Molecular Cloning and Plasmid Analysis	
T7	TAATACGACTCACTATAGGG
SP6	ATTTAGGTGACACTATAG
Apc_seq_rev	CTGCTTACTCCGGTGAGAGG
Apc_pcr_fwd	ACAGCTTGACAATAGTCAGTAATGC
Apc_pcr_rev	TGTCGATTGGCGTCAAAAGC
Id2_seq_rev	ATAAAAGACGCCCCGCCC
Id2_pcr_fwd	TCTGTCCAGGTCTCTGGTGA
Id2_pcr_rev	TGCACATAAAAGACGCCCCG
Quantitative RT-PCR	
Gcg_fwr	TCACCAGCGACTACAGCAAAT
Gcg_rev	GCAATGTTGTTCCGGTTCCT
Nts_fwr	AACTTCCCCTTGTTCTGGATGG
Nts_rev	CCTGCTGCGGCAGATTTTCT
Sct_fwr	GACCCCAAGACACTCAGACG
Sct_rev	GCTTCCCCACCAGACCCT
Gip_fwr	ACAGGAGAGCTCTTTGCCCA
Gip_rev	AGGCCAGTAGCTCTTGAATCAG
Id2_qpcr_ex1_fwd	GCATGAAAGCCTTCAGTCCG
Id2_qpcr_ex1_rev	GTCGTCCACCGGGGTTTT
Id2_qpcr_ex3_fwd	AAGGTGGAGCGTGAATACCAG
Id2_qpcr_ex3_rev	GCATTCAGTAGGCTCGTGTCA

2.7 Vectors.

gRNA sequences.

Target gene	**Sequence**
Apc	GTCTGCCATCCCTTCACGTT
Id2	TCAGTCCGGTGAGGTCCGTT
Scramble	GCACTACCAGAGCTAACTCA

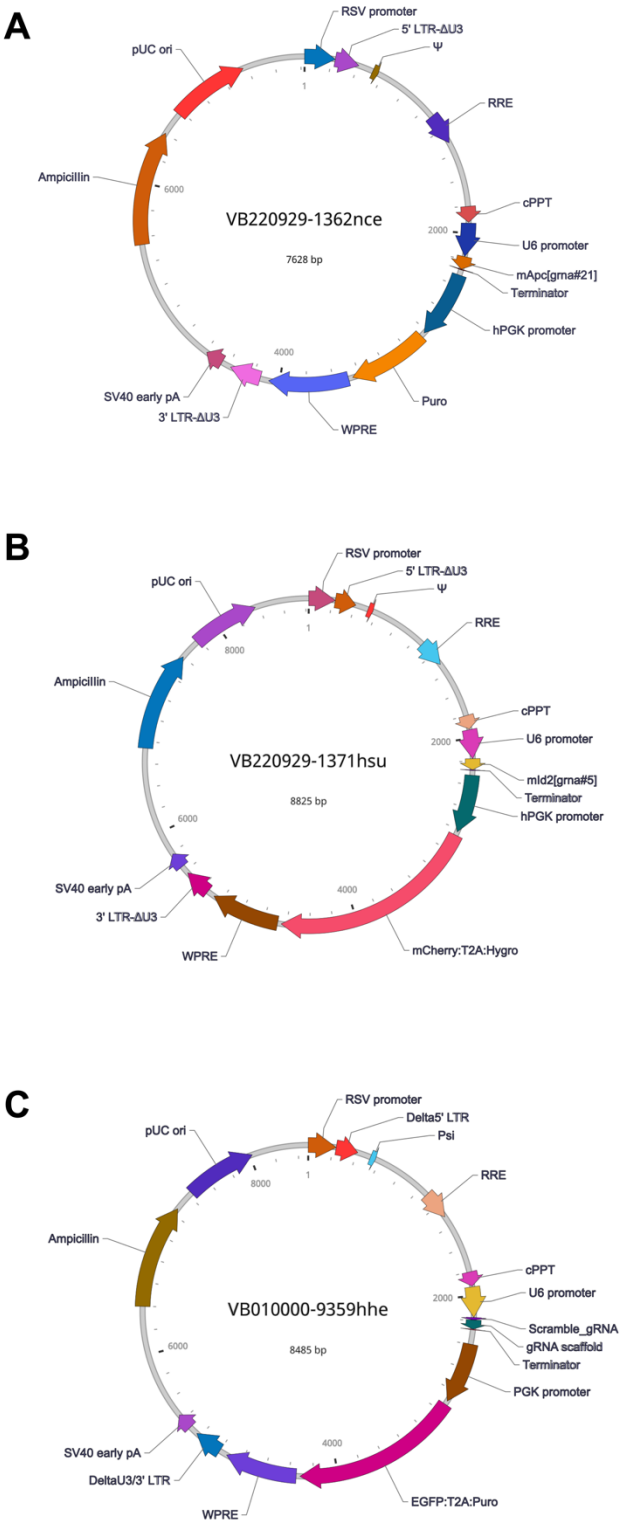

Figure 2.1 Viral vectors for the *in vitro* delivery of gRNA. A. Vector expressing *Apc* gRNA. B. Vector expressing *Id2* gRNA. C. Vector expressing *Scramble* gRNA.

2.8 PCR genotyping.

Mouse biopsies were placed in a Mouse tail lysis buffer and incubated with 100 µg/mL Proteinase K (Sigma-Aldrich) at 56°C overnight while shaking. After the incubation, Proteinase K was heat-inactivated at 80°C for 10 minutes. The DNA was then ethanol-precipitated, dissolved in water, and used for PCR. The PCR reaction was mixed as follows:

1) 10X Standard Taq Reaction Buffer (NEB) 1.5 µL
2) dNTP mix 10 mM (NEB) 0.3 µL
3) Forward primer solution 10µM 1 µL
4) Reverse primer solution 10µM 1 µL
5) DNA solution 1 µL
6) Taq polymerase (self-made) 1 µL
7) mQ 9.2 µL

The total volume for each reaction is 15 µL. PCR programs are detailed in Table 7.

PCR programs for genotyping.

PCR-program name (target sequence)	PCR-program steps
Apc^{min}	1) 94°C 4 minutes 2) 94°C 30 seconds 3) 55°C 30 seconds Steps 2-4 X35 4) 72°C 30 seconds 5) 10°C ∞
Gfp	1) 94°C 5 minutes 2) 94°C 15 seconds 3) 58°C 15 seconds Steps 2-4 X35 4) 72°C 30 seconds 5) 10°C ∞
Cre*, *CreERT2	1) 94°C 4 minutes 2) 94°C 15 seconds 3) 63°C 15 seconds Steps 2-4 X35 4) 72°C 30 seconds

	5) 10°C ∞
Id2^{flox}	1) 94°C 4 minutes 2) 94°C 15 seconds 3) 60°C 15 seconds Steps 2-4 X35 4) 72°C 30 seconds 5) 10°C ∞
Shh$^{EGFP-Cre}$	6) 94°C 4 minutes 7) 94°C 30 seconds 8) 59°C 30 seconds Steps 2-4 X30 9) 72°C 30 seconds 10°C ∞

2.9 Mouse Strains.

Id2$^{Cre-ERT2}$, *Shh$^{EGFP-Cre}$*, *Rosa26^{tdTomato}*, *Rosa26^{CreERT2}*, *Apc^{min}* and *Rosa26^{Cas9EGFP}* mice were obtained from Jackson laboratory. *Id2$^{flox/flox}$* mice were previously described (Niola *et al.*, 2012) and kindly provided by Prof. Dr. Diefenbach. C57Bl/6J mice were purchased from Charles Rivers. Mouse colonies were maintained in a certified SPF animal facility per European guidelines. All mice were housed on a 12-hour light/dark cycle with constant food and tap water access.

2.10 Quantification of Enteroendocrine and Other Epithelial Cells Using Flow Cytometry.

The procedure of crypt isolation was carried out according to the method outlined in Sato *et al.*, 2009. The small intestines were dissected from mouse embryos at E13.5 under Leica M80 Stereo Zoom Microscope and were cut into 2 mm pieces. Next, they were incubated with collagenase (Sigma-Aldrich) at a concentration of 0.15 mg/mL in PBS at 37°C with shaking at 800 rpm for 10 minutes. The cells were then collected by centrifugation at 200 g for 4 minutes, washed twice in PBS, and resuspended in PBS supplemented with 2% donkey serum. The cells were finally stained with an APC-conjugated anti-EpCAM antibody (eBioscience) at a concentration of 1:1000 for 30 minutes at room temperature. To sort living cells, DAPI-

dye exclusion was used as a gating method. DAPI dye was added right before the sorting. Fluorescence-activated cell sorting was performed using a BD FACS Aria III SORP cell sorter with a 100 µm nozzle.

The small intestines of adult mice were divided into three equal parts - Anterior, Middle, and Posterior. Each part was cut into 4 mm² pieces and placed in a 50 mL conical tube. The pieces were washed thrice with 25 mL of PBS/5 mM EDTA for 20 minutes on a rolling shaker at room temperature. The villi were removed by gentle shaking ten times and trituration using a 25 mL pipette after each 20-minute rotation in PBS/5 mM EDTA. The first two fractions of villi were discarded, and the third fraction was saved. The crypts were then separated from the intestine by vigorous shaking two times. The last third fraction of villi and crypts were mixed and collected by centrifugation at 200 g for 5 minutes and washed twice with PBS. To identify living cells, the cells were stained with Viability Dye eFlour780 (1:1000, Thermo Fisher) for 30 minutes. The cells were then fixed with 4% paraformaldehyde for 15 minutes at room temperature, washed twice with PBS, and permeabilized with a saponin-based buffer (BioLegend). Fixed cells were stained with antibodies targeting CHGA (1:1000, ImmunoStar), 5-HT (1:2000, Immunostar), DCLK (1:500, Cell Signaling Technology), UEA-FITC (1:1000, Sigma-Aldrich), CCK (1:2000, Immunostar), NTS (1:5000, Immunostar), PYY (1:500, Cell Signaling Technology), GCG-Alexa488 (1:1000, Thermo Fisher) for 2 hours at room temperature. The cells were stained with donkey anti-rabbit Alexa488 plus antibody (1:2000, Thermo Fisher) and APC-conjugated anti-EpCAM 1:1000 (eBioscience) antibody for 1 hour at room temperature. Single cells were identified based on DAPI dye intensity. Fluorescence-activated cell sorting was performed using BD FACS Aria III SORP cell sorter (100 µm nozzle) and analyzed with FlowJo software.

2.11 Intestinal Organoid and Tumoroid Cultures.

The procedure of crypt isolation and organoid culture was carried out according to the method outlined in Sato *et al.*, 2009. Intestinal organoids were generated from the intestinal crypts of 3-month-old mice. The small intestines were separated into three equal parts (anterior, middle, and posterior), and then each part was cut into pieces of 4 mm^2. These pieces were placed in 50 mL conical tubes and washed thrice with 25 mL of PBS/5 mM EDTA. The washing was done for 20 minutes at room temperature on a roller shaker. The villi were removed by gentle shaking ten

times and trituration using a 25 mL pipette after each 20-minute rotation in PBS/5 mM EDTA. Crypts were separated from the intestine by vigorously shaking the tubes twice. The collected crypt material was washed twice with PBS, resuspended in organoid medium, and mixed 1:1 with Matrigel (Corning). The mixture was then plated in 48-well plates supplemented with advanced DMEM/F12 media containing B27 supplement (Gibco), non-essential amino acids, 2 mM L-glutamine, 15 mM HEPES, and antibiotics. Growth factors, including 250 ng/mL human R-spondin1 (Peprotech), 100 ng/mL mouse Noggin (Peprotech), 100 ng/mL human EGF (R&D systems), and 10 µM Y-27632 inhibitor (Tocris), were added to both the cell culture medium and Matrigel. After the formation of organoids, they were cultured in the organoid medium containing 250 ng/mL of human R-spondin1 (Peprotech), 100 ng/mL of mouse Noggin (Peprotech), and 100 ng/mL of human EGF (R&D systems). The organoids were split and reseeded with fresh Matrigel once a week or more frequently if they became too dense. To split the organoids, they were pipetted at least 100 times using a 200 µL tip. The medium was changed every other day.

Intestinal tumoroids were generated from the posterior small intestinal tumors of 20-week-old *Apc*^{min} mice. Each tumor was dissected, cut into smaller pieces and incubated in Accutase (Sigma-Aldrich) for minutes at 37°C. After that, the dissected tumors were washed in PBS, resuspended in organoid medium and mixed 1:1 with Matrigel (Corning). The mixture was then plated in 48-well plates supplemented with advanced DMEM/F12 media containing B27 supplement (Gibco), non-essential amino acids, 2 mM L-glutamine, 15 mM HEPES, and antibiotics. Growth factors, including 0.2 µM mouse LDN (StemCell Technologies) and 100 ng/mL human EGF (R&D systems), were added to both the cell culture medium (EL medium) and Matrigel. After formation, the tumoroids were cultured for at least two weeks to ensure pure cultures of sparoid tumoroids before all assays. The medium was changed every other day. Once a week, the tumoroids were split by pipetting at least 100 times with a 200 µL tip and reseeded with fresh Matrigel.

To promote the differentiation of intestinal epithelium towards secretory lineage, organoids were cultured for 48 hours in an ENR medium. This was followed by cultivation for 96 hours in ERo medium, which contained 100 ng/mL human EGF and 1 µM RO4929097 (Peprotech). To induce differentiation of enteroendocrine cells, the organoids were cultivated for 48 hours in ENR medium, followed by cultivation for 96 hours in BERo medium (20 ng/mL BMP2 (Peprotech), 100 ng/mL human EGF,

1 μM RO4929097). To promote differentiation of intestinal tumoroids towards secretory lineage, they were cultured in EL medium for 24 hours followed by 48 hours in ERo medium. Images were acquired at different positions along the Z-axis using a Leica DM IL microscope and then merged using Adobe Photoshop software.

2.12 Tamoxifen-induction of Cre Recombinase Activity.

Tamoxifen (Sigma-Aldrich) was dissolved in peanut oil (Sigma-Aldrich) to produce a 20 mg/mL stock solution. Mice were given tamoxifen through oral gavage at a dosage of 0.12 mg/g, as it has been previously demonstrated to have higher efficiency than intraperitoneal injection (Park *et al.*, 2008).

Id2^{CreERT2}*:Rosa26*^{tdTomato} mice were given one dose of tamoxifen, whereas *Apc*$^{min/+}$*:Rosa26*^{CreERT2}*:Id2*$^{lox/lox}$ mice and their controls were treated twice with a 24-hour interval between treatments.

In cultured tumoroids, Cre recombinase was induced by treating with 1 μM of 4-hydroxytamoxifen, an active metabolite of tamoxifen, added to EL medium. When establishing the efficient working concentration of 4-hydroxytamoxifen, the recombination efficiency was monitored by CNV analysis of *Id2* exon1 and exon3.

2.13 Immunohistochemistry.

Embryonic or adult small intestines were dissected, washed in PBS and fixed for 20 minutes in 1% paraformaldehyde in PBS at room temperature, incubated overnight in 30% sucrose, embedded in OCT and kept at −80°C. Immunohistochemical analyses were performed on 10 μm cryosections. Sections were blocked with 5% goat serum in 0.1% NP-40/PBS at room temperature for 1 hour and incubated with primary APC-conjugated anti-EpCAM antibody (eBioscience) overnight at 4°C. After incubation, the sample was washed three times with PBS for five minutes. Then, the slides were stained with goat-anti-rabbit Alexa Fluor™ 647 antibody (1:1000, Thermo Fisher) for one hour at room temperature. Three washes in PBS, five minutes each, were performed to wash unbound secondary antibodies. Counterstaining of nuclei was performed with DAPI (Sigma-Aldrich). Sections were embedded in Vectashield (Vector Labs). Images were acquired with Leica SP8 2017 with HyD confocal microscope. EpCAM-staining intensity was measured in Fiji image processing package.

EdU staining on cryosections was conducted using the Click-iT™ EdU Cell Proliferation Kit for Imaging, AlexaFluor647 dye (Thermo Fisher Scientific), following the manufacturer's instructions. Counterstaining of nuclei was performed with DAPI (Sigma-Aldrich). The sections were embedded in Vectashield (Vector Labs). The images were captured using the Leica SP8 2017 with HyD confocal microscope.

To stain intestinal tumoroids for phospho-histone H3, they were first collected and fixed in 4% PFA in PBS for 20 minutes at room temperature. After that, the tumoroids were washed twice with PBS containing 0.2% Triton X-100 and 0.05% Tween-20 and then permeabilized in PBS containing 0.5% Triton X-100 for 20 minutes. Next, the tumoroids were blocked in PBS containing 0.2% Triton X-100, 0.05% Tween-20, and 5% donkey serum for one hour. They were stained overnight with anti-phospho-histone H3 antibody (Cell Signaling) in a 1:2000 dilution. The next day, the tumoroids were washed three times with PBS for five minutes each. Afterwards, the tumoroids were stained with a secondary donkey-anti-rabbit AlexaFluor488 antibody (1:1000, Thermo Fisher) for one hour at room temperature, followed by three washes in PBS for five minutes each to remove any unbound secondary antibodies. Nuclei counterstaining was performed with DAPI (Sigma-Aldrich), and tumoroids were embedded in Vectashield (Vector Labs). Images were acquired with Leica SP8 2017 HyD confocal microscope and analyzed in LAS X Life Science Microscope Software Platform.

2.14 RNA Extraction and Quantitative RT-PCR.

The intestinal organoids' total RNA was isolated using TRI reagent (Sigma-Aldrich). About 1 million cells were suspended in 500 µL of TRI reagent and incubated for 5 minutes at room temperature. Then, 100 µL of chloroform was added and vortexed for 15 seconds. After 10 minutes of incubation at room temperature, the samples were centrifuged at 13 000 g for 15 minutes at 4°C. The aqueous phase that retains RNA was transferred to a new tube. Next, 250 µL of isopropyl alcohol was added, and the samples were incubated for 10 minutes at room temperature and centrifuged again at 13 000 g for 10 minutes at 4°C. The RNA was washed once in 80% ethanol. The air-dried pellet was resuspended in 20 µL of RNase-free water (Qiagen).

The High-Capacity Reverse Transcription Kit (Applied Biosystems) was used according to the manufacturer's instructions to generate double-stranded cDNA.

Expression changes were normalized to *Tbp*. Quantitative PCR was performed with the StepOne thermocycler (Applied Biosystems) using a SYBR green-containing master mix kit (Roche). A mean quantity was calculated from triplicate reactions for each sample.

2.15 Copy Number Variation (CNV) Analysis.

Genomic DNA was extracted using ROTI Phenol/Chloroform/Isoamyl alcohol (Carl Roth) after pretreating the mouse tissue/tumoroids suspension with Proteinase K (Sigma-Aldrich) overnight at 56°C with shaking. 1 volume of ROTI Phenol/Chloroform/Isoamyl alcohol was mixed thoroughly with the suspension, followed by centrifugation at 13 000 g for 1 minute. The aqueous phase was then collected, mixed with 1 volume of chloroform, and centrifuged again at 13 000 g for 1 minute. The DNA-containing aqueous phase was collected and subjected to ethanol precipitation.

Quantitative PCR was performed with primers for *Id2* exon1 (id2_qpcr_ex1_fwd and id2_qpcr_ex1_rev) and exon3 (id2_qpcr_ex3_fwd and id2_qpcr_ex3_rev) using the StepOne thermocycler (Applied Biosystems) and SYBR green-containing master mix kit (Roche). The mean quantity was calculated from three separate PCR reactions for each sample.

2.16 Preparation of Samples for Bulk RNA-sequencing.

500 epithelial cells from the E13.5 embryo's small intestine were sorted into a Dilution Buffer containing RNase Inhibitor from the SMARTer Ultra Low RNA Kit for Illumina Sequencing (Takara Bio). The first-strand cDNA synthesis was done following the instructions provided by the manufacturer. Ds cDNA amplification was performed using a 17-cycle PCR program. Subsequently, cDNA was purified as per the manufacturer's protocol. Samples were validated using the Agilent 2100 BioAnalyzer and the High Sensitivity DNA Chip from Agilent's High Sensitivity DNA Kit. For library preparation, 1 ng of cDNA was used with the Nextera XT Library Prep kit (Illumina), following the manufacturer's instructions. Quality control of the libraries was performed using the Agilent 2100 BioAnalyzer and the High Sensitivity DNA Chip from Agilent's High Sensitivity DNA Kit. The Novogene company sequenced the libraries.

The RNA from tumoroids was extracted using the RNeasy Mini Kit from Qiagen, following the manufacturer's protocol. The number of tumoroids growing in a single well of a 48-well plate was collected for each sample. The quality control of RNA was checked using the Agilent 2100 BioAnalyzer with Agilent RNA 6000 Nano Kit. Novogene company performed the library preparation and sequencing.

2.17 Bulk RNA-sequencing Data Analysis.

Raw fastq files of samples of *Id2*-deficient and control embryos were processed using the Nextflow pipeline nf-core/rnaseq pipeline (Ewels et al., 2020) to generate raw unnormalized gene counts. Differentially expressed genes were determined using the DESeq2 software package (Love *et al.*, 2014).

For all other bulk transcriptome analyses, raw fastq files were processed to QIAGEN CLC Genomics Workbench 24 to generate raw unnormalized gene counts. Differentially expressed genes were determined in Partek Flow using DESeq2(R) method.

All gene counts were normalized using Median ratio method in Partek Flow before being processed to Gene Set Enrichment Analysis (GSEA) in GSEA 4.3.2 software (Mootha *et al.*, 2003; Subramanian *et al.*, 2005).

Heatmaps and volcano plots were generated in Flaski 3.16.12 app (Iqbal *et al.*, 2021).

2.18 Hematoxylin and Eosin (H&E) Co-staining.

Sections were deparaffinized, hydrated, and stained in Gill's hematoxylin solution 2 (Sigma-Aldrich) for 3 minutes. After that, the slides were washed in running tap water for 5 minutes, rinsed in distilled water, and dipped in 95% ethanol. Next, the eosin co-staining was performed by immersing slides in the eosin solution (Sigma-Aldrich) for 1 minute. Stained slides were washed in 95% ethanol, dehydrated and mounted with ROTI Histokitt (Carl Roth). Images were acquired on the Olympus IX2-UCB microscope.

2.19 Synthesis of RNA Probes for *in situ* Hybridization.

The DNA fragments of 600-800 bp were amplified from genomic DNA using standard PCR conditions. The PCR product was purified using the NucleoSpin Gel

and PCR Clean-up Kit (Macherey-Nagel) and then cloned into the pGEM-T vector using the pGEM-T Easy Vector Systems Kit (Promega). The ligation mix was left to incubate for 16 hours at room temperature to maximize efficiency before being transformed into JM109 competent bacteria. Bacterial clones containing the vector with an insertion were selected using blue-white screening and processed for plasmid extraction using the GeneJET Plasmid-Midiprep Kit (Thermo Fisher Scientific). The plasmids were sent for Sanger sequencing to determine the insert orientation. The vector was linearized by restriction, and *in vitro* transcription was performed from the SP6 or T7 promoter to obtain antisense RNA. The synthesis was carried out using the SP6 or T7 bacteriophage polymerase (New England Biolabs) and DIG RNA Labeling Mix (Roche), which incorporated dig-UTP into the synthesized RNA probe. The probe was then purified from non-incorporated dig-UTP using Microspin G-50 Columns (Sigma-Aldrich) and stored at -20°C or -80°C for an extended period of time.

2.20 RNA *in situ* Hybridization.

Small intestines were dissected, divided into three equal parts — anterior, mid and posterior — and fixed in 4% PFA overnight. The following day, tissues were dehydrated by incubation in a series of ethanol solutions with 30%, 50%, 70% and 99% ethanol and washed in xylol twice. Afterwards, tissues were paraffinized and sectioned on Leica RM2235 Rotary Microtome to 10 µm sections. Before proceeding to RNA in situ hybridization, slides with sections were baked, deparaffinized in xylol and rehydrated in a series of ethanol solutions with 99%, 70%, 50% and 30% of ethanol concentrations, followed by PBS. Rehydrated sections were fixed in 4% PFA for 15 minutes, bleached in 6% hydrogen peroxide for 15 minutes and treated with proteinase K 10 µg/mL solution for 10 minutes. Treated slides were immediately fixed in 4% PFA for another 15 minutes, washed twice in PBS and proceeded to acetylation in freshly prepared 0.25% acetic anhydride solution in 100 mM Tris-Cl (pH 7.5) for 10 minutes. Then, tissues were equilibrated in 2xSSC buffer, pH 5 and dehydrated in a series of ethanol solutions with 30%, 50%, 70% and 99% ethanol concentrations. Dehydrated slides were dried on air and hybridized with digoxygenin-labelled RNA probe for *Id2, Id3* or *Smoc2* overnight at 63°C. The following day, hybridized sections were washed in 5x, 2x, 1x and 0.2x SSC buffer at 60°C, proceeded to the blocking stage and incubated overnight with sheep anti-digoxigenin antibody 1:3000 (Roche).

The following day, slides were washed in TBSX buffer and stained with NBT/BCIP (Roche) until the signal was developed. Afterwards, slides were dehydrated and mounted with ROTI Histokitt (Carl Roth). Images were acquired on the Olympus IX2-UCB microscope.

2.21 CISPR-Cas9 Genome Editing of Small Intestinal Organoids.

The protocol for lentiviral transduction of small intestinal organoids was developed based on three previously published protocols – Koo *et al.*, 2013; Andersson-Rolf *et al.*, 2014; van Lidth de Jeude *et al.*, 2015. Lentiviruses were purchased from VectorBuilder https://en.vectorbuilder.com. *Rosa*^{Cas9EGFP} organoids from the small intestine's middle third were cultured for at least 2 weeks after isolation. The resulting organoids were split and plated into a new well of the 48-well plate to obtain around 50 organoids in each well. Two wells were prepared for one transduction. Freshly split organoids were cultured in the organoid culture medium supplemented with 10 µM Chir99021 (StemCell Technologies) and 10 mM nicotinamide (Carl Roth) (ENRCNic) to induce the formation of cystic hyperproliferative crypts. After two days, the organoids were collected and broken down by pipetting with a p200 micropipette 50 times to obtain 5-10 cell aggregates. It is important to break down the organoids into small enough particles but not to a single-cell state. To ensure the efficiency of breaking, it was checked under the microscope. Organoids were transferred into 15 mL conical tubes and centrifuged for 5 min at 100 g. The supernatant was removed, and organoids were resuspended in 500 µL of pre-warmed 1x trypsin (Sigma-Aldrich) and incubated for 3 min in a 37°C water bath. Trypsin was inactivated by adding 3.5 mL of the organoid culture medium, followed by centrifugation for 5 min at 500 g. The supernatant was removed, leaving approximately 40 µL. The organoids were then resuspended and transferred to a well in a 48-well plate. Two aliquots (>10^8 transducin units / mL, 25 µL each) of the lentiviral particles were resuspended in 250 µL of infection medium, prepared fresh, and spinoculation was performed by centrifuging in a pre-warmed centrifuge at 32°C at 600 g for one hour. Organoids mixed with viruses were incubated for 6 hours at 37°C in a cell culture incubator to ensure transduction. After transduction, the organoids were resuspended in 1 mL of organoid culture medium and transferred into microcentrifuge tubes. The tubes were then centrifuged at 850 g for 5 minutes to pellet the organoids, and the

supernatant was removed. The organoids were resuspended in a mixture of organoid medium and Matrigel (Corning) in a 1:1 ratio. This mixture was then plated onto a 48-well plate and cultured in ENRCNic medium with the addition of 10 µM Y27632 to prevent anoikis. After two days, the medium was refreshed, and a selection antibiotic was added. Four days after transduction, the standard organoid medium was used with the selected antibiotic. The antibiotic selection process took two weeks, during which the medium was refreshed every other day, and the Matrigel was changed once a week. Individual clones were then picked, plated, and expanded. To confirm the frame-shift mutation presence, the DNA was extracted, and the region around the gRNA target was amplified using Apc_pcr_fwd and Apc_pcr_rev, or Id2_pcr_fwd and Id2_pcr_rev primers. The PCR products were then purified with the NucleoSpin Gel and PCR Clean-up Kit (Macherey-Nagel) and sent for Sanger sequencing with Apc_seq_rev and Id2_seq_rev. After sequencing, the sequences were analyzed and checked using the Unipro UGENE v48.1 software (Okonechnikov *et al.*, 2012) and aligned with the Clustal Omega multiple sequence alignment online program, which can be found at https://www.ebi.ac.uk/jdispatcher/msa/clustalo. In cases where Sanger sequences displayed heterogenous chromatograms, frame-shift mutations for both alleles in heterozygous clones were confirmed by cloning the PCR product amplified with Apc_pcr_fwd and Apc_pcr_rev, or Id2_pcr_fwd and Id2_pcr_rev primers into the pGEM-T Easy Vector from the pGEM-T Easy Vector Systems Kit (Promega). The ligation mix was transformed into competent bacteria and plated onto LB agar plates containing 100 µg/mL ampicillin. Bacterial clones expressing vector with the insertion were selected by blue-white selection. The plasmids were extracted using GeneJET Plasmid-Midiprep-Kit (Thermo Fisher Scientific) and sent for Sanger sequencing using T7 primer.

2.22 Statistical Analysis.

Information on sample size and statistical tests used for each experiment are indicated in the figure legends. Data are provided as means with SD. Data were tested for normality with the D'Agostino and Pearson omnibus normality test and Shapiro-Wilk test. Data with a normal distribution were statistically analyzed using a two-tailed Student's t-test. The Mann-Whitney test was used instead if the data were not normally distributed. A *P*-value of ≤0.05 was considered significant. The analysis was performed using GraphPad Prism v10.

3. RESULTS

3.1 The Role of ID2 in the Differentiation of Secretory Lineages in the Mouse Small Intestinal Epithelium. *

3.1.1 *Id2*$^{+}$ Cells Mark the Enteroendocrine Lineage.

To study the role of ID2 in defining intestinal stem cell (ISC) fate, I first assessed the capacity of cells expressing *Id2* and their progenies to differentiate into distinct secretory populations. For that, I performed a lineage tracing experiment with *Id2*^{CreERT2}*:Rosa26*^{tdTomato} mice. Figure 3.1A shows the steps of the experiment. First, tamoxifen (TAM) was administered by oral gavage 3 days before analysis, which is sufficient for terminal differentiation of secretory cells. After three days, the small intestines were dissected and divided into three equal parts: anterior, middle, and posterior. From each part, the fraction of crypts and the last fraction of villi were extracted and stained for chromogranin A, a pan-marker of EECs. Serotonin, also known as 5-HT, was used to identify the largest population of EECs, specifically the enterochromaffin cells (ECs). To identify the minor populations of EECs, stainings for GLP1, marking L cells, NTS, marking N cells, PYY, produced in both L and N cells, SST, secreted by D cells, and GHRL, produced by X cells, were performed. Additionally, crypts and villi were stained for DCLK1 to analyze tuft cell lineage; Paneth cells were defined by their high reactivity with *Ulex europaeus agglutinin* (UEA), as described in Leis *et al.*, 1997. The stained populations were quantified by FACS. Figure 3.1B illustrates the FACS gating strategy involving the pre-selection of single and viable cells, followed by the selection of epithelial cells based on EpCAM staining, a pan-marker of epithelial cells. The percentage of Hormone^{+}/DCLK1^{+}/UEA^{high} cells derived from *Id2*$^{+}$ progenitors and *Id2*$^{-}$ progenitors were calculated using Q2/Q1 and Q3/Q4 division, respectively, from the final FACS plot in Figure 3.1B. The results of flow cytometry gating for each hormone, DCLK1^{+} and UEA, are illustrated in Figure 3.1C.

Based on FACS quantification, *Id2*-expressing cells accounted for approximately 2% of the entire intestinal epithelium. Analysis of enteroendocrine cells stained for CHGA and Serotonin (5-HT)-producing enterochromaffin cells revealed

* The results of this chapter were published in the following paper: Zinina, V. V., Ruehle, F., Winkler, P., Rebmann, L., Lukas, H., Möckel, S., Diefenbach, A., Mendez-Lago, M., & Soshnikova, N. (2022). ID2 controls differentiation of enteroendocrine cells in mouse small intestine. *Acta physiologica (Oxford, England)*, *234*(2), e13773. https://doi.org/10.1111/apha.13773.

that over 80% of CHGA$^+$ and 5-HT$^+$ cells either express *Id2* or stem from *Id2*$^+$ progenitors Figure 3.2 A,B).

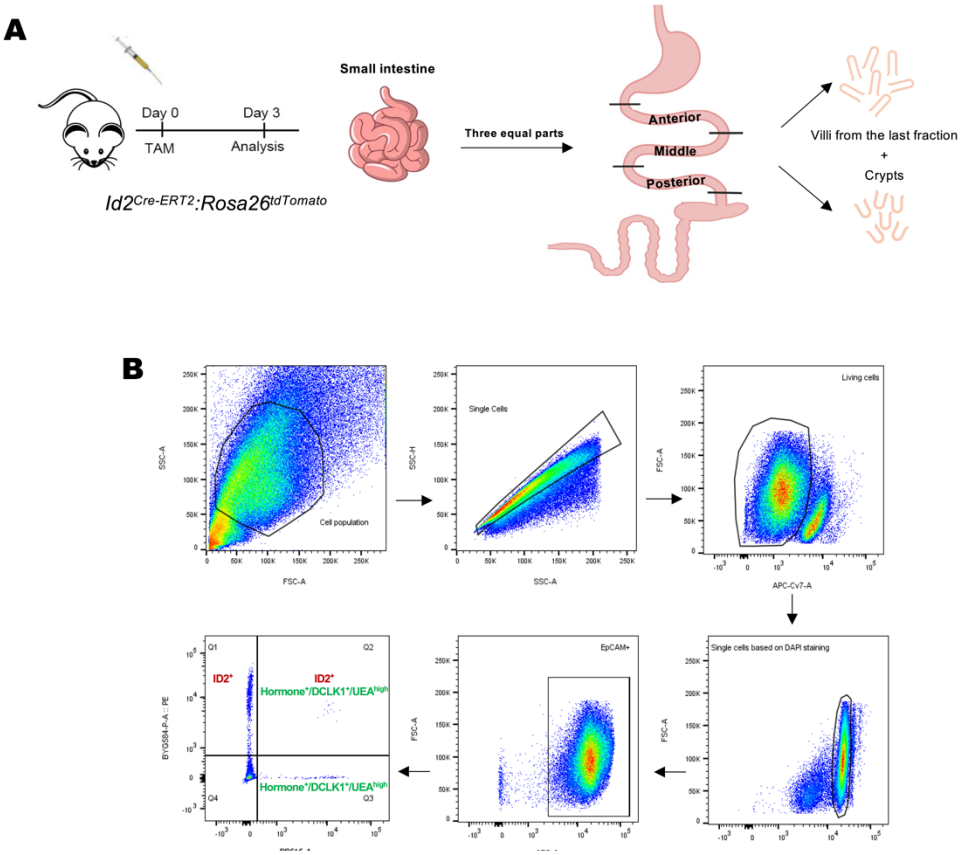

Figure legend on next page.

Cholecystokinin (CCK) is produced mainly by I cells but can also be produced by other types of peptidergic enteroendocrine cells. *Id2*$^{+}$ cells had an approximately five-fold higher proportion of CCK expression than *Id2*-negative progenitors, similar to CHGA and 5-HT counts (Figure 3.2C). Together, these results indicate that the majority of both enterochromaffin and peptidergic EECs express *Id2* or stem from *Id2*$^{+}$ progenitors.

While GLP-1 showed a slight tendency towards enrichment in *Id2*$^{+}$ progenitors, the difference did not reach statistical significance (Figure 3.2D). However, both PYY and NTS were present in *Id2*$^{+}$ populations at significantly higher frequencies than in *Id2*-negative populations (Figure 3.2E, F). Both L and N cell populations produce PYY, but the N-cell population is responsible for the significant enrichment of PYY-producing cells among *Id2*$^{+}$ progenitors. This suggests that *Id2* expression is activated during L cell differentiation towards N cells.

I further examined the population of GHRL-producing X cells and found that the frequency of X cells among *Id2*$^{+}$*tdTomato*$^{+}$ progenies tended to be higher compared to *Id2*-negative progenies, although this difference was not statistically significant due to the high deviation between individual animals used for the experiment (Figure 3.2G). Most SST-producing D cells, in contrast, stem from Id2^{-} tdTomato^{-} progenies (Figure 3.2H).

Figure 3.1 Lineage tracing of *Id2*$^{+}$ intestinal epithelial cells. A: Experimental plan. *Id2*$^{Cre\text{-}ERT2}$*:Rosa26*^{tdTomato} mice were treated with tamoxifen. Small intestine was dissected into 3 parts- anterior, middle, and posterior. Villi and crypts were extracted and used for antibody staining and FACS quantification 3 days after Cre induction. B: FACS strategy to quantify hormone-positive cells from *Id2*$^{Cre\text{-}ERT2}$*:Rosa26*^{tdTomato} mice. Dissected intestines were dissociated with EDTA to get cell suspension and stained with eFluor 780 viability dye. After fixation, the samples were stained with hormone antibodies and co-stained with donkey-anti-rabbit Alexa 488 secondary and anti-EpCAM antibodies. FACS gating strategy included single-cell selection, living cell selection based on eFluor 780 staining, and DAPI^{+}EpCAM^{+} single (based on DAPI staining) epithelial (based on EpCAM staining) cell selection. The percentage of hormone-producing cells was quantified based on Alexa 488 staining, and *Id2*$^{+}$ cells were quantified based on tdTomato expression. C: Representative flow cytometry profiles of *Id2*$^{+}$ (Q1-Q2) and *Id2*$^{-}$ (Q3-Q4) cells and their progenies in the intestinal epithelium. Enteroendocrine, tuft, and Paneth cells derived from either *Id2*$^{+}$ (Q2) or *Id2*$^{-}$ (Q3) progenies are distinguished based on the expression of specific markers.

Analysis of tuft cell population based on DCLK1 staining showed that tuft cells are generated from both *Id2*$^{+}$*tdTomato*$^{+}$ and *Id2*$^{-}$*tdTomato*$^{-}$ progenies with similar frequencies (Figure 3.2I). Moreover, analysis of Paneth cell population based on UEA staining showed that UEA^{high} Paneth cells arise from *Id2*-negative progenitors with fivefold higher frequencies (Figure 3.2J). Together these results demonstrate that *Id2* is not a marker of the common secretory progenitor.

To summarize, lineage tracing analysis shows that *Id2* is expressed in both peptidergic and enterochromaffin EECs and later reactivated during N-cell differentiation from L cells.

3.1.2 ID2 Promotes Differentiation Along Enteroendocrine Lineage but Suppresses Tuft Cell Fate.

To investigate ID2 functions, I used a mouse model with the *Id2* conditional null allele (Niola *et al.*, 2012) and the *Shh*$^{Cre\text{-}EGFP}$ (Harfe *et al.*, 2004) knock-in allele,

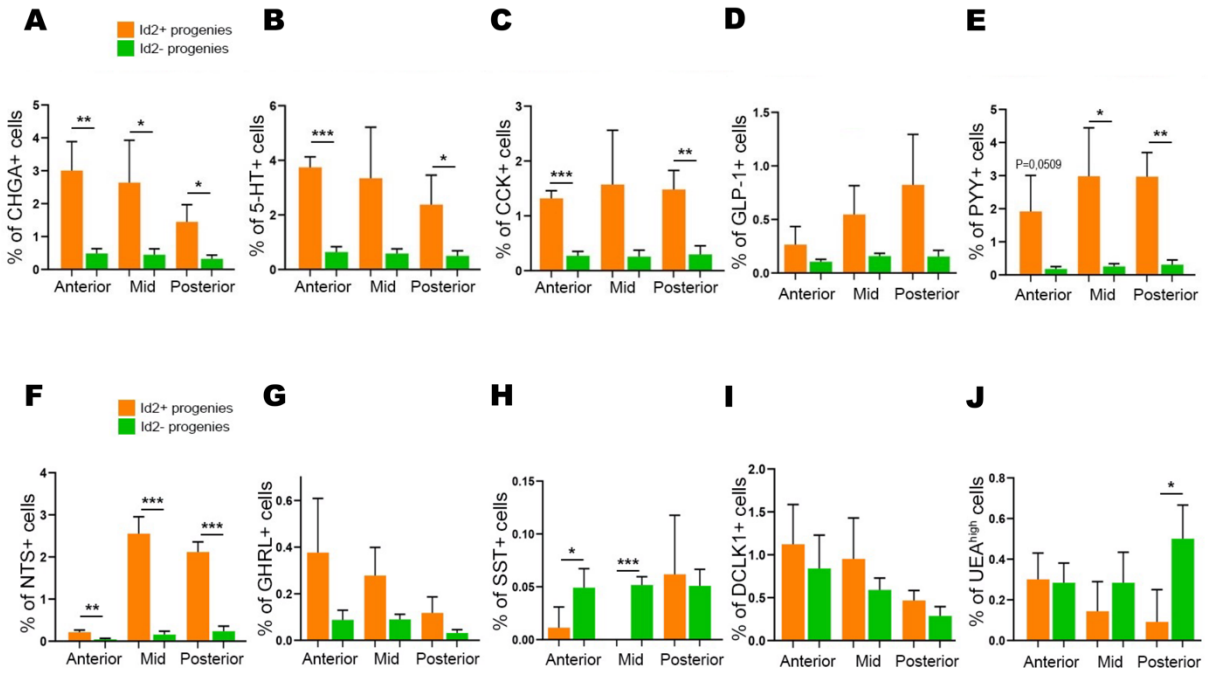

Figure 3.2 FACS quantification of hormone^{+}*Id2*$^{+}$ intestinal epithelial cells. A-J: Quantification of the numbers of hormone^{+}*Id2*$^{+}$ cells (orange) and hormone^{+}*Id2*$^{-}$ cells (green) in *Id2*$^{Cre\text{-}ERT2}$:*Rosa26*^{tdTomato} mouse small intestine by flow cytometry 3 days after tamoxifen administration. Error bars are ±SD, n = 3 mice. *P < 0.05, **P < 0.01 and ***P < 0.001 by two-tailed Student's t-test.

which activates Cre at the ventral intestinal epithelium already from embryonic day 9.5 (E9.5) and spreads throughout the whole intestinal epithelium by E11.5, which was demonstrated on small intestines derived from *Shh*$^{Cre\text{-}EGFP}$*:Rosa26*^{tdTomato} embryos (Figure 3.3A). *Id2* conditional allele contains *loxP* sites 5′ of exon1 and intron2 so that Cre recombinase deletes the entire coding region of the *Id2* gene in the first and second exon (Figure 3.3B, Niola *et al.*, 2012).

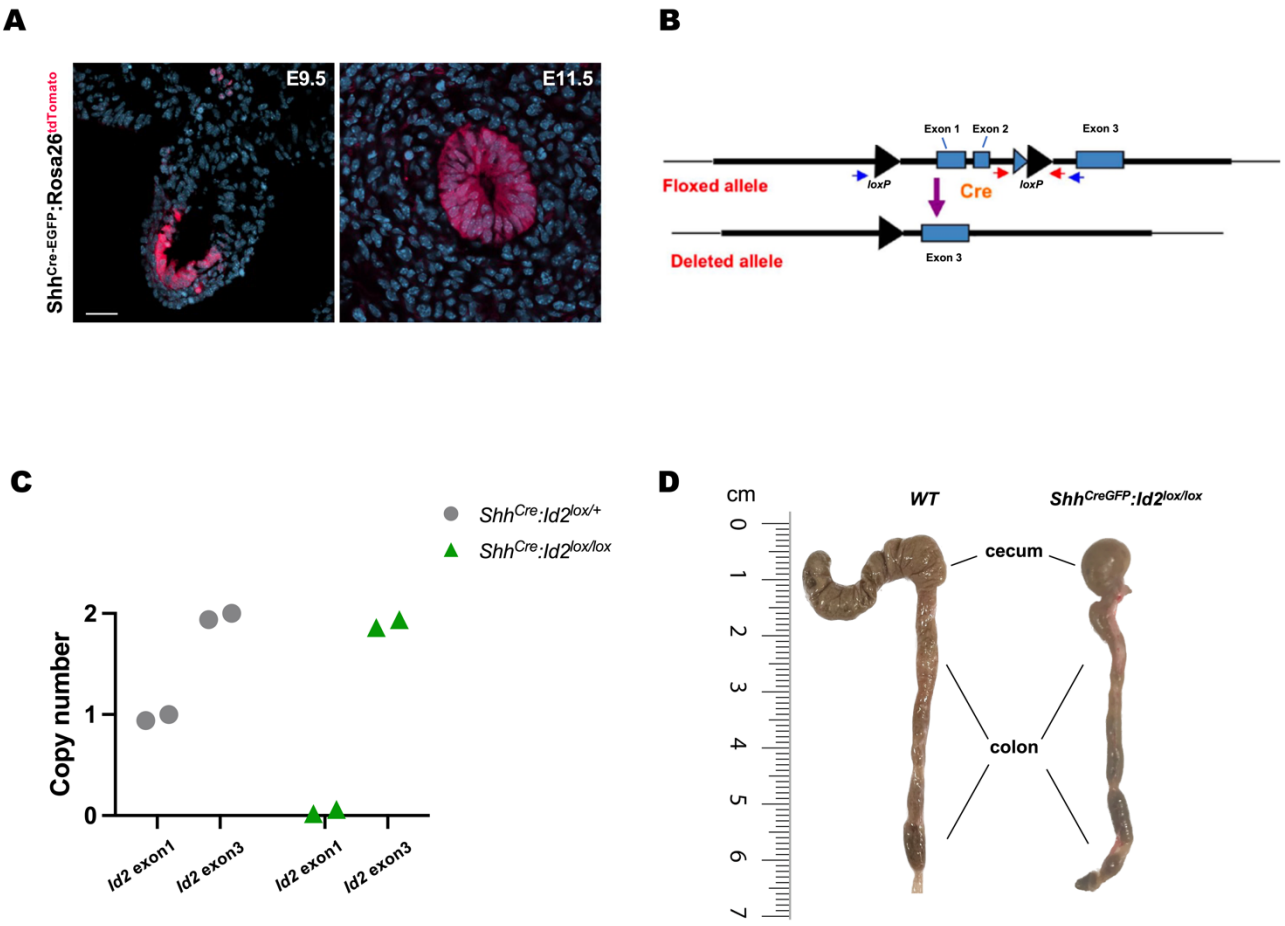

Figure 3.3 *Shh*$^{EGFP\text{-}Cre}$*:Id2*$^{lox/+}$ mouse model. A: Confocal images of transverse sections of *Shh*$^{EGFP\text{-}Cre}$*:Rosa26*^{tdTomato} mouse embryos at E9.5 and E11.5 showing Cre recombinase activity (magenta) (n = 4 embryos analysed). DAPI stains nuclei (teal). Scale bar: 30 μm E9.5 and 20 μm E11.5 B: Structure of the *Id2* floxed and deleted alleles. When Cre-mediated recombination occurs, exon1 and exon2 of the coding region of *Id2* are deleted. The figure is taken from Niola *et al.*, 2012 with modifications. C: The result of CNV analysis. *Shh*^{Cre}*:Id2*$^{lox/lox}$ mice used in the experiment lost exon1 completely. The *Shh*^{Cre}*:Id2*$^{lox/+}$ mice, used only for the assay, lost one copy of exon1 and still had both copies of the exon3 region. D: The comparison of cecums isolated from WT and *Shh*^{Cre}*:Id2*$^{lox/lox}$ mice. *Shh*^{Cre}*:Id2*$^{lox/lox}$ mice typically have a smaller bulb-shaped cecum (right) than the wild-type mice (left).

To confirm the effectiveness of Cre-mediated recombination, I conducted a Copy Number Variation (CNV) analysis using qPCR. For this purpose, I designed specific primers for the exon1 and exon3 regions of the *Id2* gene. As exon1 gets entirely deleted by Cre recombinase, the mice with *Shh*^{Cre}*:Id2*$^{lox/lox}$ genotype should lose both copies of exon1. In contrast, the exon3 region serves as a control, and both *Shh*^{Cre}*:Id2*$^{lox/lox}$ and wild-type mice should have two copies of the exon3 region. Figure 3.3C shows the result of CNV analysis, which indicates that *Shh*^{Cre}*:Id2*$^{lox/lox}$ mice used in the experiment entirely lost exon1. Meanwhile, *Shh*^{Cre}*:Id2*$^{lox/+}$ mice (only used for this assay and not for the experiment) lost only one copy of exon1 and still had both copies of the exon3 region. Furthermore, I also checked the cecums of the mice used in the experiment, as *Shh*^{Cre}*:Id2*$^{lox/lox}$ mice typically have a smaller bulb-shaped cecum than the wild-type mice (Figure 3.3D).

To study the role of ID2 in regulating differentiation along secretory lineage, I conducted an experiment using *Shh*^{Cre}*:Id2*$^{lox/lox}$ (*Id2*^{KO}) and C57BL/6 (*WT*) mice. I

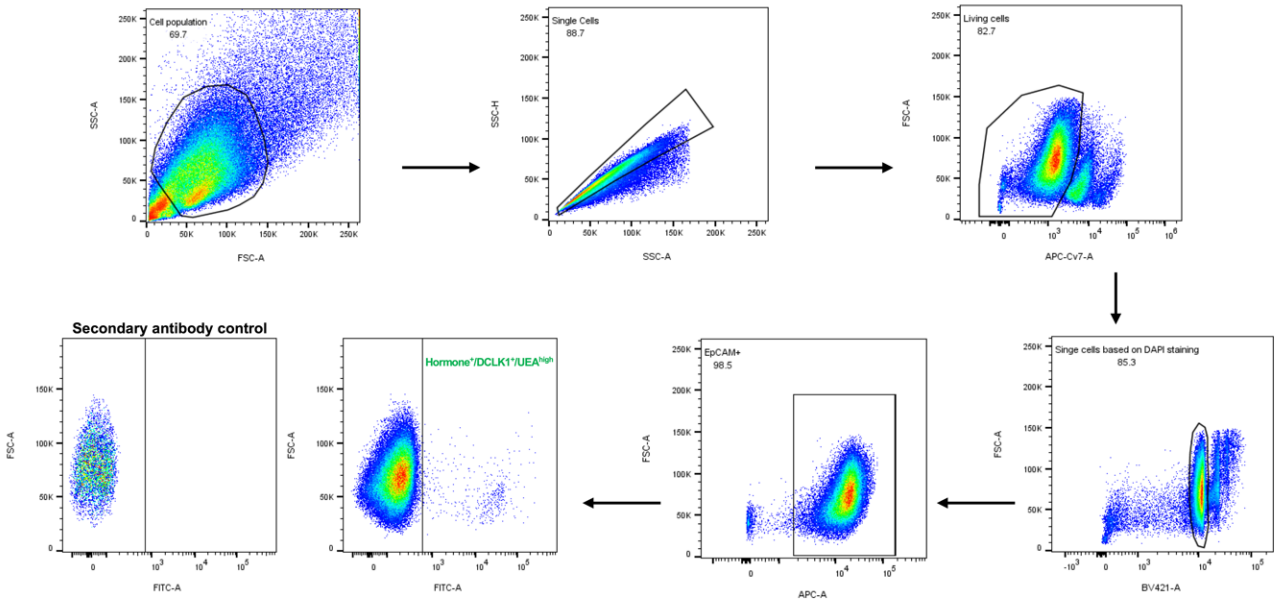

Figure 3.4 FACS strategy to quantify hormone-producing cells from *Shh*^{Cre}*:Id2*$^{lox/lox}$ and WT mice. Dissected intestines were dissociated with EDTA to get cell suspension and stained with eFluor 780 viability dye. After fixation, the samples were stained with hormone antibodies and co-stained with donkey-anti-rabbit Alexa 488 secondary and anti-EpCAM antibodies. FACS gating strategy included single-cell selection, living cell selection based on eFluor 780 staining, and DAPI^{+}EpCAM^{+} single epithelial cell selection. The percentage of hormone-producing cells was quantified based on Alexa 488 staining.

aimed to determine the number of different secretory populations in each group. To do this, I dissected the small intestines, divided them into three equal parts, and extracted crypts mixed with the last fraction of villi (the same way as discussed above for the lineage tracing experiment). Cell suspensions were stained for CHGA, 5-HT, CCK, PYY, GLP1, NTS, GHRL, SCT and SST to analyze EECs. Tuft and Paneth cells were analyzed by performing DCLK1 and UEA staining, respectively. The FACS strategy for quantification is shown in Figure 3.4 and includes single-cell selection, living cell selection based on eFluor 780 staining, and DAPI$^+$EpCAM$^+$ single epithelial cell selection. The percentage of hormone-producing cells was determined by staining with specific hormone antibodies and co-staining with donkey-anti-rabbit Alexa 488 secondary antibody.

The analysis of FACS counts revealed a 1.8-fold reduction in CHGA$^+$ cells upon deletion of *Id2*, meaning that ID2 promotes differentiation along EE lineage (Figure 3.5A). Interestingly, the number of EC cells producing serotonin (the largest

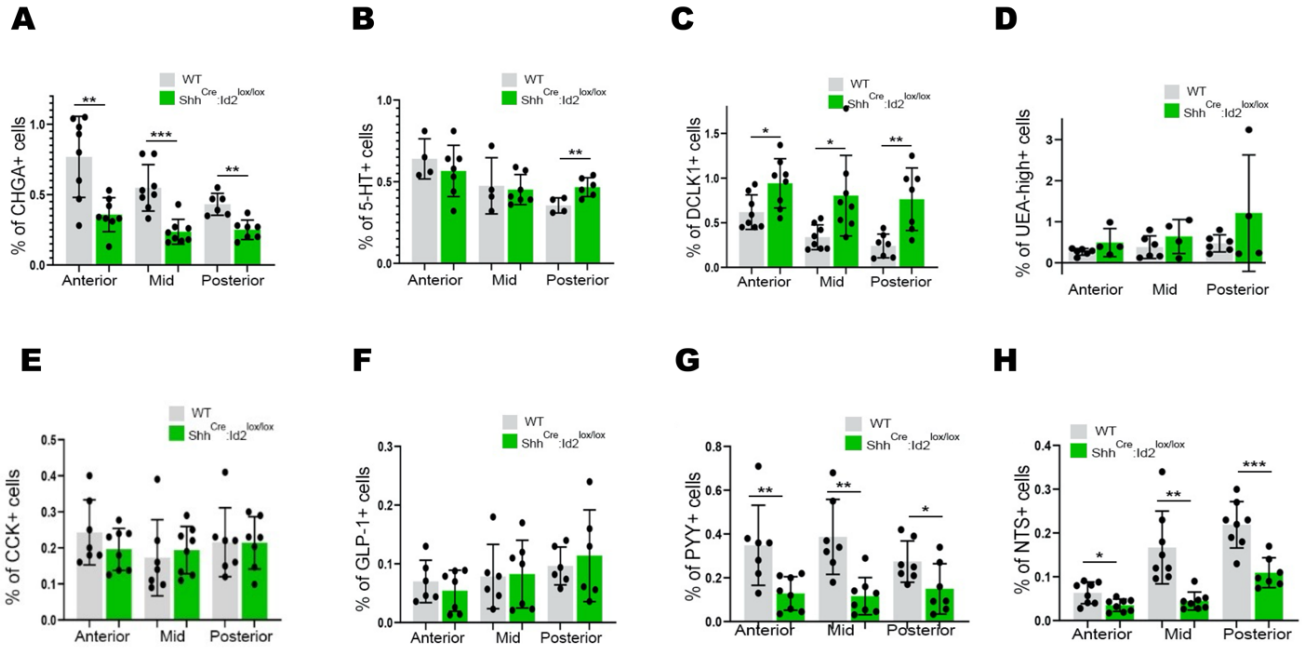

Figure 3.5 ID2 promotes differentiation along enteroendocrine lineage but suppresses tuft cell fate. FACS quantification of hormone-producing cells from *Shh^{Cre}:Id2$^{lox/lox}$* and WT mice: frequency of CHGA$^+$ EpCAM$^+$ (A), 5-HT$^+$ EpCAM$^+$ (B), DCLK1$^+$ EpCAM$^+$ (C), UEA$^+$ EpCAM$^+$ (D), CCK$^+$ EpCAM$^+$ (E), GLP1$^+$ EpCAM$^+$ (F), PYY$^+$ EpCAM$^+$ (G), NTS$^+$ EpCAM$^+$ (H) in the Anterior, Mid and Posterior parts of the small intestine of wild-type (WT, grey) and *Shh$^{EGFP-Cre}$:Id2$^{flox/flox}$* (green) mice. Error bars are ±SD, n = 4-8 mice. *P < 0.05, **P < 0.01 and ***P < 0.001 by two-tailed Student's t-test.

population of EE cells) was unchanged in the anterior and middle small intestines but increased 1.3 times in the posterior part of *Id2*^{KO} mice compared to *WT* (Figure 3.5B). Serotonin-producing cells in the gut are distributed in an anterior-posterior gradient, with the highest number in the anterior part. This means that ID2 is essential for the maintenance of this gradient by suppressing EC cell differentiation in the posterior part of the small intestine.

The number of DCLK1^{+} tuft cells was over 1.5 times higher in *Id2*-deficient mice, indicating that ID2 inhibits tuft cell differentiation in the gut (Figure 3.5C). Conversely, no significant difference in Paneth cell numbers was observed based on UEA staining (Figure 3.5D).

Together, these results demonstrate ID2's promoting effect on EEC differentiation but its inhibitory effect on tuft cell lineage.

3.1.3 ID2 is Necessary for the Differentiation of Enteroendocrine N cells.

Next, I investigated the role of ID2 in the differentiation of individual EE populations, starting with CCK-producing cells, which are mainly I cells. The analysis of FACS counts did not reveal a significant difference in I cell numbers between *Id2*^{KO} and *WT* mice (Figure 3.5E). In line with lineage tracing results, I did not detect any difference in GLP1^{+} L cell population (Figure 3.5F). At the same time, the numbers of PYY-producing cells were dramatically decreased in all parts of the small intestine in *Id2*-deficient mice: 3 times in the anterior, almost 4 times in the middle and 2.3 times in the posterior part (Figure 3.5G). As discussed earlier, PYY is produced by both L cells, which are found in the crypts, and N cells, mostly present in the villi and arising from L cells. Therefore, the number of NTS-producing N cells was examined, as they could impact the difference in PYY-producing cells. The study found that NTS^{+} N cells were significantly decreased in mice lacking *Id2*: 1.8 times in the anterior, 3 times in the middle, and 2 times in the posterior part (Figure 3.5H). These results demonstrate that the differentiation of the enteroendocrine N cell lineage requires ID2, which is in agreement with the lineage tracing results.

3.1.4 ID2 Mediates BMP Signaling During N cell Differentiation.

The results of lineage tracing and *Id2*-deficient mice showed the requirement of ID2 for the differentiation of N cell lineage. Beumer *et al.* (2018) found that BMP signaling induces *Nts* expression, causing L cells in crypts with low BMP levels to

differentiate into N cells more abundant in villi with high BMP. To investigate the impact of ID2 on the regulation of BMP-induced differentiation of EECs, I utilized a small intestinal organoid model system *ex vivo*. Crypts were isolated from WT and *Shh*^{Cre}*:Id2*$^{lox/lox}$ mice and were cultured in a standard organoid medium that contained EGF, Noggin, and R-spondin (ENR medium, Figure 3.6A). EGF promotes proliferation and maintains *ex vivo* organoid cultures. The undifferentiated state is supported by Noggin antagonizing BMP ligands and R-spondin activating Wnt signaling. Isolated

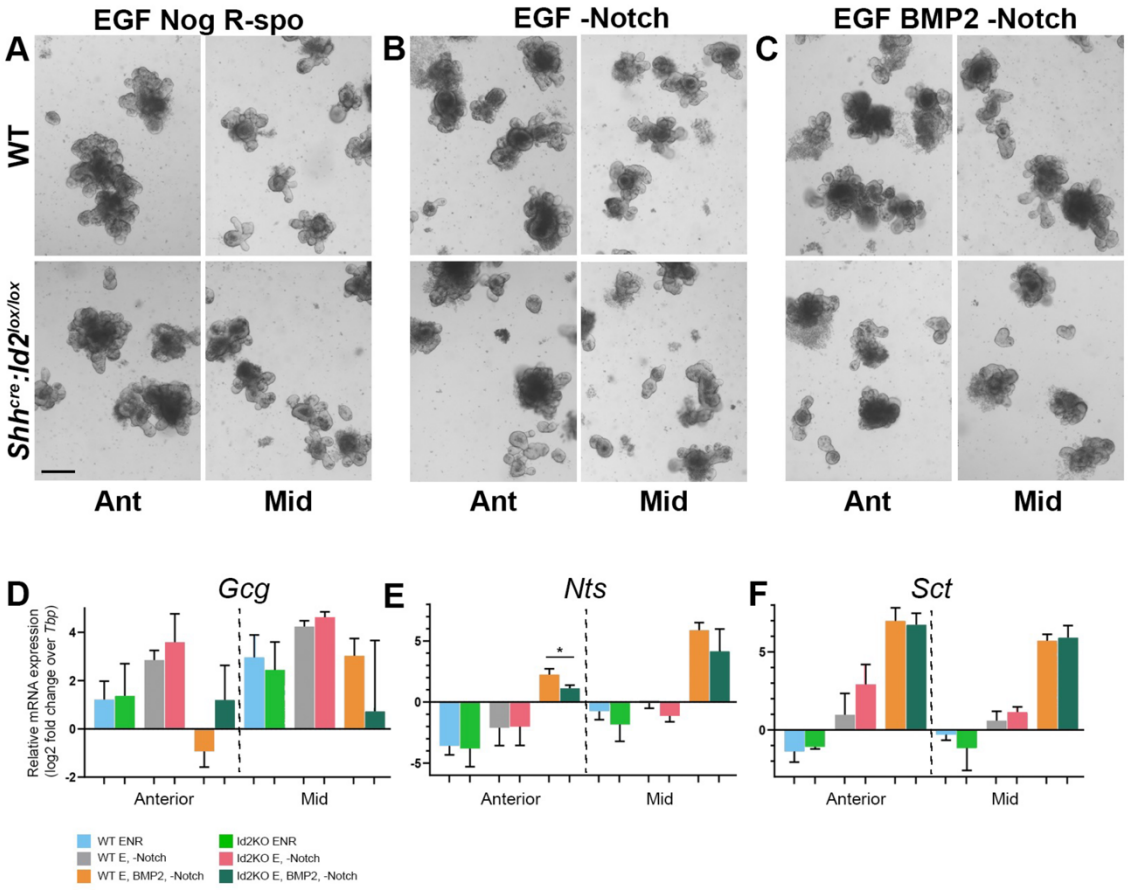

Figure 3.6 ID2 acts downstream of BMP signaling during N cell differentiation. A-C: Representative images of organoids derived from the small intestinal epithelium of either wild-type or *Shh*$^{EGFP\text{-}Cre}$*:Id2*$^{flox/flox}$ mice cultured in the medium containing EGF, Noggin and R-spondin1 (A), EGF and Notch inhibitor RO4929097 (B) BMP2, EGF and Notch inhibitor RO4929097 (C). Scale bar: 200 µm. D-F: qRT-PCR analysis showing expression of *Glucagon* (*Gcg*) (D), *Neurotensin* (*Nts*) (E) and *Secretin* (*Sct*) (F) in the small intestinal organoids derived from wild-type (blue) or Id2 mutant (green) mice cultured in ENR, and organoids derived from wild-type (grey) or *Id2* mutant (red) mice cultured for 4 days in the presence of Notch inhibitor RO4929097 (E, -Notch medium), as well as organoids derived from wild-type (orange) or Id2 mutant (teal) mice cultured for 4 days in the presence of BMP2 and Notch inhibitor RO4929097 (BE, -Notch medium) (n = 3). *Tbp* expression was used as a normalizing control. Error bars are ±SD. *P < 0.05 by two-tailed Student's t-test.

crypts were cultured for at least 2 weeks until budding structured organoids formed. It is noteworthy that organoids derived from the anterior and middle parts of the small intestine were cultured successfully for several months, while those from the posterior section displayed a lower clonogenic capacity and were lost after three passages. As a result, all subsequent assays were conducted only with the organoids obtained from the anterior and middle thirds of the small intestine.

To induce differentiation of EECs in cultured organoids, the medium was supplied by the gamma-secretase inhibitor RO4929097, which prevents the activation of Notch signaling and thus pushes differentiation towards the secretory lineage. Noggin and R-spondin were removed. EGF was added to maintain cell viability and proliferation (ERo conditional medium, Figure 3.6B). In order to activate BMP signaling, the ERo conditional medium was supplemented with BMP2 (BERo conditional medium, Figure 3.6C).

Based on the results of the quantitative reverse-transcription PCR (qRT-PCR) analysis, both the *Id2* mutant and wild-type organoids displayed increased expression of *Glucagon* (*Gcg*) after being cultured for 96 hours on ERo conditional medium (Figure 3.6D). This finding supports the conclusion that *Id2* does not influence the differentiation program of L cells. Furthermore, when BMP2 was added to the culture, *Gcg* expression was notably inhibited in both the wild-type and *Id2* mutant organoids (Figure 3.6D). This suggests that ID2 does not act downstream of BMP signaling to suppress *Gcg* transcription during L cell transition towards N cells.

After being cultured in BERo medium, both wild-type and *Id2* mutant organoids showed a significant increase in the expression of *Nts*, as displayed in Figure 3.6E. However, the levels of *Nts* were considerably lower in *Id2*-deficient anterior organoids than in control. In particular, Nts was upregulated over 50-fold in wild-type and 25-fold in *Id2* mutant organoids (Figure 3.6E). These results suggest that ID2 is crucial in mediating the BMP signaling during N cell specification.

It is interesting to note that there were no significant differences in *Nts* expression between wild-type and mutant organoids that were derived from the middle part of the small intestine. This observation could be due to the fact that high doses of BMP2 can stimulate the expression of ID1 and/or ID3, which might compensate for the lack of ID2 in an *ex vivo* environment.

The expression of *Secretin* (*Sct*) is activated during the differentiation of various enteroendocrine cells. In my experiment, the addition of BMP2 significantly

increased *Sct* expression in both wild-type and *Id2* mutant organoids. The increase was about 300-fold in the anterior and 65-fold in the middle organoids (Figure 3.6F). These findings suggest that ID2 is not essential for the terminal differentiation of all enteroendocrine cells. Instead, the data confirm that ID2 has a specific role downstream of BMP signaling for N cell differentiation.

3.1.5 ID2 Negatively Regulates the Differentiation of X cells.

To precisely determine the role of *Id2* in the specification of enteroendocrine progenitors along other cell types, including Ghrelin (GHRL) producing X cells and Somatostatin (SST) producing D cells, I measured the expression of these hormones in wild-type and *Id2*-deficient mice. Moreover, because of the lack of antibodies reliably labelling Gastric Inhibitory Peptide (GIP) positive K cells, I used organoids derived from wild-type and *Id2* mutant mice.

According to FACS quantification, the loss of *Id2* results in an increase in $GHRL^+$ cell numbers (threefold) in the posterior part of the small intestine (Figure 3.7A). It implies that ID2 suppresses the differentiation of the enteroendocrine progenitors towards X cell fate in the ileum. Furthermore, the fluorescence intensity of $GHRL^+$ cells was higher in the anterior part of the small intestine of *Id2* mutant mice than controls (Figure 3.7B). As per qRT-PCR analysis, *Ghrl* expression levels were three times higher in anterior organoids of *Id2* mutants than in those of wild-type organoids when both were cultured in ERo medium. (Figure 3.7C).

Inhibition of Notch signaling in intestinal organoids led to an up-regulation in the expression of *Gip*. This effect was over fivefold enhanced in the absence of *Id2* (Figure 3.7D). It suggests that *Id2* negatively regulates the differentiation of K cells. However, *Gip* transcripts were also detected in other intestinal epithelial cells (Zinina *et al*., 2022), so it is not clear whether differences in *Gip* levels reflect the increase in K cell numbers in *Id2* mutant organoids.

SST^+ D cell numbers did not change in *Id2* mutants compared to wild type (Figure 3.7E). In summary, these data show that *Id2* negatively regulates enteroendocrine X cell differentiation.

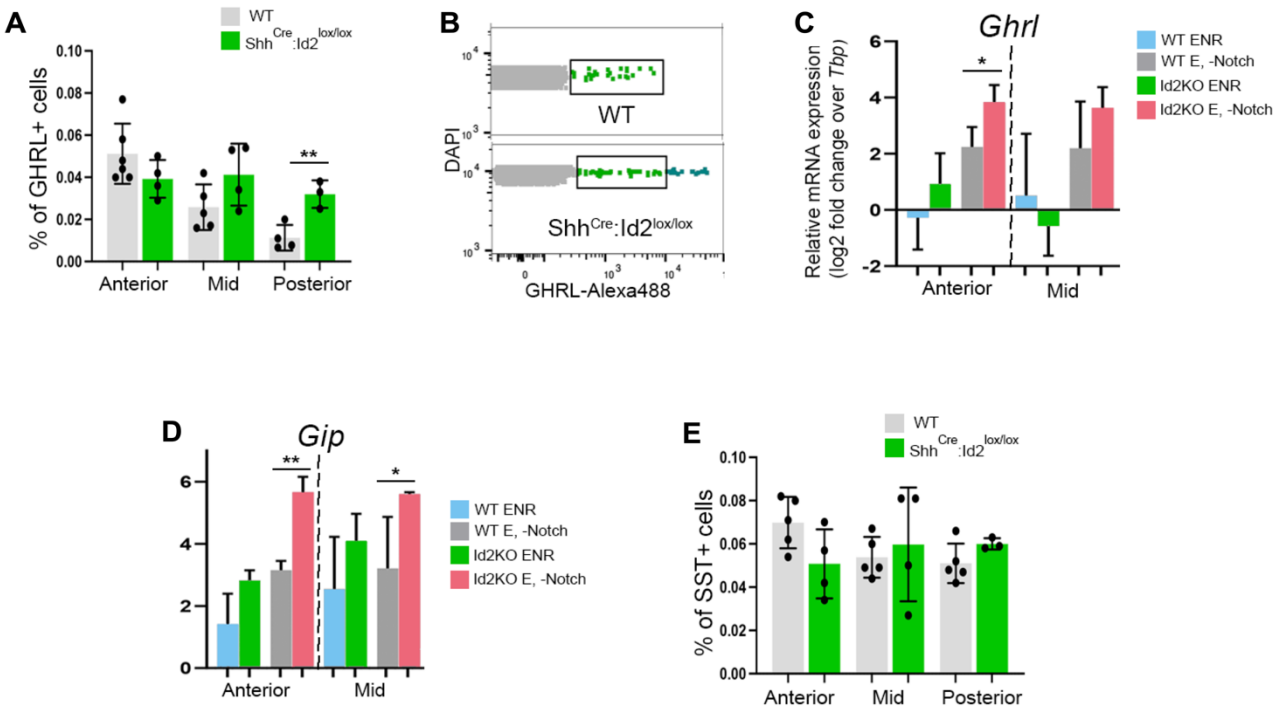

Figure 3.7 ID2 suppresses the differentiation of X cells. A: FACS Quantification of GHRL^{+}EpCAM^{+} cells using FACS from wild-type (WT, grey) and *Shh*$^{EGFP\text{-}Cre}$*:Id2*$^{flox/flox}$ (green) mice in the Anterior, Mid and Posterior parts. Error bars are ±SD, n = 4-8 mice. $^{**}P < 0.01$ by two-tailed Student's *t*-test. B: Fluorescence intensity of GHRL^{+} cells in the Anterior part of the small intestine of wild-type and *Shh*$^{EGFP\text{-}Cre}$*:Id2*$^{flox/flox}$ mice measured by FACS. C and D: qRT-PCR analysis showing the expression of X cell marker *Ghrelin* (*Ghrl*) (C) and K-cell marker *Gastric Inhibitory Peptide* (*Gip*) (D) in the small intestinal organoids derived from wild-type (blue) or *Id2* mutant (green) mice cultured in ENR, and in organoids derived from wild-type (grey) or *Id2* mutant (red) mice cultured for 4 days in the presence of Notch inhibitor RO4929097 (E, -Notch medium) (n = 3). *Tbp* expression was used as a normalizing control. Error bars are ±SD. $^{*}P < 0.05$ and $^{**}P < 0.01$ by two-tailed Student's *t*-test. E: FACS quantification of SST^{+}EpCAM^{+} cells in the Anterior, Mid and Posterior parts of the small intestine of wild-type (WT, grey) and *Shh*$^{EGFP\text{-}Cre}$*:Id2*$^{flox/flox}$ (green) mice. Error bars are ±SD, n = 4-8 mice.

3.2 The Oncogenic Role of ID2 in the Small Intestinal Epithelium.

3.2.1 The Depletion of *Id2* in the Small Intestinal Epithelium Causes a Significant Reduction in Tumor Numbers in *Apc*^{min} mice.

Previous studies have shown that ID2 plays a vital role in the development of tumors in *Apc*^{min} mice. However, these studies used mouse models in which *Id2* was knocked out constitutively. This makes it difficult to determine if the effect observed was due to the epithelial function of ID2 or the disruption of type 2 innate lymphoid cell lineage, which was earlier shown to promote the progression of colorectal cancer. (Wang, S. *et al.*, 2020).

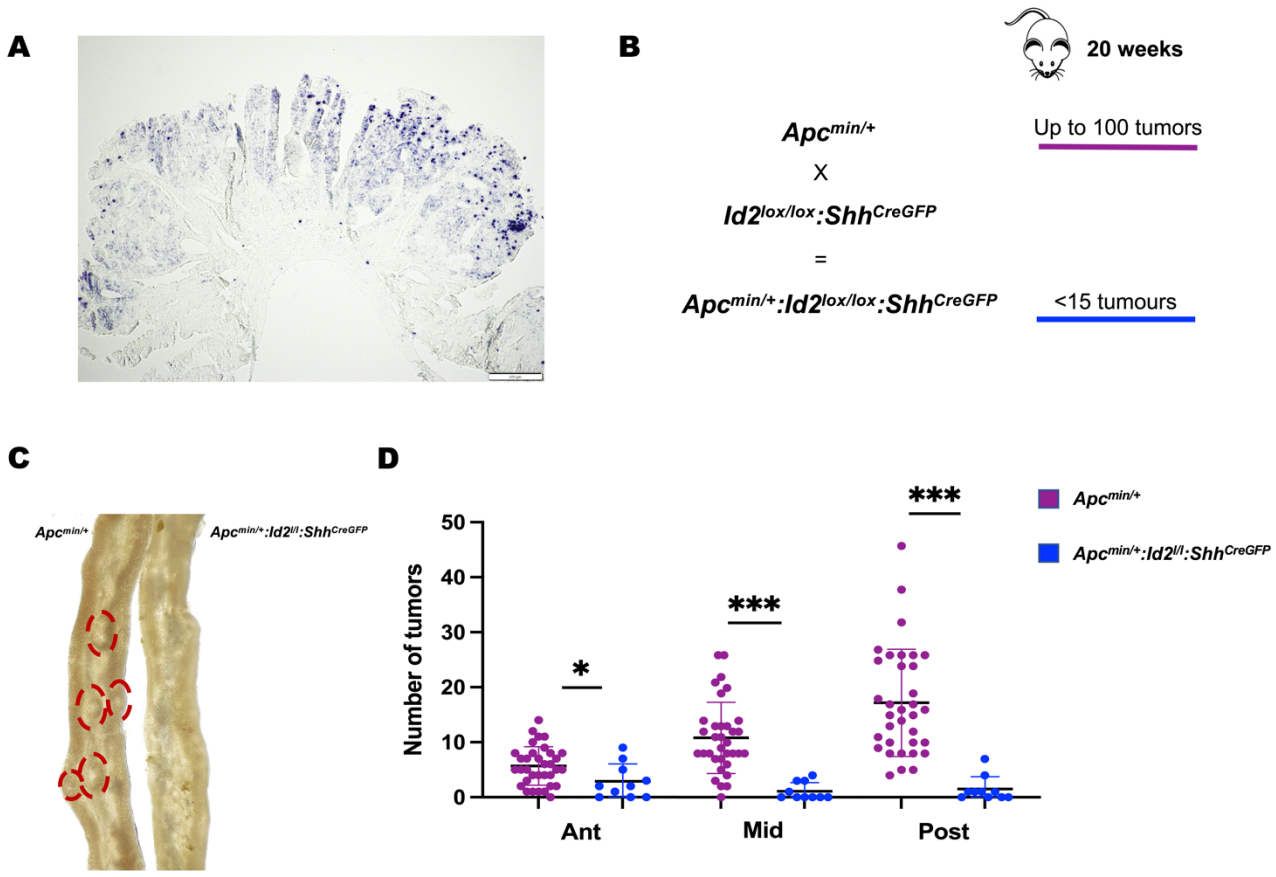

Figure 3.8 The depletion of *Id2* in the small intestinal epithelium significantly reduces tumor numbers in *Apc*^{min} mice. A: RNA *in situ* hybridization analysis showing the expression of *Id2* in tumors from *Apc*^{min} mice. Scale bar: 200 µm. B: Genetic mouse cross scheme with the indication of the observed tumor numbers at the age of 20 weeks. C: Dissected small intestines of *Apc*$^{min/+}$ and *Apc*$^{min/+}$*:Shh*^{CreGFP}*:Id2*$^{lox/lox}$ mice. The dotted circles highlight the tumors. D: Tumor counts performed for *Apc*$^{min/+}$ (magenta) and *Apc*$^{min/+}$*:Shh*^{CreGFP}*:Id2*$^{lox/lox}$ (blue) mice in the anterior (Ant), middle (Mid) and posterior (Post) parts of the small intestine. Error bars are ±SD *P < 0.05, ***P < 0.001 by the Mann-Whitney test, n=10-34 mice.

I conducted an RNA *in situ* hybridization analysis to identify the expression of *Id2* in small intestinal tumors of *Apc*^{min} mice. Figure 3.8A displays the outcome of the analysis, which clearly demonstrates that *Id2* is broadly expressed in intestinal tumors. To further investigate the role of ID2 in small intestinal tumor formation, I used an *Apc*^{min}*:Shh*^{Cre}*:Id2*$^{lox/lox}$ mouse model. This model allows for gut epithelium-specific depletion of *Id2* in *Apc*^{min} mice. As discussed earlier, Cre activity starts in the ventral part of the developing small intestinal epithelium as early as E9.5 (Figure 3.3A). When the mice reached 20 weeks of age, they were sacrificed, and their small intestines were examined for tumor counts. *Apc*^{min} mice of the same age were used as the control group. The analysis of tumor counts indicated that *Apc*^{min} mice normally develop up to 14 tumors in the anterior, 26 in the middle, and 46 in the posterior third of the small intestine and up to 80 in total. However, when *Apc*^{min} mice with epithelial-specific *Id2* depletion were analyzed, the total number of tumors in all parts was less than 15 (as shown in Figure 3.8B). Figure 3.8C shows the fragments of dissected small intestines of *Apc*$^{min/+}$ and *Apc*$^{min/+}$*:Shh*^{CreGFP}*:Id2*$^{lox/lox}$ mice, with tumors highlighted. The difference was particularly significant in the middle and posterior thirds of the small intestine, as illustrated in Figure 3.8D. These results demonstrate that depletion of *Id2* during early embryogenesis significantly reduces the number of tumors in *Apc*^{min} mice.

3.2.2 *Id2*-deficient Developing Small Intestines Display a Stomach-like Transcriptome Signature and an Increased Number of Stem Cells.

The previous studies of the group have shown that *Id2* is expressed in the embryonic small intestine as early as E9.0 (Dzama *et al.*, 2017) but decreases by E14.5 (Kazakevych *et al.*, 2017). To investigate the effect of *Id2* knock-out on the developing small intestinal epithelium, I conducted a bulk transcriptome analysis of embryonic small intestinal epithelial cells isolated from *Shh*^{Cre}*:Id2*$^{lox/lox}$ (*Id2*^{KO}) and *Id2*$^{lox/lox}$ (WT) mice at E13.5. The small intestines were mechanically disrupted, treated with collagenase, and stained for EpCAM, as shown in Figure 3.9A. The strategy for FACS sorting involved pre-selecting living cells based on DAPI staining and epithelial cells based on EpCAM staining, as shown in Figure 3.9B. I was only able to isolate around 3000 epithelial cells from the small intestine of one embryo at E13.5. Therefore, I isolated 500 cells per sample and processed them using the SMART-Seq v4 Kit for ultra-low amounts of RNA. The Nextera XT Kit was used to prepare libraries,

which underwent size distribution assessment, as shown in Figure 3.9C, for quality control.

Comparative analysis of *Id2KO* and WT embryo transcriptomes revealed 411 differentially expressed genes (|log2FC|≥*1*, FDR<0.05). 251 genes were up-regulated in *Id2*^{KO} embryos. The figure 3.10A depicts a heatmap that displays the expression of selected genes. Among them are genes previously shown to be up-regulated in *Id2*^{KO} developing intestine (Nigmatullina *et al.*, 2017; Mori *et al.*, 2019) and previously shown to be expressed in stomach endoderm: *Cym*, *Irx3*, *Irx5*, *Krt15, Foxa2, Adcy8* (Houweling *et al.*, 2001; Sherwood *et al.*, 2009; Lloyd *et al.*, 1995; Monaghan *et al.*, 1993; Visel, 2004). In addition to that, well-known markers of stem cells were also

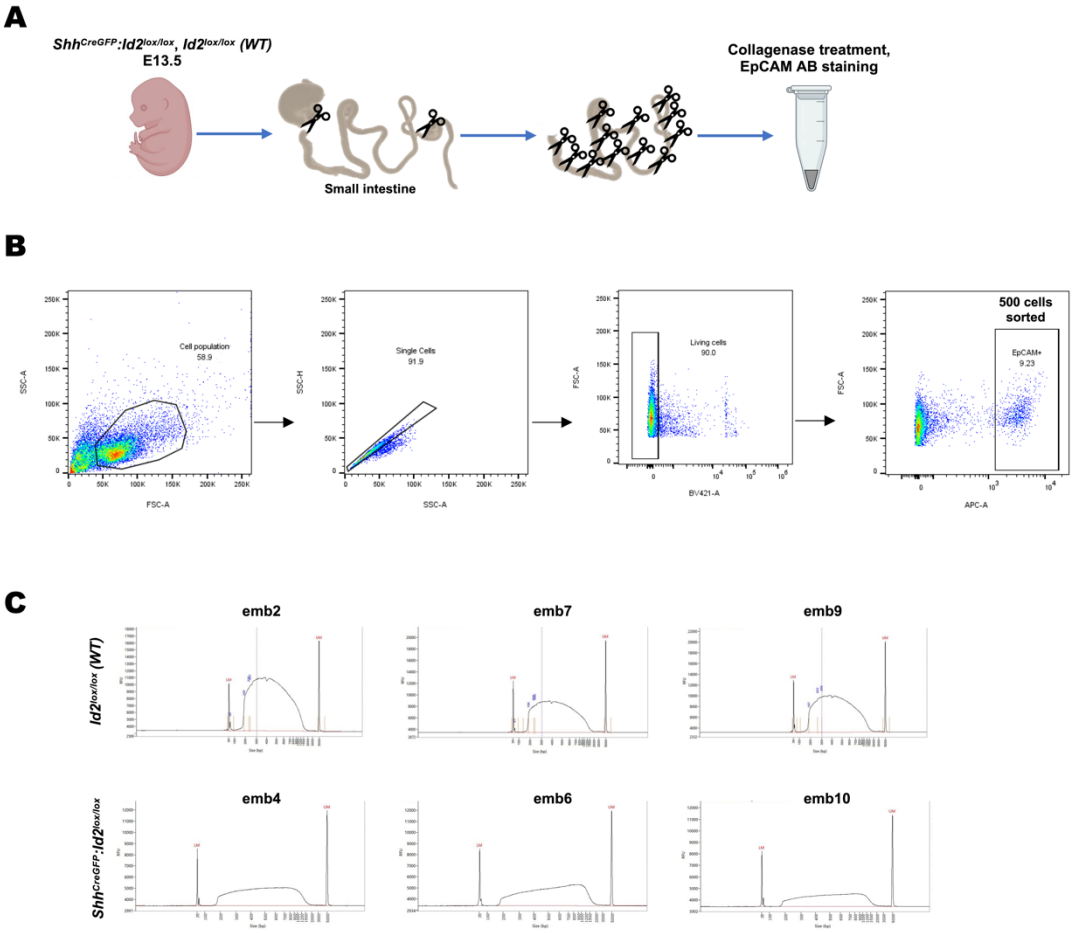

Figure 3.9 Isolation of epithelial cells from the developing gut. A: Preparation of E13.5 developing small intestines for FACS sorting. Small intestines of *Shh*^{Cre}*:Id2*$^{lox/lox}$ (*Id2*^{KO}) and *Id2*$^{lox/lox}$ (WT) embryos were mechanically disrupted, treated with collagenase, and stained for EpCAM, B: FACS sorting strategy to select small intestinal epithelial cells from E13.5 developing small intestines. After single-cell selection, the viable cells were selected based on DAPI staining. Each sample was sorted to collect 500 DAPI^{-}EpCAM^{+} cells. C: Library quality control with the size assessment.

up-regulated in *Id2*^{KO} embryos (*Pdgfa*, *Slc12a2*, *Smoc2*) (Nigmatullina *et al.*, 2017) and genes encoding transcription factors from SOX-family: *Sox2*, known to regulate the development of the stomach (Raghoebir *et al.*, 2012), *Sox17* and *Sox21*. There also was an increased expression of genes, encoding two secreted ligands of the TGF-beta (transforming growth factor-beta) superfamily of proteins: *Bmp2* and *Bmp3,* and the gene encoding a secreted Wnt family member protein *Wnt11*. In addition, *Id2*^{KO} embryos showed an increased expression of *Runx1* gene, encoding a transcription factor with previously shown tumor-suppressive function in *Apc*^{min} mice (Fijneman *et al.*, 2012). Finally, there was a compensatory enriched expression of genes encoding two other members of ID-family transcriptional regulators *Id1* and *Id3*

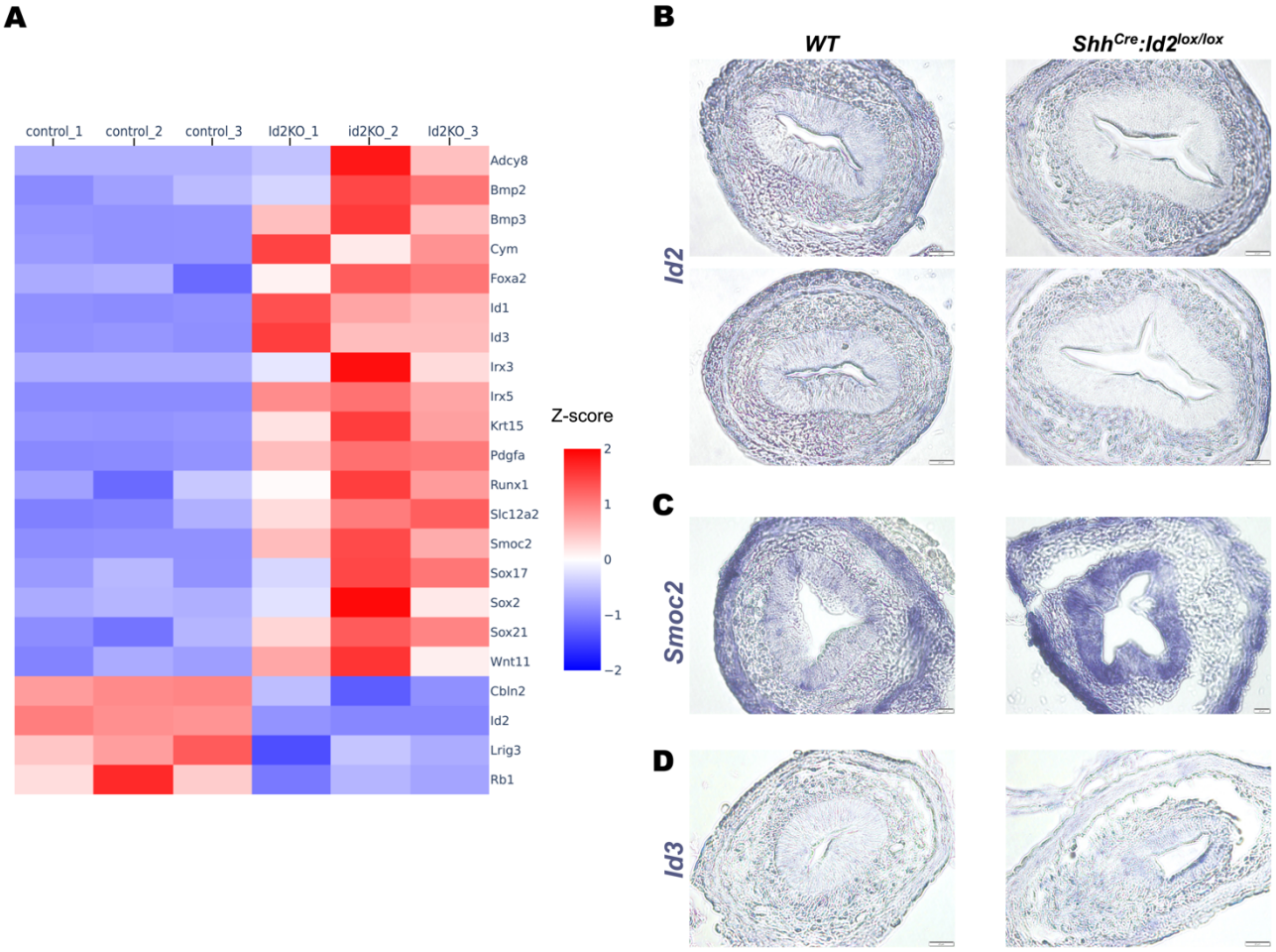

Figure 3.10 *Id2*-deficient developing small intestines display a stomach-like transcriptome signature. A: Z-score hierarchical clustering heatmap showing top up- and down-regulated genes in *Id2* mutant epithelial cells from E13.5 small intestine compared to controls. The annotation bar indicates normalized expression for each gene. B-D RNA *in situ* hybridization analyses showing the expression of *Id2* (B), *Smoc2* (C) and *Id3* (D) on transverse sections of *Shh*^{Cre}:*Id2*$^{lox/lox}$ (*Id2*^{KO}) and *Id2*$^{lox/lox}$ (WT) mouse embryos at E13.5 (n = 3 embryos analyzed). Scale bars 20 μm.

in *Id2*^{KO} embryos (Nigmatullina *et al.*, 2017) In *Id2*^{KO} embryos, the expression of 160 genes was down-regulated. Among these genes, there were *Cbln2*, which is enriched in the posterior small intestine (Zinina *et al.*, 2022), *Rb1* encoding for retinoblastoma protein, a known negative regulator of the cell cycle, and *Lrig3* - that restricts the number of stem cells in the colon (Stevenson *et al.*, 2022). The RNA *in situ* hybridization analysis confirmed the results of bulk transcriptome analysis by showing the expression of *Id2* (Figure 3.10B), *Smoc2* (Figure 3.10C), and *Id3* (Figure 3.10D) in the small intestines of *Id2*^{KO} and *WT* embryos at E13.5.

As bulk transcriptome analysis revealed an up-regulation of stem cell marker genes, I further performed EdU staining of embryonic guts from WT and *Id2*^{KO} isolated

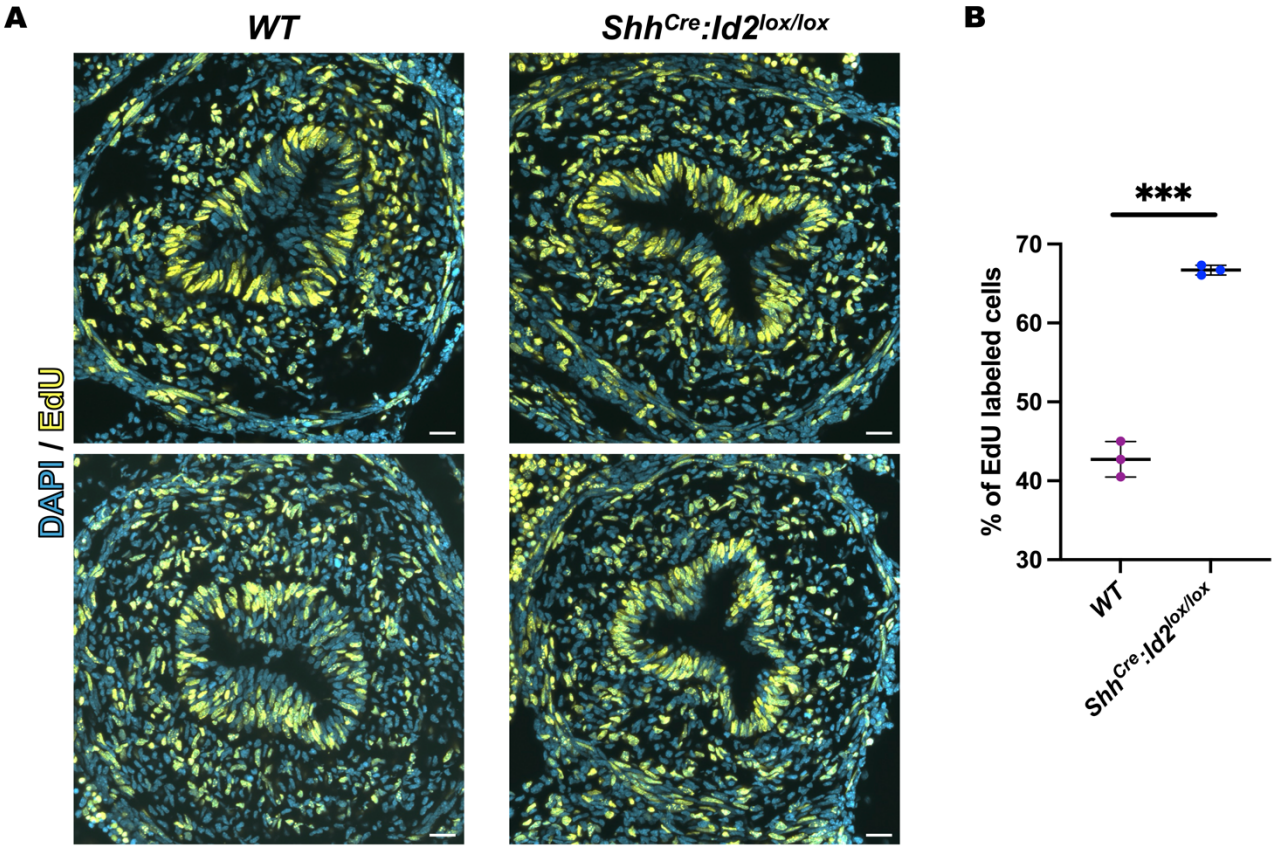

Figure 3.11 *Id2*-deficient developing small intestines display an increased number of stem cells. A: Confocal images of transverse sections of *WT* and *Shh*^{Cre}*:Id2*$^{lox/lox}$ mouse embryos at E14.5 showing EdU stained cells (yellow) (n = 3 embryos analyzed). DAPI stains nuclei (teal). Scale bar: 20 μm. B: Quantification of EdU labelled cells in the small intestinal epithelium of *WT* (magenta) and *Shh*^{Cre}*:Id2*$^{lox/lox}$ (blue) mouse embryos at E14.5. Error bars are ±SD ***P < 0.001 by two-tailed Student's t-test.

from embryos around E14.5 to compare the numbers of proliferative cells (Figure 3.11A). The quantification of EdU-stained cells revealed a significantly higher proportion of proliferative cells in *Id2*^{KO} small intestines compared to WT (Figure 3.11B). Furthermore, in agreement with the results of bulk transcriptome analysis, the middle segments of small intestines isolated from *Id2*^{KO} embryos displayed a morphology of anterior segments, where pseudostratified epithelium starts to remodel and form villus structures earlier than in posterior segments (Walton *et al.*, 2012, Chin *et al.*, 2017), which can be seen in Figure 3.11A.

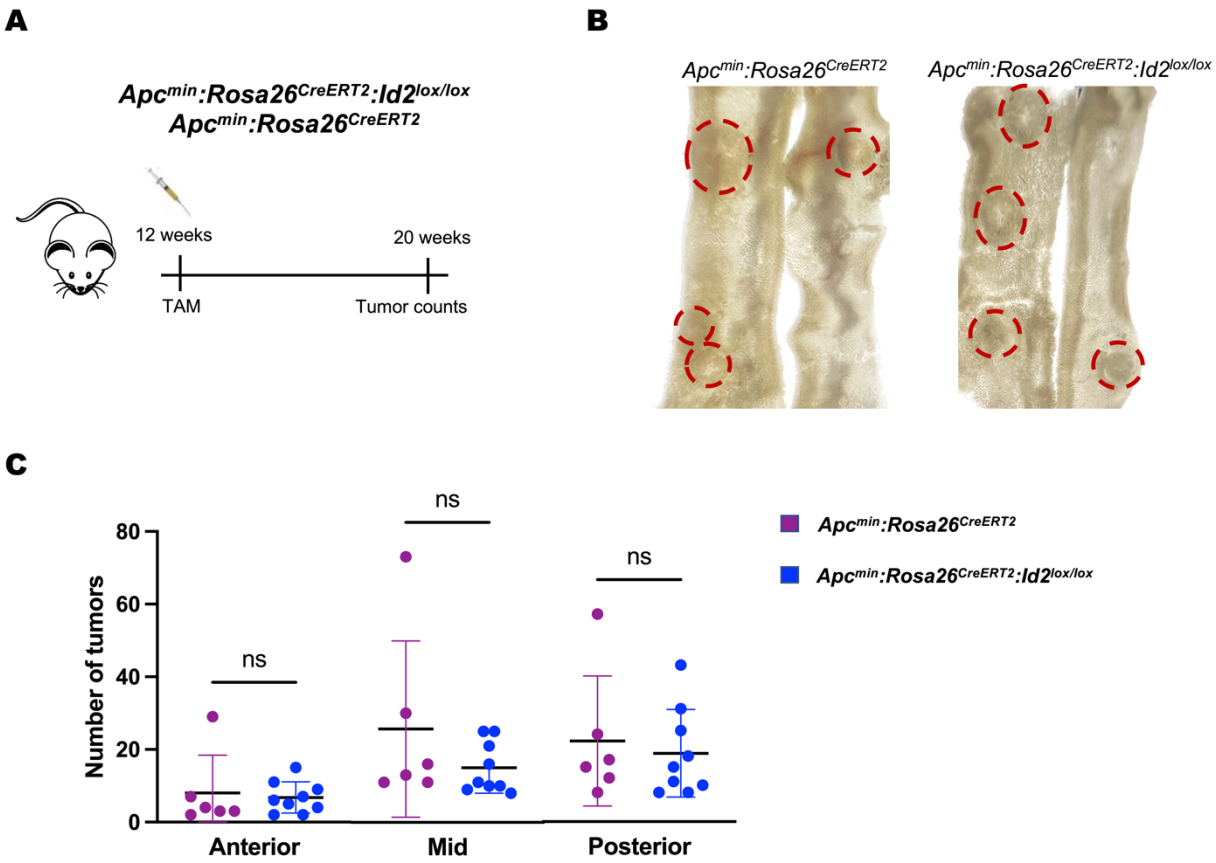

Figure 3.12 Induced *Id2*-deficiency in mice with developed small intestinal tumors. A: The experimental outline for inducing *Id2* deficiency in mice with developed tumors. Tamoxifen was given twice to *Apc*$^{min/+}$*:Rosa26*^{CreERT2}*:Id2*$^{lox/lox}$ mice, 24 hours apart, to induce Cre recombinase. *Apc*$^{min/+}$*:Rosa26*^{CreERT2} were used as controls. All mice were treated at 12 weeks old and analyzed at 20 weeks old, including small intestine dissection and tumor count. B: Dissected small intestines of *Apc*$^{min/+}$*:Rosa26*^{CreERT2} and *Apc*$^{min/+}$*:Rosa26*^{CreERT2}*:Id2*$^{lox/lox}$ mice. The dotted circles highlight the tumors. C: Tumor counts performed for *Apc*$^{min/+}$*:Rosa26*^{CreERT2} (magenta) and *Apc*$^{min/+}$*:Rosa26*^{CreERT2}*:Id2*$^{lox/lox}$ (blue) mice in the anterior (Ant), middle (Mid) and posterior (Post) parts of the small intestine. Error bars are ±SD by the Mann-Whitney test, ns stands for not significant, n=6-9 mice.

Taken together, the analysis of the developing small intestines revealed a stomach-like transcriptome signature and a higher number of stem cells in *Id2*-deficient embryos compared to WT.

3.2.3 ID2 Inhibits Differentiation of Intestinal Tumor Cells in *Apc*$^{min/+}$ Mice.

To further study the role of ID2 in tumorigenesis, I used *Apc*$^{min/+}$*:Rosa26*^{CreERT2}*:Id2*$^{lox/lox}$ mice with ubiquitously expressed *Rosa26* locus as a Cre-driver. The *Id2* loss was induced by two times tamoxifen treatment (24 hours between treatments) of *Apc*$^{min/+}$*:Rosa26*^{CreERT2}*:Id2*$^{lox/lox}$ mice and *Apc*$^{min/+}$*:Rosa26*^{CreERT2} control mice at the age of 12 weeks. The scheme of the experiment is shown in Figure 3.12A. This time point was selected because previous research (Oikarinen *et al.*, 2007) and my own experience with the mouse model has shown that *Apc*$^{min/+}$ mice show a sharp increase in the number and size of tumors after 12 weeks of age. Analysis of this timepoint allows to study the effect of *Id2* depletion in already formed tumors. The analysis of mice at 20 weeks showed no steady difference in tumor size. Both groups developed large and small tumors with similar frequencies and variations between individual animals from the same group. Figure 3.12B shows an exemplary picture of dissected intestines with tumors from *Id2*-deficient and control mice. The comparison of tumor counts did not reveal any difference between groups, as shown in Figure 3.12C, meaning that *Id2* depletion does not prevent the progression of already-formed tumors.

After conducting further histological analysis of tumors from both groups of mice, I observed a difference in tumor morphology. To assess the degree of differentiation in the tumors, I performed H&E staining and estimated the tumor grade. Pathologists use tumor grade to describe how differentiated a tumor is. Lower-grade tumors are well-differentiated, while higher-grade tumors are poorly differentiated. Upon analyzing the H&E stainings, I observed that tumors from *Id2*-deficient mice

have a lower grade, as they look more like normal well-differentiated small intestinal epithelium than control tumors (Figure 3.13A).

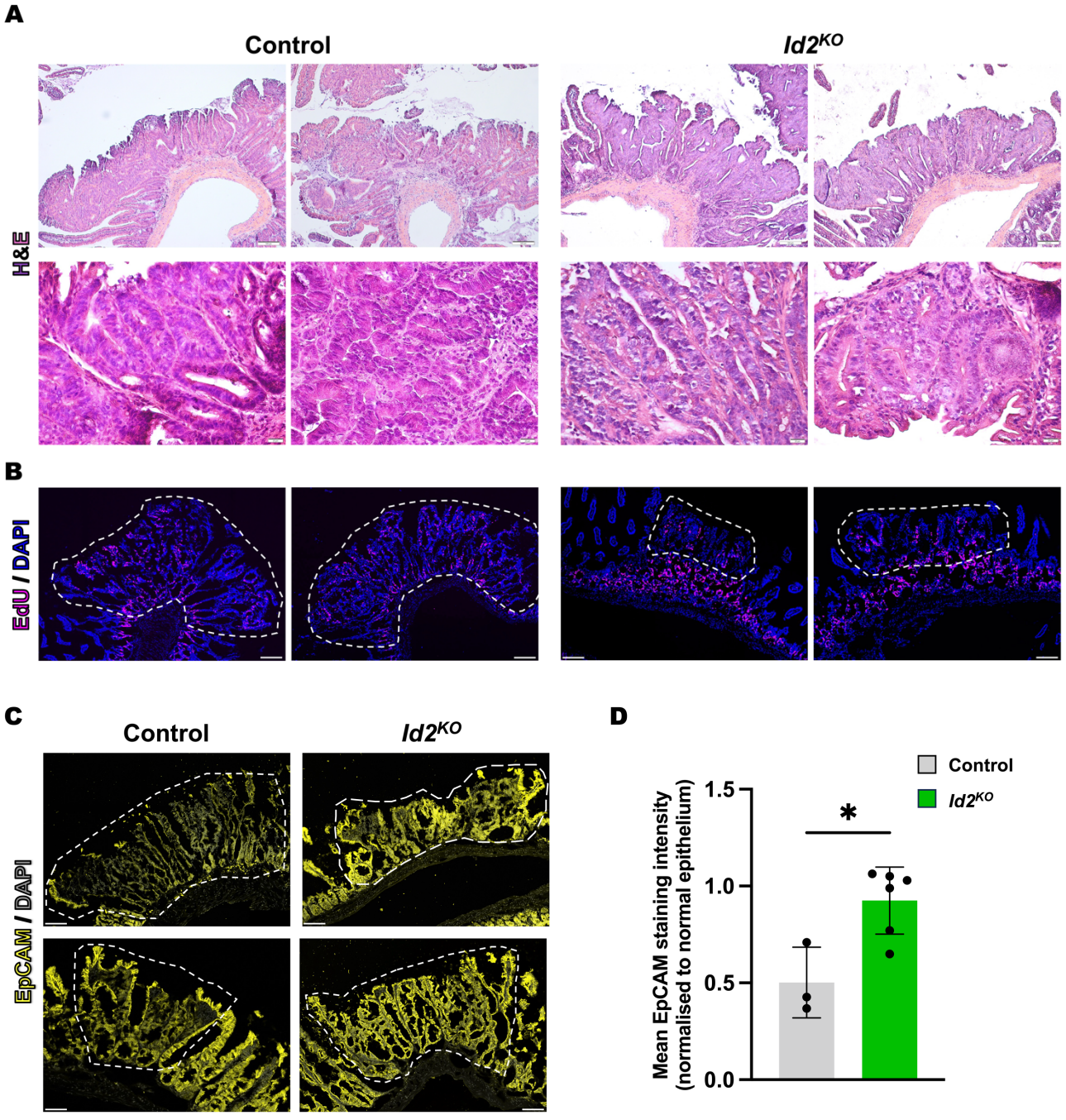

Figure legend on next page.

I additionally performed EdU staining to label proliferative cells in *Id2*-deficient and control tumors. The analysis showed that *Id2*-deficient tumors had underlying normal intestinal epithelium, distinguishable from the tumors by the presence of round, non-hyperplastic crypts. In contrast, control tumors exhibited hyperplastic crypts and lacked underlying normal epithelium (Figure 3.13B).

Furthermore, tumors that lacked *Id2* showed increased expression of *EpCAM*, as demonstrated by anti-EpCAM antibody staining on slides (Figure 3.13C) and confirmed by measuring staining intensity (Figure 3.13D) in tumors from both control and *Id2*-deficient mice. Normally, Apc^{min} tumors show lower *Epcam* expression than the normal small intestinal epithelium. Therefore, in conjunction with H&E staining analysis, higher EpCAM staining intensity suggests a lower grade of Apc^{min} tumors with *Id2* deficiency, indicating a role for ID2 in inhibiting the differentiation of tumor cells in these tumors. Additionally, EdU staining indicates that the normal intestinal epithelium underlying *Id2*-deficient tumors may substitute for tumor cells.

3.2.4 *Id2* Depletion Reduces the Clonogenicity of Small Intestinal Tumoroids.

As the $Apc^{min/+}$:$Rosa26^{CreERT2}$:$Id2^{lox/lox}$ mouse model depletes *Id2* in all cells, I additionally utilized an *ex vivo* tumoroid model system, which allows to investigate the epithelial-specific effect of *Id2* depletion in formed tumoroids. To generate tumoroids, I mechanically disrupted tumors from $Apc^{min/+}$:$Rosa26^{CreERT2}$:$Id2^{lox/lox}$ and $Apc^{min/+}$ mice and grew them in the standard organoid medium with EGF and LDN193189 (EL medium) for at least 2 weeks to ensure pure cultures of sparoid tumoroids. LDN193189 is a cost-effective alternative to Noggin and is added to the medium for

---

Figure 3.13 *Id2*-deficient $Apc^{min/+}$ tumors exhibit a lower grade. A: H&E stained small intestinal tumors from tamoxifen-treated $Apc^{min/+}$:$Rosa26^{CreERT2}$ (control) and $Apc^{min/+}$:$Rosa26^{CreERT2}$:$Id2^{lox/lox}$ (Id^{KO}) mice. *Id2*-deficient mouse tumors look more like normal small intestinal epithelium than control tumors, thus exhibiting a lower grade (n=3 mice). B: EdU staining (magenta) in tumors from tamoxifen-treated control and Id^{KO} mice. *Id2*-deficient tumors had underlying normal intestinal epithelium with round, non-hyperplastic crypts, while control tumors exhibited hyperplastic crypts. DAPI stains nuclei (blue) (n=3 mice). The boundaries of tumors are shown with a dotted line. C: EpCAM staining (yellow) in tumors from tamoxifen-treated control and Id^{KO} mice (n=3 mice). The boundaries of tumors are shown with a dotted line. D: Mean EpCAM staining intensity in tumors of control (grey) and Id^{KO} (green) mice (n=3-6 tumors) normalized to normal epithelium. Error bars are ±SD *P < 0.05 by two-tailed Student's t-test. Scale bars: 100 µm top row A, B, C; 20 µm bottom row A.

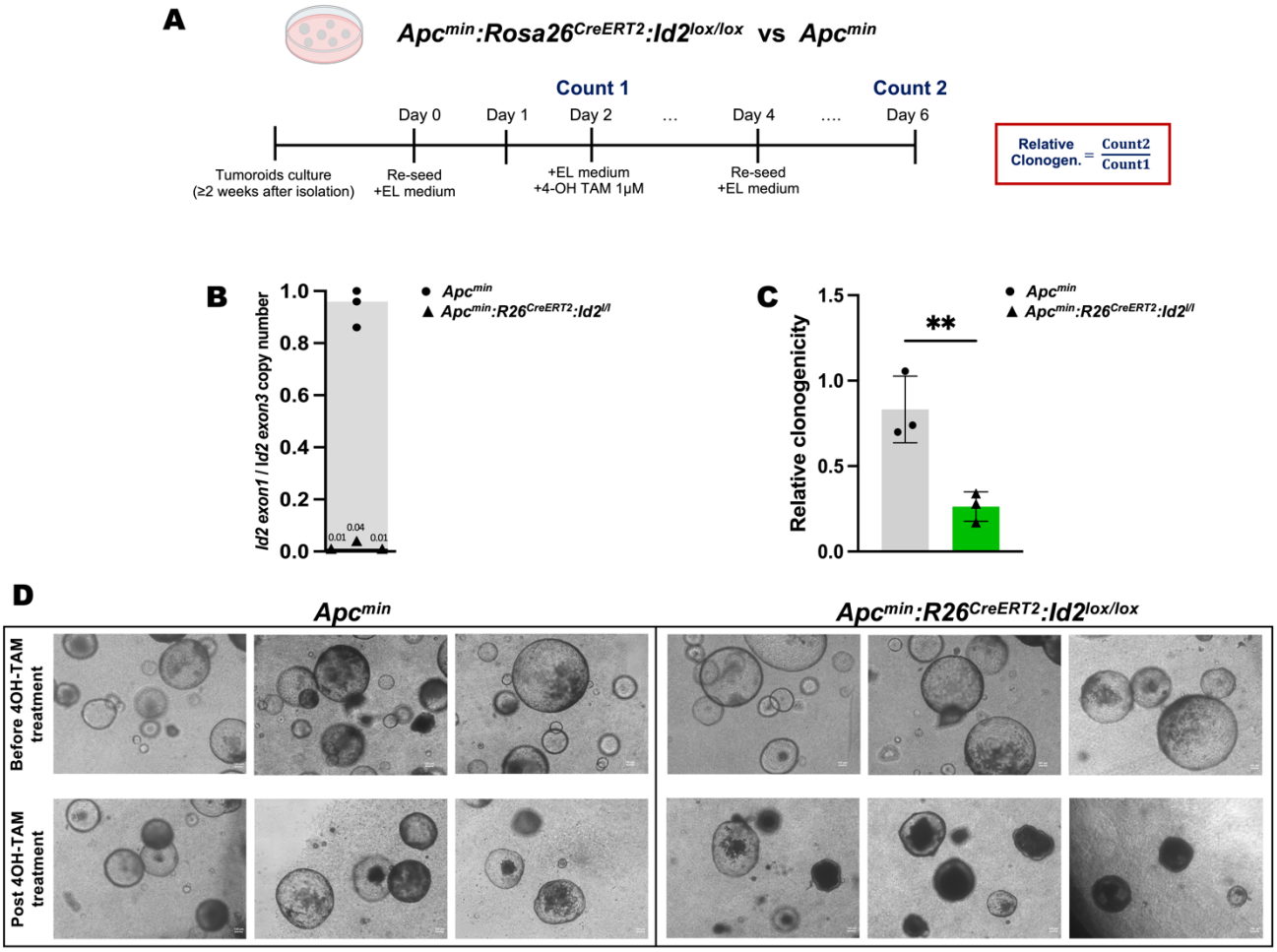

Figure 3.14 *Id2* depletion reduces the clonogenicity of small intestinal tumoroids. A: The experimental outline for inducing *Id2* deficiency in $Apc^{min/+}$:$Rosa26^{CreERT2}$:$Id2^{lox/lox}$ tumoroids. Apc^{min} tumoroids were used as controls. Tumoroids were treated with 1μM 4OH-tamoxifen for 2 days to activate Cre-recombinase. Prior to treatment, the number of tumoroids per well was counted. After treatment, the tumoroids were re-seeded and counted again after 2 days. Relative clonogenicity is the ratio of the second count to the first. B: The results of CNV analysis of *Id2* exon1 confirm the efficiency of Cre-recombination in 4OH-tamoxifen treated $Apc^{min/+}$:$Rosa26^{CreERT2}$:$Id2^{lox/lox}$ tumoroids. C: Relative clonogenicity of 4OH-tamoxifen treated $Apc^{min/+}$ (grey) and Apc^{min}:$Rosa26^{CreERT2}$:$Id2^{lox/lox}$ (green) tumoroids. Error bars are ±SD **P < 0.01 by two-tailed Student's t-test, n=3 mice. D: Imaging of $Apc^{min/+}$ and Apc^{min}:$Rosa26^{CreERT2}$:$Id2^{lox/lox}$ tumoroids before (top row) and after (bottom row) 4OH-tamoxifen treatment; n=3 mice; scale bar 100 μm.

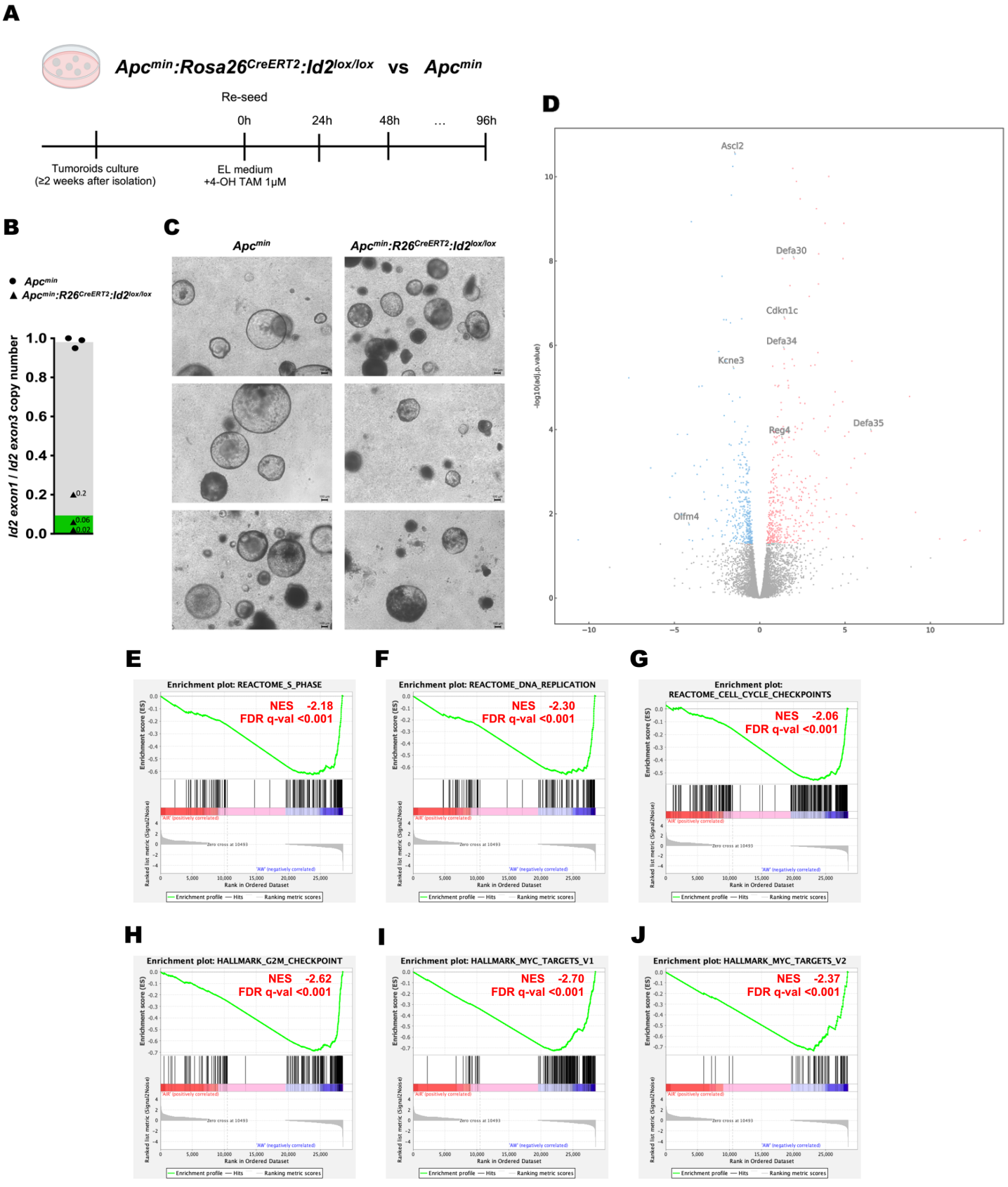

Figure legend on next page.

BMP signaling inhibition. The addition of R-spondin is unnecessary since *Apc*-deficient tumoroids have constitutively active Wnt signaling, and culture in an R-spondin-free medium allows for their selection.

To investigate how the deletion of *Id2* affects the clonogenic capacity of tumoroids, I treated them with 1μM 4OH-tamoxifen for 2 days to activate Cre-recombinase in *Apc*$^{min/+}$*:Rosa26*^{CreERT2}*:Id2*$^{lox/lox}$ tumoroids. Before the treatment, I counted the number of tumoroids per well. After the treatment, I re-seeded and counted them again after another 2 days. To determine the relative clonogenicity, the second count was divided by the first to obtain a ratio. The steps of the experiment are summarized in Figure 3.14A. I established the working concentration of 4OH-tamoxifen to be sufficient for efficient recombination, confirmed by CNV analysis of *Id2* exon1 (Figure 3.14B). The analysis of performed counts revealed a significant reduction in clonogenic capacity for *Apc*^{min} *Id2*-deficient tumoroids compared to *Apc*^{min} (Figure 3.14C). Imaging before and after treatment showed that *Id2* depletion resulted in smaller tumoroid size, reduced transparency, and less defined spheroid structure in *Apc*^{min} *Id2*-deficient tumoroids, while control *Apc*^{min} tumoroids were unaffected by the treatment (Figure 3.14D).

To understand the molecular changes that caused the reduction of the clonogenic capacity, I performed bulk transcriptome analysis of treated *Apc*$^{min/+}$*:Rosa26*^{CreERT2}*:Id2*$^{lox/lox}$ and *Apc*^{min} tumoroids. Two groups of tumoroids were grown in EL medium with 1μM 4OH-tamoxifen for four days. The treatment time was

---

Figure 3.15 Tumoroids with *Id2* depletion show a reduced expression of stem cell marker genes. A: The experimental outline for inducing *Id2* deficiency in *Apc*$^{min/+}$*:Rosa26*^{CreERT2}*:Id2*$^{lox/lox}$ tumoroids. *Apc*^{min} tumoroids were used as controls. Tumoroids were treated with 1μM 4OH-tamoxifen for 4 days to activate Cre-recombinase. After treatment, tumoroids were collected for transcriptome analysis. B: The results of CNV analysis of *Id2* exon1 confirm the efficiency of Cre-recombination in 4OH-tamoxifen treated *Apc*$^{min/+}$*:Rosa26*^{CreERT2}*:Id2*$^{lox/lox}$ tumoroids. C: Imaging of *Apc*$^{min/+}$ and *Apc*^{min}*:Rosa26*^{CreERT2}*:Id2*$^{lox/lox}$ tumoroids after 4OH-tamoxifen treatment; n=3 mice; scale bar 100 μm. D: Volcano plot of differentially expressed genes identified between the *Apc*^{min}*:Id2*^{KO} vs *Apc*$^{min/+}$ tumoroids. The blue dots denote down-regulated gene expression, the red dots denote up-regulated gene expression, and the grey dots denote the gene expression with an FDR>0.05. E-H: GSEA enrichment plots for top decreased sets from Reactome (E-G) and Hallmark (H-J) collections in *Apc*^{min}*:Id2*^{KO} vs *Apc*$^{min/+}$ tumoroids. E- S-phase, F- DNA-replication, G- cell cycle checkpoints, H- G2M checkpoint, I- MYC targets v1, J- MYC targets v2. NES stands for Normalized Enrichment Score; FDR stands for False Discovery Rate.

extended due to a higher seeding density than the clonogenic assay. The experiment's scheme is shown in Figure 3.15A. After 96 hours of treatment, the CNV analysis of *Id2* exon1 was performed to ensure efficient recombination (Figure 3.15B). Both groups of tumoroids were imaged post-treatment. In accordance with the results of the clonogenic assay, *Apc*$^{min/+}$*:Rosa26*^{CreERT2}*:Id2*$^{lox/lox}$ tumoroids formed fewer, smaller, and less defined spheroids compared to *Apc*$^{min/+}$ tumoroids (Figure 3.15C).

Comparative transcriptome analysis of *Apc*$^{min/+}$*:Rosa26*^{CreERT2}*:Id2*$^{lox/lox}$ and *Apc*^{min} tumoroids revealed 388 differentially expressed genes (|log2FC|≥ *1*, FDR<0.05). 249 genes were up-regulated in *Apc*$^{min/+}$*:Rosa26*^{CreERT2}*:Id2*$^{lox/lox}$ tumoroids. Among them were *Cyclin-dependent kinase inhibitor 1C* (*Cdkn1c*), a cell cycle inhibitor, and genes that are specifically expressed in mature intestinal cell populations, such as Paneth (*Defa30*, *Defa34*, *Defa35*) and enteroendocrine cells (*Regenerating islet-derived family member 4*, *Reg4*, which is most abundant in goblet and Paneth cells, according to Zinina *et al.*, 2022). Among 139 down-regulated genes

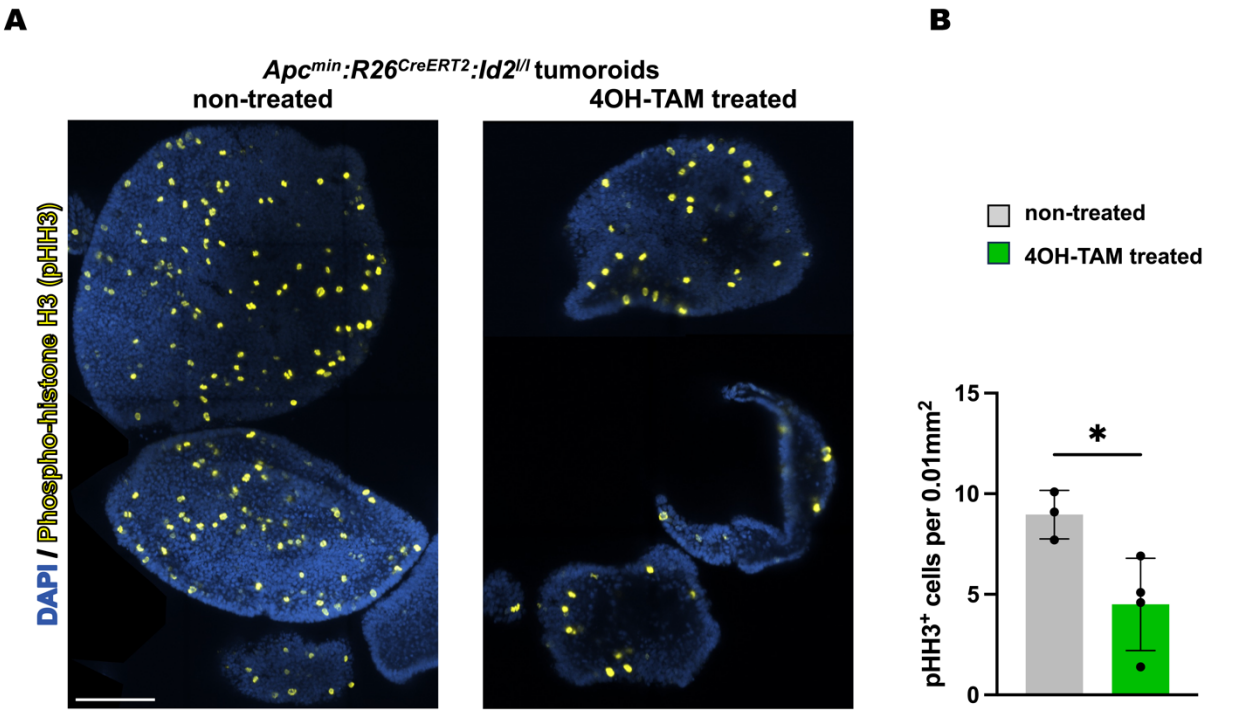

Figure 3.16 *Id2* depletion reduces the number of proliferating cells in *Apc*$^{min/+}$ tumoroids. A: Phospho-histone H3 (pHH3) staining (yellow) in non-treated (left) and 4OH-tamoxifen-treated (right) *Apc*$^{min/+}$*:Rosa26*^{CreERT2}*:Id2*$^{lox/lox}$ tumoroids. DAPI stains nuclei (blue). Scale bar 100 µm. B: Quantification of Phospho-histone H3 (pHH3)-stained cells in non-treated (grey) and 4OH-tamoxifen-treated (green) *Apc*$^{min/+}$*:Rosa26*^{CreERT2}*:Id2*$^{lox/lox}$ tumoroids. Error bars are ±SD *P < 0.05 by two-tailed Student's t-test, n=3-4 tumoroids.

are markers of stem cells, such as *Ascl2*, *Olfm4*, *Kcne3*. The results of bulk transcriptome analysis are presented on the volcano plot in Figure 3.15D. In addition, I conducted Gene Set Enrichment Analysis (GSEA) and found that there was a decrease in the expression of Reactome gene sets that are associated with regulating S-phase (Figure 3.15E), DNA replication (Figure 3.15F), and cell cycle checkpoints (Figure 3.15G), as well as Hallmark gene set related to regulating the G2M checkpoint (Figure 3.15H) in $Id2^{KO}$ tumoroids. Furthermore, GSEA indicated a decrease in the expression of Hallmark gene sets associated with MYC target genes in $Id2^{KO}$ tumoroids (Figure 3.15I-J), consistent with findings from Biyajima *et al.* (2015). Their study demonstrated that *Id2* deficiency led to reduced c-MYC protein levels and increased mRNA levels of its antagonist, *Mxd1*, in the ileal crypts of $Apc^{\Delta 716}$ mice.

To verify the results of bulk transcriptome analysis, I performed immuno-fluorescent staining of 4OH-tamoxifen treated and non-treated $Apc^{min/+}$:$Rosa26^{CreERT2}$:$Id2^{lox/lox}$ tumoroids against phospho-histone H3 (pHH3) to image cells undergoing M-phase of cell cycle (Figure 3.16A). The number of $pHH3^{+}$ cells was reduced in 4OH-tamoxifen-treated $Apc^{min/+}$:$Rosa26^{CreERT2}$:$Id2^{lox/lox}$ tumoroids compared to untreated ones (Figure 3.16B).

Taken together, the depletion of *Id2* in $Apc^{min/+}$ tumoroids significantly reduces their clonogenic capacity and alters gene expression, notably decreasing the expression of stem cell markers, cell cycle regulators, and MYC target genes while increasing the expression of genes specific to mature intestinal cells.

3.2.5 ID2 is Necessary for Tumorigenesis in Small Intestinal Epithelium: Insights from CRISPR-Cas9 Genome Editing of Intestinal Organoids.

I have shown the effect of *Id2* depletion on tumors *in vivo* and *in vitro* on tumoroids. However, it remains unclear if ID2 is necessary for tumor initiation. To answer this question, I established CRISPR-Cas9 genome editing on small intestinal organoids to generate clones with *Apc* and *Id2* loss-of-function mutations. For this, I isolated small intestinal organoids from $Rosa26^{Cas9EGFP}$ mice and cultured them on ELR medium additionally supplied with CHIR, GSK3β inhibitor, to activate Wnt signaling and enrich cultures with stem cells. CHIR pre-treated $Rosa^{Cas9EGFP}$ organoids formed spheroids already after 3 days of treatment. After 7 days of treatment, I transduced organoids with lentivirus expressing gRNA targeting the *Apc* gene and *Id2*

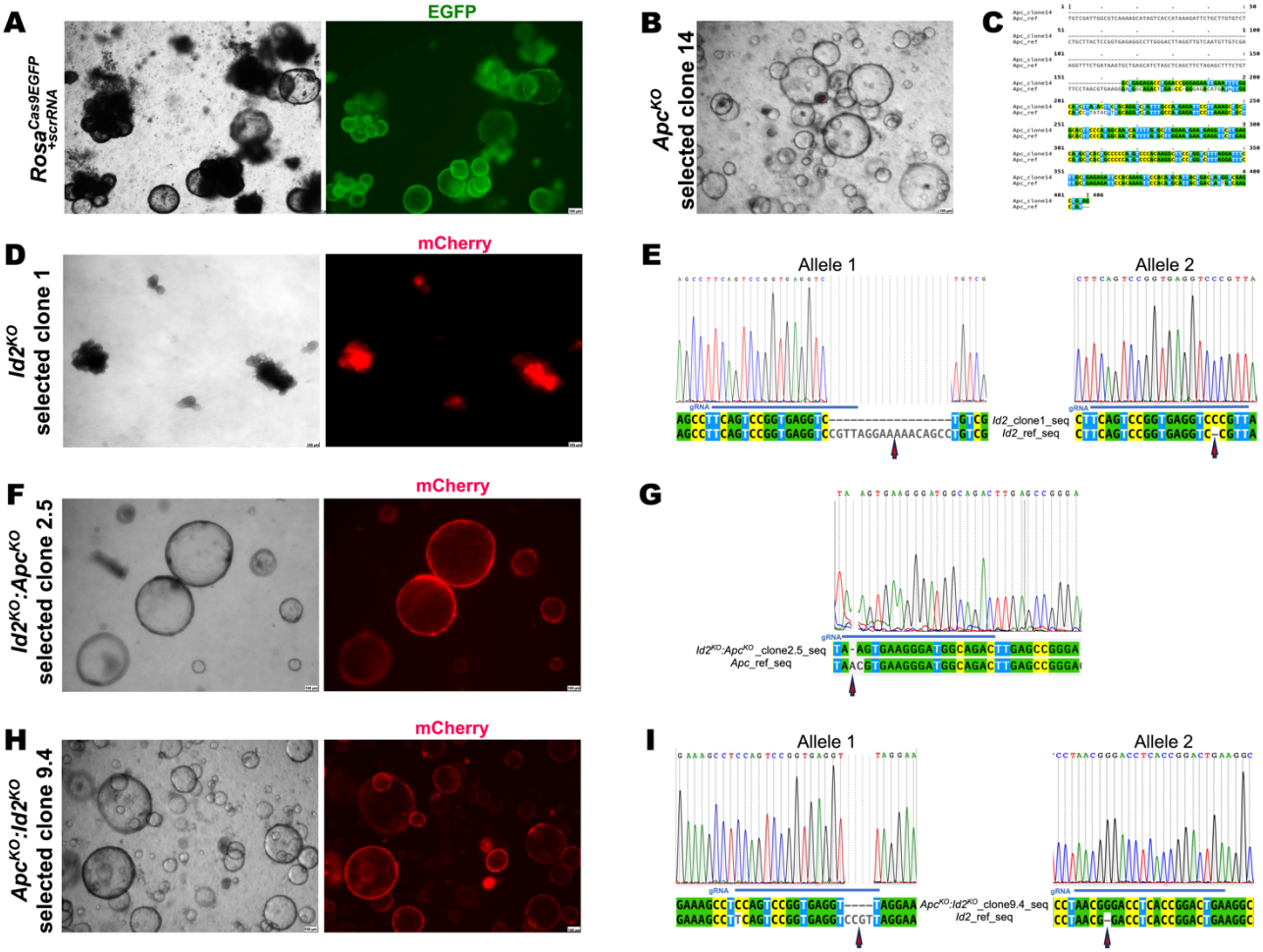

Figure 3.17 Generation of CRISPR-Cas9-mediated *Apc*^{KO}, *Id2*^{KO}, *Apc*^{KO}*:Id2*^{KO}, *Id2*^{KO}*:Apc*^{KO} clones. A: Brightfield (left) and fluorescent (right) images of generated *Rosa*$^{Cas9EGFP+scrRNA}$ organoids. Organoids obtained by transduction of *Rosa*^{Cas9EGFP} organoids with lentivirus expressing scrambled gRNA. B: Brightfield image of generated and selected *Apc*^{KO} clone 14. Organoids obtained by transduction of *Rosa*^{Cas9EGFP} organoids with lentivirus expressing gRNA targeting the *Apc* gene. C: Sanger sequence verifying *Apc* loss-of-function mutation in homozygous *Apc*^{KO} clone 14. D: Brightfield (left) and fluorescent (right) images of generated and selected *Id2*^{KO} clone 1. Organoids obtained by transduction of *Rosa*^{Cas9EGFP} organoids with lentivirus expressing gRNA targeting the *Id2* gene and expressing mCherry-reporter. E: Sanger sequence verifying *Id2* loss-of-function mutation for both alleles in heterozygous *Id2*^{KO} clone 1. F: Brightfield (left) and fluorescent (right) images of generated and selected *Id2*^{KO}*:Apc*^{KO} clone 2.5. Organoids obtained by transduction of *Id2*^{KO} organoids with lentivirus expressing gRNA targeting the *Apc* gene. G: Sanger sequence verifying *Apc* loss-of-function mutation in homozygous *Id2*^{KO}*:Apc*^{KO} clone 2.5. H: Brightfield (left) and fluorescent (right) images of generated and selected *Apc*^{KO}*:Id2*^{KO} clone 9.4. Organoids obtained by transduction of *Apc*^{KO} organoids with lentivirus expressing gRNA targeting the *Id2* gene and expressing mCherry-reporter. I: Sanger sequence verifying *Id2* loss-of-function mutation for both alleles in heterozygous *Apc*^{KO}*:Id2*^{KO} clone 9.4. Scale bar in A-B, D, F, H: 100 µm.

gene to generate loss-of-function mutants. To serve as a control, I used lentivirus expressing scrambled gRNA to transduce organoids and selected them on ELR medium supplied with the selective antibiotic. Figure 3.17A shows *Rosa*$^{Cas9EGFP+scrRNA}$ organoids 7 days after transduction and selection. *Apc* gRNA-transduced organoids were selected on EL-medium without R-spondin1 supplied with the selective antibiotic to ensure the survival of *Apc* loss-of-function mutants. After one month of selection, I performed a single-clone selection when pure cultures of spheroid tumoroids were generated. *Apc* loss-of-function was confirmed by Sanger sequencing of both alleles. The selected clone 14 (Figure 3.17B) had a large deletion of over 150 nucleotides downstream gRNA sequence (Figure 3.17C). *Id2* gRNA-transduced organoids were selected on ELR medium supplied with the selective antibiotic. Transduction efficiency was controlled by the expression of mCherry-reporter contained in the vector. Several selected clones were sent for Sanger sequencing to verify *Id2* loss-of-function alleles.

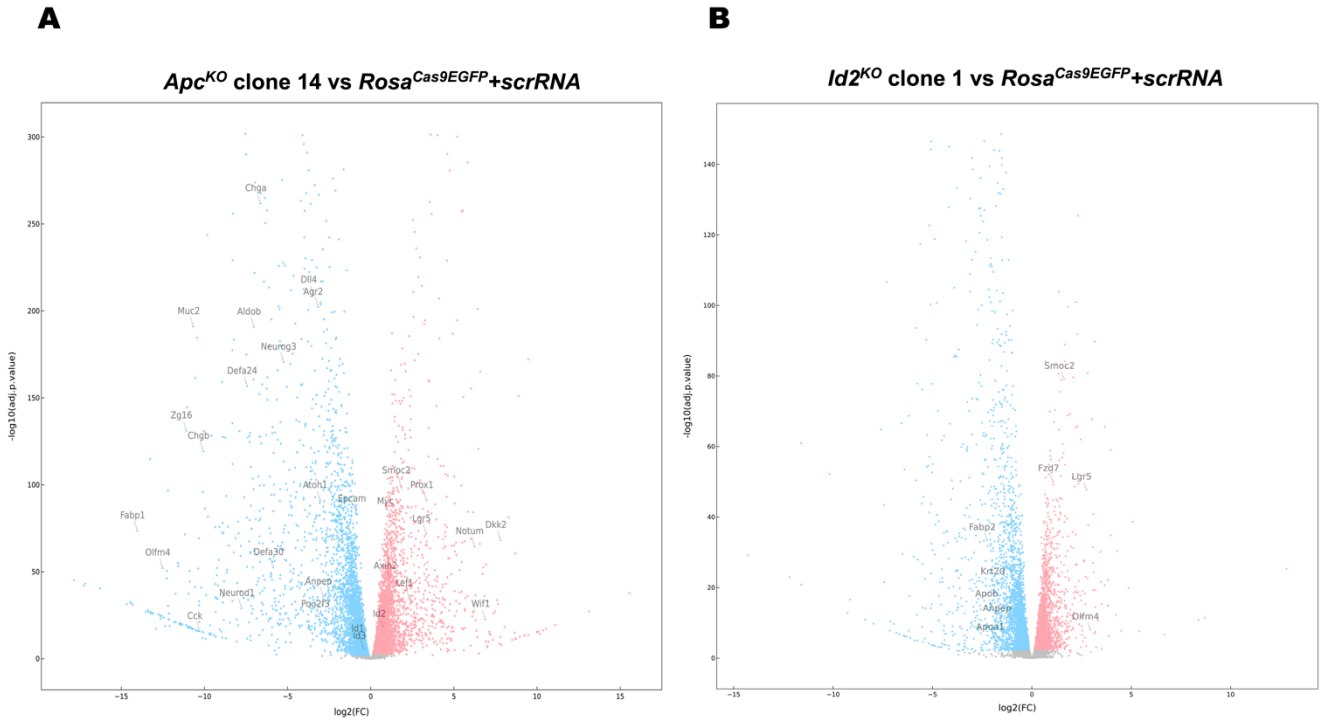

Figure 3.18 Bulk transcriptome analysis of *Apc*^{KO} clone 14 and *Id2*^{KO} clone 1. A: Volcano plot of differentially expressed genes identified between the *Apc*^{KO} vs *Rosa*$^{Cas9EGFP+scrRNA}$ organoids. The blue dots denote down-regulated gene expression, the red dots denote up-regulated gene expression, and the grey dots denote the gene expression with an FDR>0.05. B: Volcano plot of differentially expressed genes identified between the *Id2*^{KO} vs *Rosa*$^{Cas9EGFP+scrRNA}$ organoids. The blue dots denote down-regulated gene expression, the red dots denote up-regulated gene expression, and the grey dots denote the gene expression with an FDR>0.05.

The selected clone 1 (Figure 3.17D) had a confirmed frame-shift mutation for both alleles (Figure 3.17E).

In a comparative bulk transcriptome analysis of *Apc*^{KO} clone 14 and *Rosa*$^{Cas9EGFP+scrRNA}$ organoids, 3630 differentially expressed genes were identified (|log2FC|≥ 1, FDR<0.01). Of these, 1551 genes were enriched, and 2079 genes were lost in *Apc*^{KO} clone 14 (Figure 3.18A). Among the enriched genes were Wnt signaling target genes, including *Lgr5*, *Axin2*, *Myc*, *Prox1, Lef1*. *Prox1* has previously been shown to promote tumor progression, while *Lef1* has been found to be induced after *Apc* deletion in small intestinal stem cells (Heino *et al.*, 2021). *Smoc2*, a stem cell marker gene and BMP antagonist, was also upregulated in *Apc*^{KO} tumoroids. Additionally, the expression of three other Wnt target coding genes – *Dkk2* (223 times),

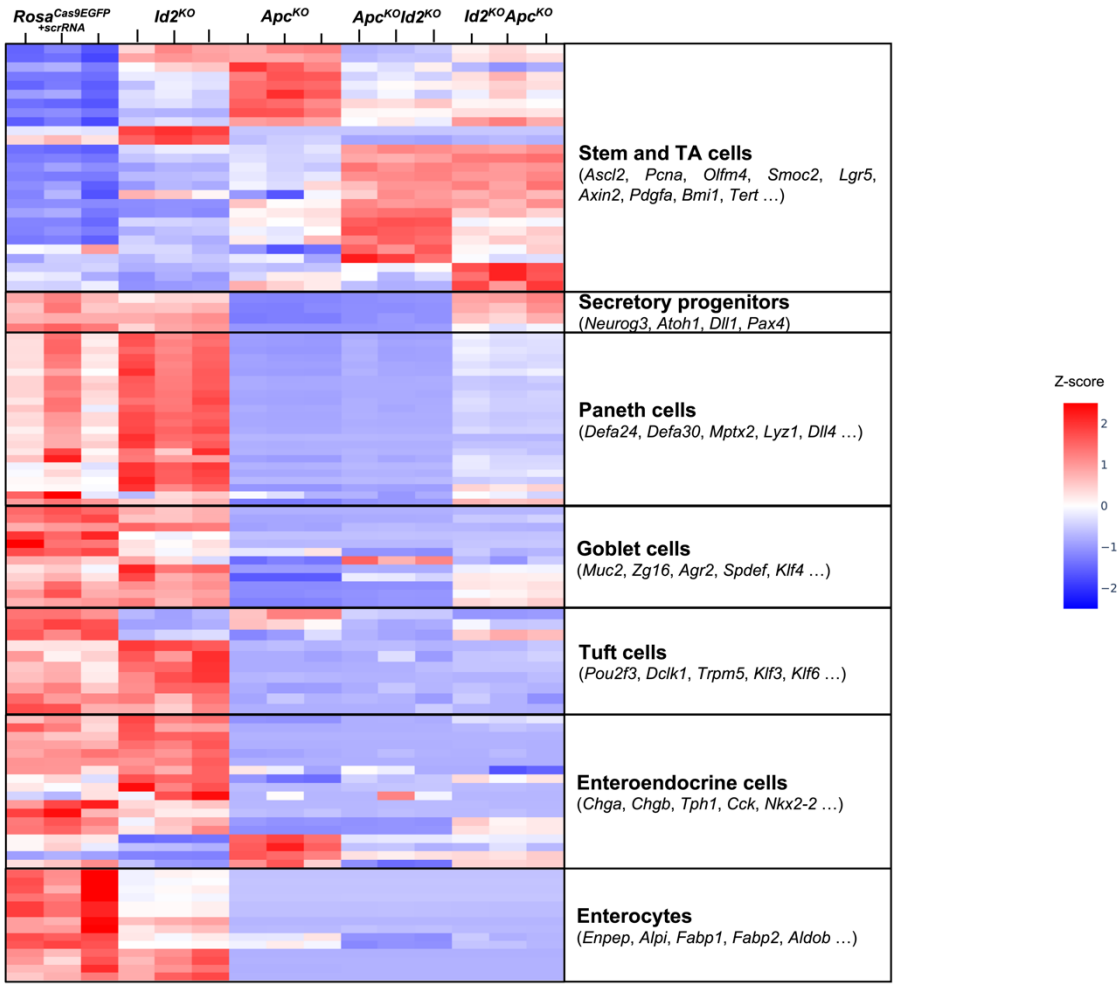

Figure 3.19 Z-score hierarchical clustering heatmap visualization displaying the expression of various marker genes for different small intestinal populations in *Rosa*$^{Cas9EGFP+scrRNA}$, *Id2*^{KO}, *Apc*^{KO}, *Apc*^{KO}*:Id2*^{KO}, *Id2*^{KO}*:Apc*^{KO} organoids; colors represent scaled expression values, with blue for low expression and red for the high expression levels.

Notum (75 times), and *Wif1* (117 times) - was upregulated in Apc^{KO} tumoroids. These genes code for negative regulators of Wnt signaling, which have been previously shown to be overexpressed in intestinal tumors and inhibit the proliferation of neighboring wild-type crypts (Flanagan *et al.*, 2021, van Neerven *et al.*, 2021). In agreement with my previous results, *Id2* expression was 1.72 times upregulated in Apc^{KO} tumoroids, while two other ID-family members, *Id1* and *Id3,* showed a reduced expression (1.43 and 1.31 times, respectively). Among other down-regulated genes were *Epcam*, markers of mature intestinal epithelial cells, such as enterocytes (*Aldob*, *Anpep, Fabp1, Fabp2*), enteroendocrine cells (*Neurog3, Neurod1, Chga, Chgb, Cck*), goblet cells (*Muc2*, *Zg16, Agr2*), Paneth cells (*Dll4*, *Lyz1*, *Defa*), tuft cells (*Pou2f3*) and common secretory progenitors (*Atoh1*). It is worth noting that the *Olfm4* stem cell marker gene was down-regulated, consistent with the previous study indicating that OLFM4 has oncosuppressive function (Liu *et al.*, 2016). In summary, the comparative bulk transcriptome analysis reveals that Apc^{KO} clone 14 displays a distinct molecular signature, characterized by upregulated Wnt signaling target genes and downregulated markers of mature intestinal epithelial cells. Additionally, the significant upregulation of negative regulators of Wnt signaling, such as *Dkk2*, *Notum*, and *Wif1*, even in monocultures of tumoroids, highlights the impact of *Apc* deletion. The increased expression of *Id2* in Apc^{KO} tumoroids confirms its oncogenic role.

In a comparative bulk transcriptome analysis of $Id2^{KO}$ clone 1 and $Rosa^{Cas9EGFP+scrRNA}$ organoids, 1749 differentially expressed genes were identified ($|\log2FC| \geq 1$, FDR<0.01, Figure 3.18B). Of these, 544 genes were enriched, and 1205 genes were lost in $Id2^{KO}$ clone 1. Among upregulated genes were stem cell markers *Lgr5, Smoc2, Olfm4, Fzd7*. Enterocyte markers (*Anpep*, *Apoa1*, *Apob*, *Fabp2*) and intestinal keratins, including *Krt20*, significantly expressed in villi (Mun *et al.*, 2022), were down-regulated.

To determine if ID2 is necessary for tumorigenesis, the chosen clone 1 of $Id2^{KO}$ was transduced with lentivirus expressing gRNA targeting the *Apc* gene. After more than two weeks of being cultured on a selective EL medium, spheroid tumoroids were formed. The expression of mCherry-reporter verified the efficiency of the transduction. However, it's worth noting that the first spheroid tumoroids from $Id2^{KO}$ organoids transduced with lentivirus expressing *Apc* gRNA occurred as late as after 10 days of culture on a selective medium. This is a longer time than $Rosa^{Cas9EGFP}$ organoids, transduced with lentivirus expressing *Apc* gRNA, which formed sparoids

already after 3 days of selection on EL medium supplied with the antibiotic. This means that ID2 is important for tumorigenesis, as well as to promote tumoroids growth. Generated clones were analysed by Sanger sequencing to ensure frame-shift mutation for both alleles. Selected clone *Id2*^{KO}*:Apc*^{KO} 2.5 (Figure 3.17F) had verified *Apc* loss-of-function mutation for both alleles (Figure 3.17G). In parallel, I also generated *Apc*^{KO}*:Id2*^{KO} tumoroids by transduction of *Apc*^{KO} clone 14 with lentivirus expressing gRNA targeting the *Apc* gene. Selected clone *Apc*^{KO}*:Id2*^{KO} 9.4 (Figure 3.17H) was analysed by Sanger sequencing and had a confirmed frame-shift mutation for both *Id2* alleles (Figure 3.17I). The first *Apc*^{KO}*:Id2*^{KO} sparoids were formed already after 3 days of selection on EL medium supplied with the antibiotic, albeit at a slightly lower density than *Apc*^{KO}.

Considering that fewer *Id2*^{KO}*:Apc*^{KO} clones formed and after a significantly longer time than was observed with *Apc*^{KO} clone generation, I conclude that ID2 is necessary for tumorigenesis in the small intestinal epithelium.

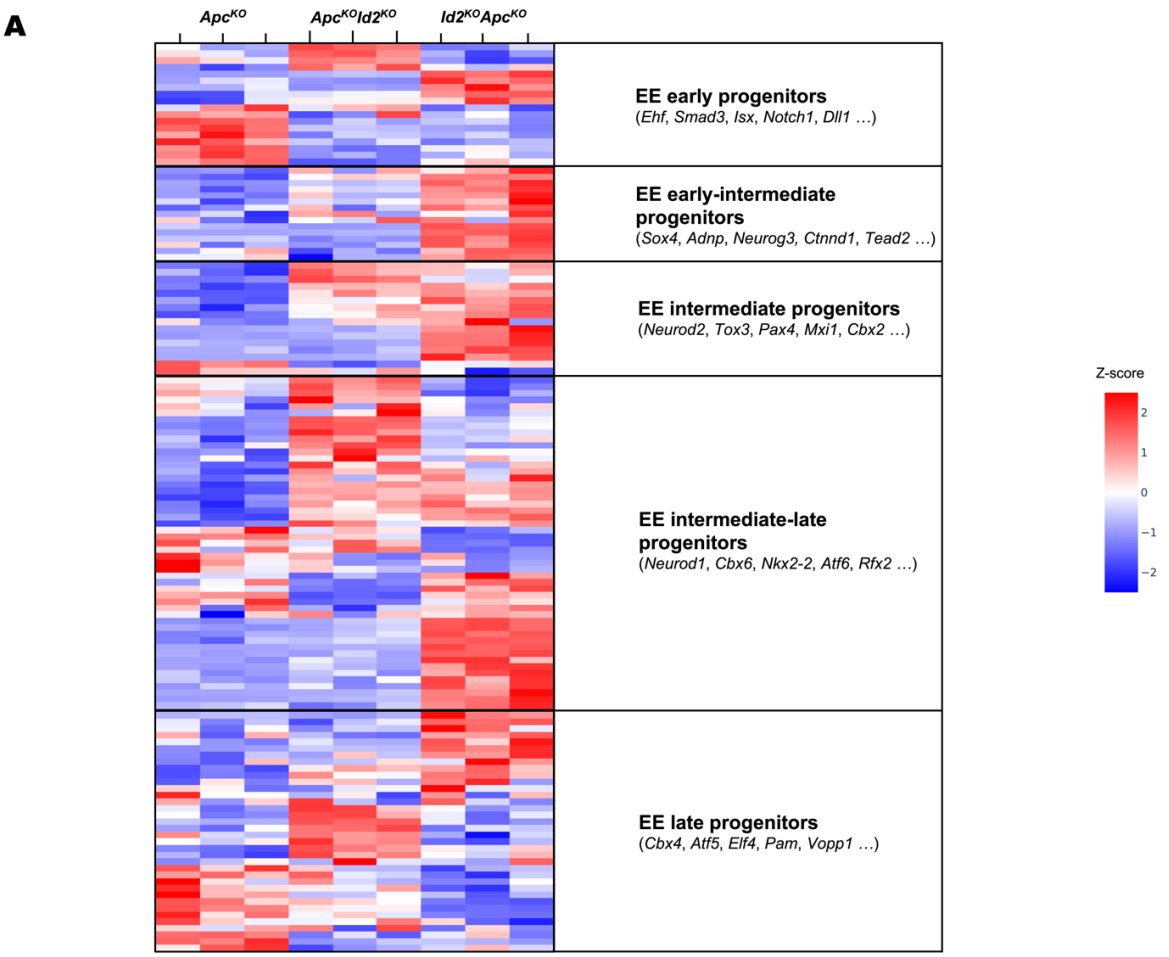

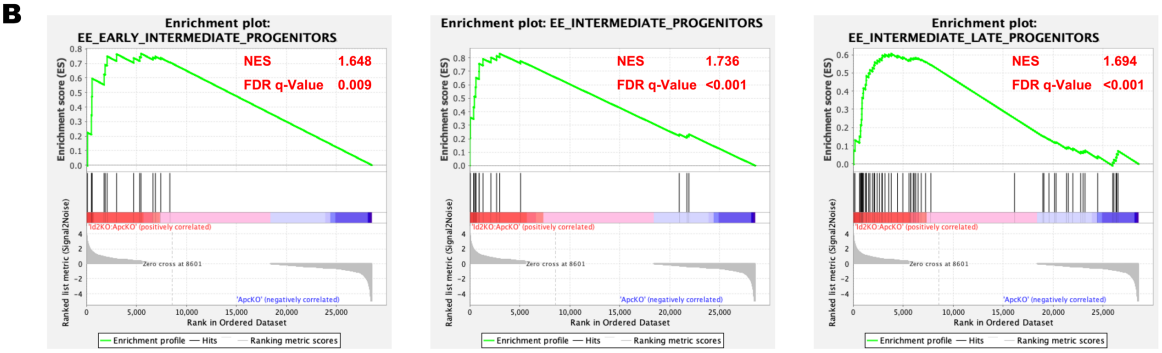

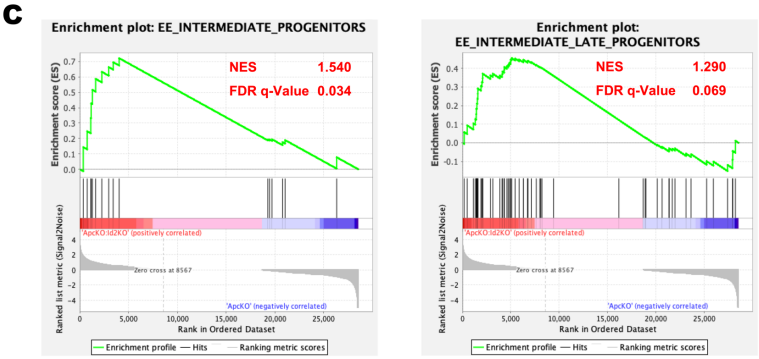

Figure legend on next page.

3.2.6 ID2 Prevents Differentiation of Intestinal Cancer Stem Cells.

I conducted a bulk transcriptome analysis of selected clones to study the molecular signature of two types of organoids - *Id2KO* organoids with knocked-out *Apc* and Apc^{KO} tumoroids with knocked-out *Id2*. I examined the expression of signature genes of various cell populations in all the clones generated by CRISPR-Cas9 to reveal their differential expression. The analysis revealed that $Id2^{KO}$:Apc^{KO} tumoroids showed increased expression of secretory progenitor marker genes compared to Apc^{KO} and Apc^{KO}:$Id2^{KO}$ (Figure 3.19). The best-characterized secretory progenitors are enteroendocrine (EE) progenitors, due to the study by Gehart *et al.* (2019), who performed a time-resolved transcriptome analysis of EE lineage. Therefore, I checked the expression of early and late enteroendocrine progenitor markers, determined by Gehart *et al.* (2019), in Apc^{KO}, Apc^{KO}:$Id2^{KO}$, and $Id2^{KO}$:Apc^{KO} tumoroids. The results showed that $Id2^{KO}$:Apc^{KO} tumoroids enriched early-intermediate, intermediate and intermediate-late EE progenitors (Figure 3.20A). To confirm this observation, I performed Gene Set Enrichment Analysis (GSEA), which confirmed 1.6-time enrichment of early-intermediate progenitors, 1.7-time enrichment of intermediate, and intermediate-late EE progenitors in $Id2^{KO}$:Apc^{KO} tumoroids over Apc^{KO} (Figure 3.20B). GSEA analysis also showed a slight enrichment of intermediate and intermediate-late progenitors in Apc^{KO}:$Id2^{KO}$ compared to Apc^{KO} (1.5 and 1.3 times, respectively, Figure 3.20C). It can be inferred from the results that ID2 is necessary to prevent the differentiation of cancer stem cells.

To investigate whether progenitor cells can differentiate into mature secretory populations, I conducted an experiment where I cultured Apc^{KO}, Apc^{KO}:$Id2^{KO}$, and $Id2^{KO}$:Apc^{KO} tumoroids in ERo medium for two days to induce differentiation towards secretory lineage. Afterwards, I assessed the expression of genes specific to mature secretory cell populations. The experiment plan is shown in Figure 3.21A. Imaging of

---

Figure 3.20 Tumoroids generated from *Id2*-deficient organoids show an increased expression of EE progenitor marker genes. A: Z-score hierarchical clustering heatmap visualization displaying the expression of EE progenitors in Apc^{KO}, ApcKO:Id2KO, and $Id2^{KO}$:Apc^{KO} organoids; colors represent scaled expression values, with blue for low expression and red for the high expression levels. B: GSEA enrichment plots for enriched sets of early-intermediate, intermediate and intermediate-late EE progenitor marker genes in $Id2^{KO}$:Apc^{KO} vs Apc^{KO}. C: GSEA enrichment plots for enriched sets of intermediate and intermediate-late EE progenitor marker genes in Apc^{KO}:$Id2^{KO}$ vs Apc^{KO}. NES stands for Normalized Enrichment Score; FDR stands for False Discovery Rate.

the tumoroids before and after being cultured in a conditional ERo medium showed that while the *Apc*^{KO} tumoroids were unaffected by the treatment, *Apc*^{KO}*:Id2*^{KO} and *Id2*^{KO}*:Apc*^{KO} tumoroids showed reduced transparency and a broken spheroid structure, as shown in Figure 3.21B. Based on the results of the quantitative reverse-transcription PCR (qRT-PCR) analysis showed an induced expression of *Nts*, N-cell marker (Figure 3.21C), and *Sct*, expressed in almost all enteroendocrine cells (Figure 3.21D), in *Apc*^{KO}*:Id2*^{KO} and *Id2*^{KO}*:Apc*^{KO} tumoroids over *Apc*^{KO} tumoroids.

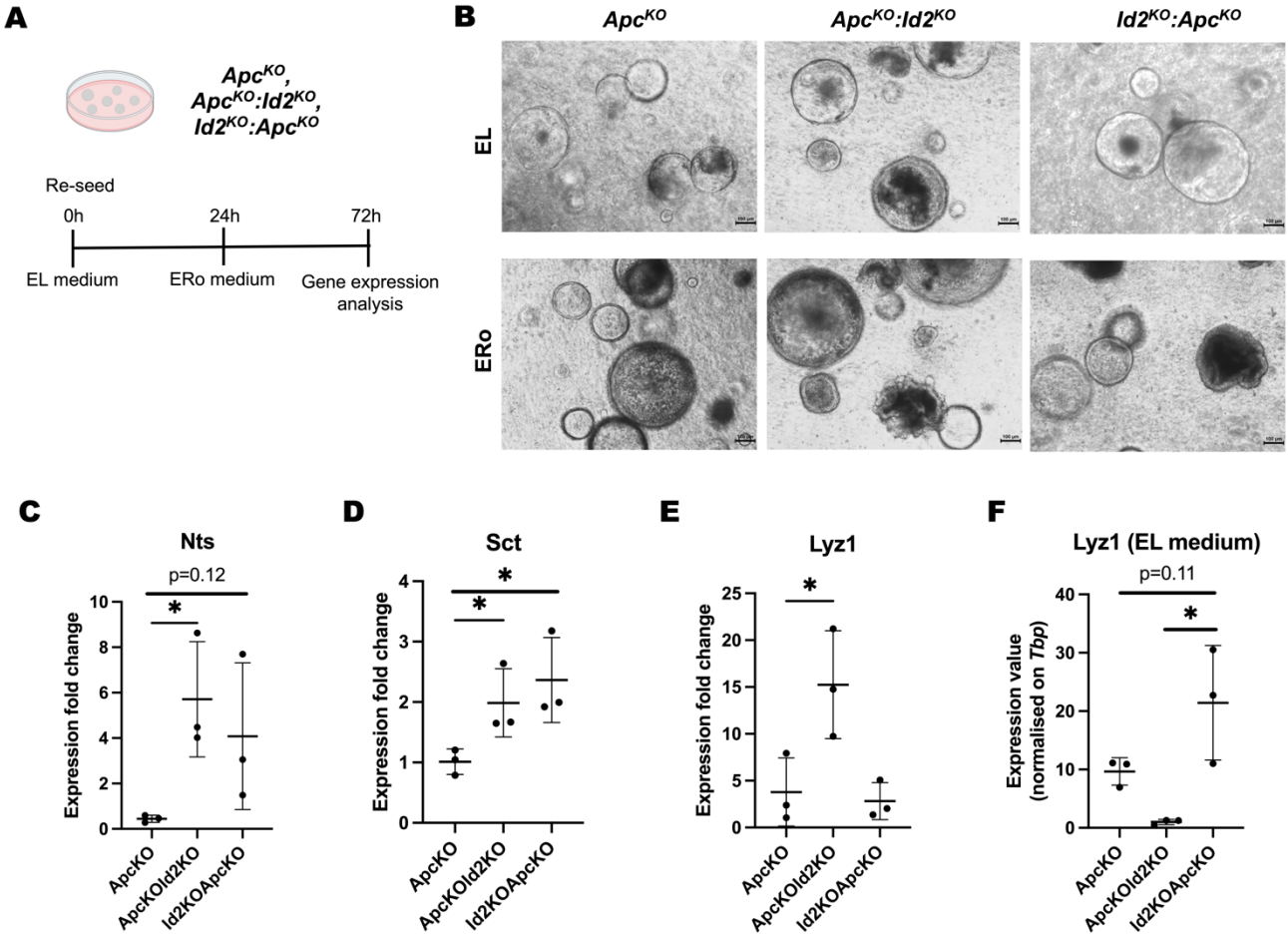

Figure 3.21 *Id2* depletion induces differentiation of intestinal cancer stem cells. A: The experimental outline for inducing secretory lineage differentiation in *Apc*^{KO}, *Apc*^{KO}*:Id2*^{KO} and *Id2*^{KO}*:Apc*^{KO} tumoroids. Tumoroids were cultured in ERo conditional medium for 2 days before being collected for gene expression analysis. B: Imaging of *Apc*^{KO}, *Apc*^{KO}*:Id2*^{KO} and *Id2*^{KO}*:Apc*^{KO} tumoroids in standard EL tumoroid medium (top row) and after 2 days of culture in ERo conditional medium (bottom row); n=3 technical replicates; scale bar 100 µm. C-F qRT-PCR analysis showing expression of *Nts* (C), *Sct* (D), *Lyz1* (E) after 2 days of culture in ERo medium and *Lyz1* after culture in EL medium (F).

The expression of *Lyz1*, a Paneth cell marker, was only induced in Apc^{KO}:$Id2^{KO}$ tumoroids, but not in $Id2^{KO}$:Apc^{KO} tumoroids (Figure 3.21E). This could be because the expression of *Lyz1* in $Id2^{KO}$:Apc^{KO} tumoroids was already high in the standard tumoroid medium (Figure 3.21F); also, other Paneth cell marker expression was enriched in $Id2^{KO}$:Apc^{KO} tumoroids, as shown on the heat-map in Figure 3.19 and separately shown for tumoroids only in Figure 3.22A. Gene Set Enrichment Analysis (GSEA) confirmed the enrichment of Paneth cell marker gene set expression in $Id2^{KO}$:Apc^{KO} tumoroids over Apc^{KO} tumoroids (NES 2.2), and the enrichment of Paneth cell marker gene set expression in Apc^{KO}:$Id2^{KO}$ tumoroids compared to Apc^{KO} tumoroids (NES 1.4; Figure 3.22B).

Together, these results suggest that the depletion of *Id2* in Apc^{KO} tumoroids induces differentiation, fostering the emergence of enteroendocrine-like and Paneth-like cells, thereby highlighting the critical role of ID2 in maintaining tumor cells in an undifferentiated state.

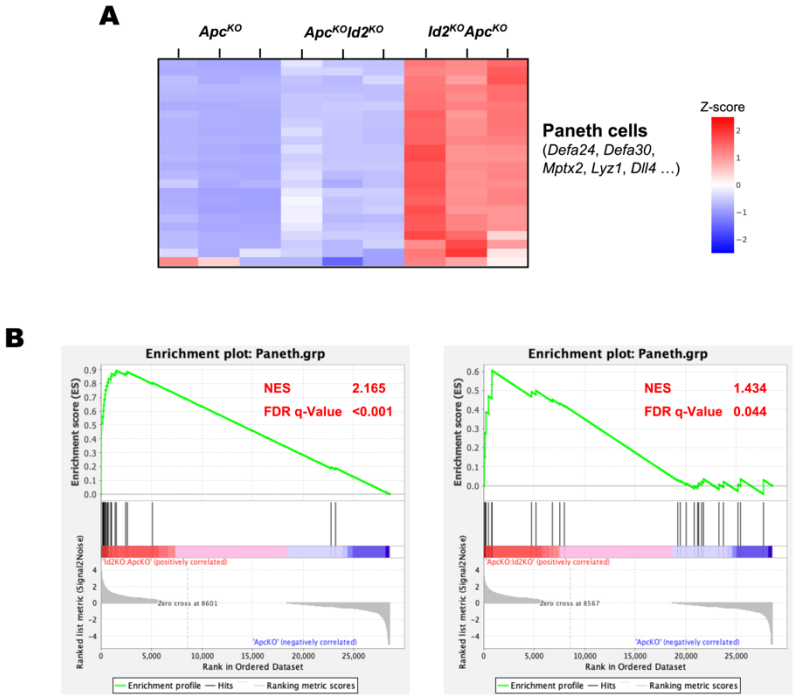

Figure 3.22 Tumoroids generated from *Id2*-deficient organoids show an increased expression of Paneth cell marker genes. A: Z-score hierarchical clustering heatmap visualization displaying the expression of Paneth cell marker genes in Apc^{KO}, ApcKO:Id2KO, and $Id2^{KO}$:Apc^{KO} tumoroids; colors represent scaled expression values, with blue for low expression and red for the high expression levels. B: GSEA enrichment plots for the set of Paneth cell marker genes in $Id2^{KO}$:Apc^{KO} vs Apc^{KO} tumoroids (left plot) and Apc^{KO}:$Id2^{KO}$ vs Apc^{KO} tumoroids (right plot). NES stands for Normalized Enrichment Score; FDR stands for False Discovery Rate.

4. DISCUSSIONS

4.1 The Role of ID2 in the Differentiation of Secretory Lineages in the Mouse Small Intestinal Epithelium.

ID2 is well-known for specifying embryonic intestinal stem cell progenitors (Nigmatullina *et al.*, 2017). However, its function in adult secretory intestinal epithelial progenitors has not been studied. My research has uncovered specific functions of ID2 in determining the fate of secretory progenitors. Firstly, ID2 prevents secretory progenitors from differentiating into tuft cells. Secondly, ID2 is crucial in mediating BMP signalling during the differentiation of L and I cells into $PYY^{+}NTS^{+}$ N cells. Additionally, ID2 inhibits the differentiation of $GHRL^{+}$ X cells and $Serotonin^{+}$ ($5\text{-}HT^{+}$) enterochromaffin cells in the ileum. This ensures that these cell types are distributed in a gradient along the anterior-posterior axis of the gut.

It is important to note that when discussing the first function of ID2, which is to restrict the differentiation towards tuft cell lineage, scRNA-sequencing did not reveal *Id2* expression in the tuft cell cluster. Moreover, the lineage tracing experiment did not show a higher capacity of $Id2^{+}$ progenitors to differentiate into tuft cells. These results indicate that ID2 functions in secretory epithelial progenitors rather than in mature tuft cells to restrict the commitment towards tuft cell fate. The mechanism of this regulation remains to be further researched. Previous studies have shown that ID2 is a direct target of BMP signaling, which is involved in tuft cell expansion induced by IL-13. A recent study conducted by Lindholm *et al.* in 2022 revealed that IL-13 triggers the BMP pathway, which in turn acts as a negative feedback mechanism to regulate immune type 2-driven tuft cell hyperplasia. This feedback loop involves suppressing the expression of *Sox4* to potentially limit the tuft cell progenitor population. The study found that blocking the BMP signaling with the inhibitor dorsomorphin homolog 1 (DMH1) resulted in greater tuft cell numbers both *in vitro*, in the small intestinal organoids, and *in vivo*, as it interrupted the feedback mechanism. Based on these findings, I hypothesise that ID2 may play a role in regulating the BMP-mediated process that controls tuft cell differentiation.

In the anterior jejunum, approximately 10% of the epithelial cells express *Id2*. These include secretory and enterocyte progenitors, as well as differentiated goblet cells and enterocytes. However, enteroendocrine cells express *Id2* at a higher level,

with around 40% of them showing strong expression. It's worth noting that *Id2* expression varies between different types of enteroendocrine cells. As demonstrated by Beumer *et al.* in 2018, some hormone expression is regulated by BMP signaling. In my research, *Id2* expression was shown to correlate with the expression of hormones, sensitive to the BMP signaling induction. Thus, *Sct* expression, which is upregulated when stimulated by BMP, correlates with *Id2* expression. Furthermore, while a significant number of CCK^+ I cells or NTS^+ N cells show *Id2* positivity, SST^+ D cells and GIP^+ K cells do not.

Based on the results of lineage tracing, it has been found that cells expressing *Id2* have higher levels of CHGA, CCK, and 5-HT, nearly five times higher than those that do not express *Id2*. Additionally, PYY and NTS are expressed at frequencies ten times higher in *Id2*-positive cells. These results are consistent with the reduced numbers of $CHGA^+$ and PYY^+NTS^+ cells observed after the loss of *Id2*. Mechanistically, as demonstrated by organoid assay, ID2 acts downstream of BMP signaling to mediate the differentiation of N cells. In contrast to Ncells, the number of 5-HT^+ enterochromaffin cells remains unchanged upon losing *Id2* in the anterior and middle small intestine. This suggests that other ID family members, such as ID1 and ID3, may compensate for ID2's functions.

Some enteroendocrine cell populations showed no decrease upon loss of *Id2* and were even increased, but only in a specific part of the small intestine. Thus, in the absence of *Id2*, the number of Serotonin+ enterochromaffin cells in the posterior small intestine increased to the levels found in the middle. Moreover, the number of $GHRL^+$ X cells was found to be higher in both the mid and posterior parts of the small intestine of *Id2* mutant mice than in wild-type mice. Both enterochromaffin and X cells are distributed in the anterior-posterior gradient along the small intestine, with the highest number in the anterior and the lowest number in the posterior small intestine. These findings suggest that ID2 serves another purpose, namely to maintain the gradient distribution of enterochromaffin and X cells by preventing their differentiation in the posterior small intestine. In other words, ID2 acts as a posteriorizing factor. This is consistent with previous research (Mori *et al.*, 2018; Mori *et al.*, 2019) and with the results of my transcriptome analysis of *Id2*-deficient embryos. The analysis revealed that there was an increased expression of the genes known to be expressed in stomach endoderm in *Id2*-deficient embryos, including *Cym*, *Irx3*, *Irx5*, *Krt15*, *Foxa2*, and *Adcy8* (Houweling *et al.*, 2001; Sherwood *et al.*, 2009; Lloyd *et al.*, 1995;

Monaghan *et al*., 1993; Visel, 2004) when compared to control embryos. It is also worth noting that the expression of *Id2* is not uniform along the anterior-posterior axis of the small intestine. *Id2*-positive cells are more abundant in the anterior small intestine and decrease towards the posterior end. This suggests that ID2 not only regulates BMP signaling gradient along the crypt-villus axis, ensuring proper differentiation of crypt L and I cells towards villi N cells, but also affects the distribution of BMP signals along the anterior-posterior gradient.

To sum up, my research demonstrates that ID2 plays a crucial role in the appropriate specification and differentiation of enteroendocrine and tuft cells. I suggest that ID2 acts as a posteriorizing factor, creating a differentiation gradient for enterochromaffin and X cells along the small intestinal anterior-posterior axis. By regulating BMP signaling, ID2 aids in establishing a crypt-villi gradient, which is crucial for differentiating L and I cells towards N cell type. The functions of ID2 for gut homeostasis are summarized in Figure 4.1. These findings provide valuable insights into how enteroendocrine cells differentiate during gut homeostasis and the potential mechanisms involved that may be relevant for studying metabolic disorders.

4.2 The Oncogenic Role of ID2 in the Small Intestinal Epithelium.

Only a few studies have been conducted on the role of ID2 in the formation of tumors in the small intestine of Apc^{min} mice. Previous studies used mouse models with a constitutive knockout of *Id2*, which is not ideal. In this study, I demonstrated *Id2* expression in Apc^{min} small intestinal tumors using RNA *in situ* hybridization. I also showed that ID2 has an oncogenic function in the small intestinal epithelium of Apc^{min} mice. ID2 is necessary for the small intestinal epithelium to promote oncogenesis, and its deletion during early embryogenesis significantly reduces tumor numbers. In the formed tumors, ID2 functions to support the undifferentiated state and clonogenicity.

I utilized a mouse model (Apc^{min}:Shh^{Cre}:$Id2^{lox/lox}$) that allows the depletion of *Id2* in the epithelium of the small intestine of Apc^{min} mice. The results showed that the *Id2*-deficient mice had significantly fewer tumors, particularly in the middle and posterior thirds of the small intestine. This result confirms the oncogenic function of ID2 in Apc^{min} mice and, importantly, demonstrates that it functions in the small intestinal epithelium to promote tumorigenesis.

Two possibilities were considered to understand the reduction in tumor numbers. Firstly, ID2 may be necessary for tumorigenesis, and its deletion in early embryogenesis can prevent this event. Secondly, ID2 might not prevent small intestinal tumor formation but rather promote progression in already formed tumors, with its deletion preventing the expansion of clones with *Apc* LOH. Previous studies have shown that *Id2* is expressed in the intestine as early as E9.0 (Dzama *et al.*, 2017; Nowotschin *et al.*, 2019). In Apc^{min}:Shh^{Cre}:$Id2^{lox/lox}$ mice, Cre recombinase activity was detected at E9.5 and spread throughout the entire intestinal epithelium by E11.5, allowing depletion of *Id2* during early embryogenesis. However, this does not clarify if ID2 promotes oncogenesis since the timing of *Apc* LOH is unknown. Some studies using chemical carcinogens or anti-inflammatory drugs (Shoemaker *et al.*, 1995; Sansom *et al.*, 2001) suggest adenoma formation during embryonic development, but the exact stage remains unidentified. The reduction in tumor numbers in Apc^{min}:Shh^{Cre}:$Id2^{lox/lox}$ mice may result from either failure in tumor formation or the inability of formed tumors to progress without ID2. Therefore, to investigate if ID2 is necessary for tumor formation, I generated CRISPR-Cas9-mediated $Id2^{KO}$ organoids and further knocked out the *Apc* gene. Although I could generate clones, it is worth noting that only a few clones were produced after being cultured in a selective medium for over a week. This result demonstrated the function of ID2 in promoting tumorigenesis.

ID2 functions as a posteriorizing factor during gut development (discussed in Chapter 4.1). Critical developmental events and cell specifications of the gastrointestinal tract are regulated by mesenchymal-epithelial interactions (Zhao *et al.*, 2022). The analysis of transverse sections of developing small intestines with epithelial-specific deletion of *Id2* at E14.5 confirmed the anteriorization of the small intestine upon *Id2*-deficiency. Specifically, the villi formation process was determined at this stage in the middle small intestines of Shh^{Cre}:$Id2^{lox/lox}$ mice but not control, and according to the previous studies, the villi formation typically occurs around E14.5 starting from the anterior small intestine (discussed in chapter 1.4). As *Id2* was not deleted in the mesenchyme, these results confirm its function in the small intestinal epithelium when regulating the proper anterior-posterior specification of the small intestine.

The results of my transcriptome analysis of the developing small intestines at E13.5 showed an increased expression of stem cell marker genes in *Id2*-deficient

(*Shh*^{Cre}*:Id2*$^{lox/lox}$) embryos, as *Pdgfa*, *Slc12a2* and *Smoc2*. I compared the number of proliferating cells in *Shh*^{Cre}*:Id2*$^{lox/lox}$ and control developing guts and verified that increased expression of stem cell marker genes was due to their increased number in *Shh*^{Cre}*:Id2*$^{lox/lox}$ embryos. These results demonstrate the epithelial function of ID2 in restricting the number of stem cells in the developing guts.

To understand the role of ID2 in formed tumors, I induced *Id2*-deletion in *Apc*^{min} mice when tumors were already present at the age of 12 weeks. The analysis revealed that *Id2*-deficient tumors were of a lower grade compared to those in *Apc*^{min} mice, as shown by H&E staining and confirmed by the increased intensity of EpCAM staining in *Id2*-deficient tumors. However, there was no decrease in the number of tumors observed in mice with induced *Id2*-deficiency. This means that only the deletion of *Id2* during early embryogenesis has an effect on tumor numbers, while the deletion of *Id2* later after tumor formation only lowers tumor progression.

I verified the *in vivo* findings through the *in vitro* experiments. Tumoroids with induced *Id2* depletion showed reduced clonogenicity. Transcriptome analysis showed a reduced expression of stem cell marker genes such as *Olfm4*, *Ascl2*, and *Kcne3*, but significantly increased expression of mature secretory populations that normally do not present in tumoroids like Paneth cells (*Defa30*, *Defa34*, *Defa35* and *Reg4*). The GSEA analysis confirmed a decreased proliferation, and the analysis of hallmark pathways showed that Myc and its target transcripts were decreased in *Apc*^{min} *Id2*-deficient tumoroids compared to *Apc*^{min} ones, which is consistent with the previous study of Biyajima *et al.*, 2015. Together, these results show the opposite effect of *Id2* deletion on tumors and neighboring normal epithelium. While in tumors it results in a reduced number of proliferating cells, in the normal epithelium, it increases the number of proliferating cells, confirmed by the transcriptome analysis of the developing guts and transcriptome analysis of CRISPR-Cas9 generated *Id2*^{KO} organoids, which showed the increased expression of stem cell markers such as *Lgr5*, *Smoc2*, *Olfm4*, and *Fzd7*. Increased expression of Wnt target genes, such as *Lgr5* (7-fold) and *Fzd7* (2-fold), suggests that the *Id2*-deficient small intestinal epithelium may resist the secretion of Wnt inhibitors by tumor cells. This resistance could allow normal epithelial cells to outcompete cancer cells, leading to a lower tumor grade in *Id2*-deficient tissues. This competitive advantage implies that the cancer cells might be substituted by normal epithelium, contributing to reduced tumor progression in the absence of ID2. The result of EdU staining in tumors with induced *Id2* deficiency supports this

hypothesis, as it revealed normal epithelium underlying *Id2*-deficient tumors, suggesting the substitution of tumor cells by normal epithelium.

To further validate this hypothesis, additional experiments are required. Van Neerven *et al*. (2022) have established a protocol for studying cell competition *in vitro*. The protocol involves performing two parallel co-cultures: $Id2^{KO}$ organoids + $Id2^{KO}Apc^{KO}$ tumoroids and WT organoids + Apc^{KO} tumoroids as control. $Id2^{KO}$ organoids, Apc^{KO}, and $Id2^{KO}Apc^{KO}$ tumoroids can be generated using CRISPR-Cas9. Lentiviruses are used for the transduction of vectors, which express *Apc* targeting gRNA and *Id2* targeting gRNA. These lentiviruses must express different reporters, for instance, GFP in *Apc* vector and mCherry in *Id2* vector. WT organoids should be transduced with lentiviruses expressing scrRNA and mCherry reporter. The expression of different reporters in tumoroids and co-cultured organoids allows for further analysis using fluorescent microscopy with quantification of organoids and tumoroids, or quantification by FACS. A higher percentage of mCherry-expressing cells in the *Id2*-deficient co-culture than the control one will indicate that *Id2*-deficient normal epithelium overcomes the competition with *Id2*-deficient cancer cells.

As previously discussed, I successfully generated several CRISPR-Cas9-mediated $Id2^{KO}Apc^{KO}$ clones. The clone demonstrating the highest clonogenicity was chosen for transcriptome analysis. In parallel, I generated Apc^{KO} tumoroids with further deleted *Id2*, which were cultured for over a month without losing clonogenicity and were used for transcriptome analysis. Both $Apc^{KO}Id2^{KO}$ and $Id2^{KO}Apc^{KO}$ tumoroids showed an increased expression of *Olfm4*, which was almost 6 times up-regulated in $Apc^{KO}Id2^{KO}$ and 223 times in $Id2^{KO}Apc^{KO}$ tumoroids compared to Apc^{KO}. *Olfm4* was the most enriched stem cell marker in CRISPR-Cas9-generated *Id2*-deficient tumoroids. This means that the cultures of *Id2*-deficient tumoroids were strongly enriched with OLFM4+ stem cells, especially $Id2^{KO}Apc^{KO}$ tumoroids.

In contrast, *Olfm4* was strongly down-regulated in Apc^{min}:$Rosa26^{CreERT2}$:$Id2^{lox/lox}$ based on the transcriptome analysis after tamoxifen-induced *Id2* deletion. The recent study by Sakahara *et al.*, 2024 showed that OLFM4+ stem cells obtained from patients with advanced colorectal cancers were able to differentiate into absorptive and secretory lineage cells, specifically Paneth-like cells, which normally do not exist in the colon. These cells form the niche for cancer cells and can undergo de-differentiation. Similarly, I observed the enrichment of Paneth cell markers in $Apc^{KO}Id2^{KO}$ and especially in $Id2^{KO}Apc^{KO}$ tumoroids compared to Apc^{KO}.

The effect of *Id2* deletion observed in *Apc^{min}:Rosa26^{CreERT2}:Id2$^{lox/lox}$* tumoroids, which showed increased expression of Paneth cell markers, was confirmed in CRISPR-Cas9 generated organoids. However, in the latter, this effect might be partly impacted by OLFM4+ stem cells. Together, these results demonstrate the role of ID2 in maintaining the clonogenicity and undifferentiated state of tumor cells.

I observed a loss of clonogenicity upon induced *Id2* deletion in *Apc^{min}:Rosa26^{CreERT2}:Id2$^{lox/lox}$* tumoroids. At the same time, CRISPR-Cas9-generated tumoroids from *Id2*-deficient organoids, even though took time to generate, maintained their clonogenic capacity for over a month of culture. I hypothesize that this was mainly supported by OLFM4+ stem cells, which were enriched during prolonged culture in *Apc^{KO}Id2^{KO}* and especially *Id2^{KO}Apc^{KO}* tumoroids.

Interestingly, while *Apc^{min}:Rosa26^{CreERT2}:Id2$^{lox/lox}$* tumoroids treated with 4OH-tamoxifen showed an increased compensatory expression of other ID-family transcription factors *Id1* and *Id3*, CRISPR-Cas9 generated *Apc^{KO}Id2^{KO}* and *Id2^{KO}Apc^{KO}* tumoroids opposite showed a strong decrease in *Id1* and *Id3* expression. This suggests that the selected cancer stem cells are not dependent on ID-factors to maintain their clonogenicity.

Taken together, my results show that ID2's oncogenic function is epithelial-specific. ID2 is necessary for promoting oncogenesis in the small intestinal epithelium, and its epithelial-specific deletion at early embryogenesis leads to a dramatic decrease in *Apc^{min}* tumour numbers. Moreover, *Id2* is expressed in the formed small intestinal tumors and functions to maintain the proliferation and undifferentiated state of tumor cells. The functions of ID2 in intestinal oncogenesis are summarized in Figure 4.1. These results open new therapeutic approaches to attenuate colorectal cancer progression. The effect of a known inhibitor of ID2 Helichrysetin was demonstrated to restrict gastric cancer growth both *in vivo* and *in vitro* (Wang *et al.*, 2022). The application of Helichrysetin in the treatment of FAP patients is a subject of further research.

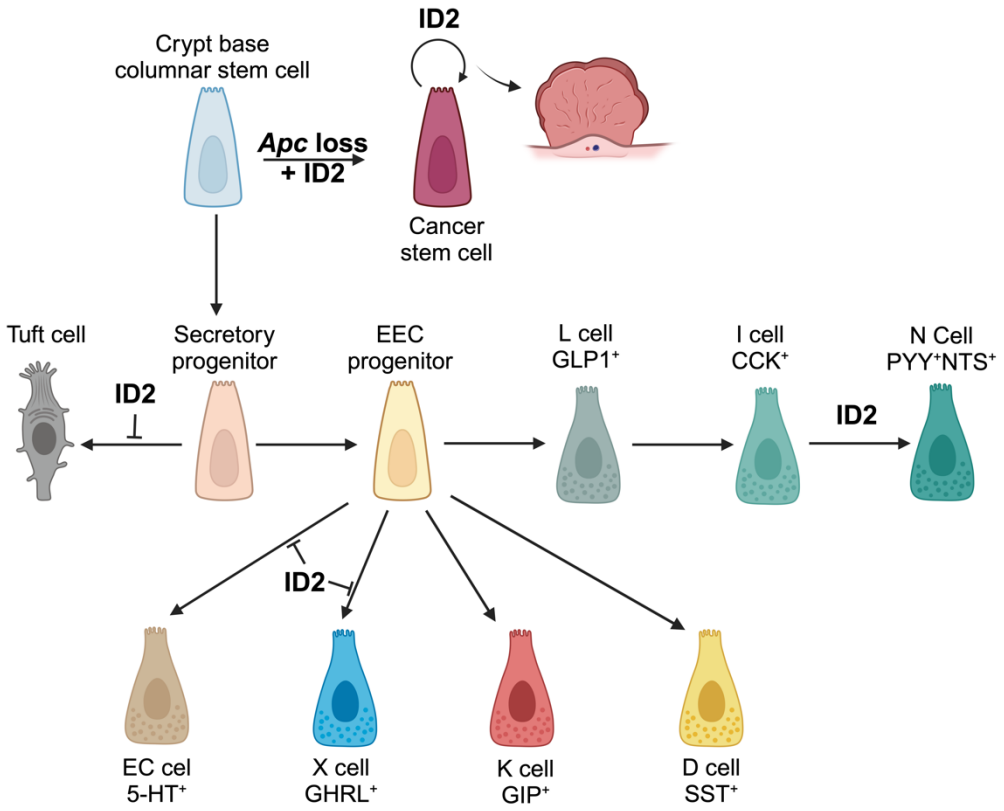

Figure 4.1 Working model showing functions of ID2 in gut homeostasis and cancer. Created with BioRender.com.

5. REFERENCES

- Ahlgren, U., Pfaff, S. L., Jessell, T. M., Edlund, T., & Edlund, H. (1997). Independent requirement for ISL1 in formation of pancreatic mesenchyme and islet cells. *Nature*, *385*(6613), 257–260. https://doi.org/10.1038/385257a0

- Ahlman, H., & Nilsson (2001). The gut as the largest endocrine organ in the body. *Annals of oncology : official journal of the European Society for Medical Oncology*, *12 Suppl 2*, S63–S68. https://doi.org/10.1093/annonc/12.suppl_2.s63

- Ambort, D., Johansson, M. E., Gustafsson, J. K., Nilsson, H. E., Ermund, A., Johansson, B. R., Koeck, P. J., Hebert, H., & Hansson, G. C. (2012). Calcium and pH-dependent packing and release of the gel-forming MUC2 mucin. *Proceedings of the National Academy of Sciences of the United States of America*, *109*(15), 5645–5650. https://doi.org/10.1073/pnas.1120269109

- Andersson-Rolf, A., Fink, J., Mustata, R. C., & Koo, B. K. (2014). A video protocol of retroviral infection in primary intestinal organoid culture. *Journal of visualized experiments : JoVE*, (90), e51765. https://doi.org/10.3791/51765

- Atanga, R., Singh, V., & In, J. G. (2023). Intestinal Enteroendocrine Cells: Present and Future Druggable Targets. *International journal of molecular sciences*, *24*(10), 8836. https://doi.org/10.3390/ijms24108836

- Auclair, B. A., Benoit, Y. D., Rivard, N., Mishina, Y., & Perreault, N. (2007). Bone morphogenetic protein signaling is essential for terminal differentiation of the intestinal secretory cell lineage. *Gastroenterology*, *133*(3), 887–896. https://doi.org/10.1053/j.gastro.2007.06.066

- Ayabe, T., Satchell, D. P., Pesendorfer, P., Tanabe, H., Wilson, C. L., Hagen, S. J., & Ouellette, A. J. (2002). Activation of Paneth cell alpha-defensins in mouse small intestine. *The Journal of biological chemistry*, *277*(7), 5219–5228. https://doi.org/10.1074/jbc.M109410200

- Ayabe, T., Satchell, D. P., Wilson, C. L., Parks, W. C., Selsted, M. E., & Ouellette, A. J. (2000). Secretion of microbicidal alpha-defensins by intestinal Paneth cells in response to bacteria. *Nature immunology*, *1*(2), 113–118. https://doi.org/10.1038/77783

- Bachmanov, A. A., Bosak, N. P., Lin, C., Matsumoto, I., Ohmoto, M., Reed, D. R., & Nelson, T. M. (2014). Genetics of taste receptors. *Current pharmaceutical design*, *20*(16), 2669–2683. https://doi.org/10.2174/13816128113199990566

- Ballantyne G. H. (2006). Peptide YY(1-36) and peptide YY(3-36): Part I. Distribution, release and actions. *Obesity surgery*, *16*(5), 651–658. https://doi.org/10.1381/096089206776944959

- Bardot, E. S., & Hadjantonakis, A. K. (2020). Mouse gastrulation: Coordination of tissue patterning, specification and diversification of cell fate. *Mechanisms of development*, *163*, 103617. https://doi.org/10.1016/j.mod.2020.103617

- Barker N. (2014). Adult intestinal stem cells: critical drivers of epithelial homeostasis and regeneration. *Nature reviews. Molecular cell biology*, *15*(1), 19–33. https://doi.org/10.1038/nrm3721

- Barker, N., Ridgway, R. A., van Es, J. H., van de Wetering, M., Begthel, H., van den Born, M., Danenberg, E., Clarke, A. R., Sansom, O. J., & Clevers, H. (2009). Crypt stem cells as the cells-of-origin of intestinal cancer. *Nature*, *457*(7229), 608–611. https://doi.org/10.1038/nature07602

- Barker, N., van Es, J. H., Kuipers, J., Kujala, P., van den Born, M., Cozijnsen, M., Haegebarth, A., Korving, J., Begthel, H., Peters, P. J., & Clevers, H. (2007). Identification of stem cells in small intestine and colon by marker gene Lgr5. *Nature*, *449*(7165), 1003–1007. https://doi.org/10.1038/nature06196

- Barker, N., van Oudenaarden, A., & Clevers, H. (2012). Identifying the stem cell of the intestinal crypt: strategies and pitfalls. *Cell stem cell*, *11*(4), 452–460. https://doi.org/10.1016/j.stem.2012.09.009

- Barreto E Barreto, L., Rattes, I. C., da Costa, A. V., & Gama, P. (2022). Paneth cells and their multiple functions. *Cell biology international*, *46*(5), 701–710. https://doi.org/10.1002/cbin.11764

- Bastide, P., Darido, C., Pannequin, J., Kist, R., Robine, S., Marty-Double, C., Bibeau, F., Scherer, G., Joubert, D., Hollande, F., Blache, P., & Jay, P. (2007). Sox9 regulates cell proliferation and is required for Paneth cell differentiation in the intestinal epithelium. *The Journal of cell biology*, *178*(4), 635–648. https://doi.org/10.1083/jcb.200704152

- Batlle, E., Henderson, J. T., Beghtel, H., van den Born, M. M., Sancho, E., Huls, G., Meeldijk, J., Robertson, J., van de Wetering, M., Pawson, T., & Clevers, H. (2002). Beta-catenin and TCF mediate cell positioning in the intestinal epithelium by controlling the expression of EphB/ephrinB. *Cell*, *111*(2), 251–263. https://doi.org/10.1016/s0092-8674(02)01015-2

- Bayer, F., Dremova, O., Khuu, M. P., Mammadova, K., Pontarollo, G., Kiouptsi, K., Soshnikova, N., May-Simera, H. L., Endres, K., & Reinhardt, C. (2021). The Interplay between Nutrition, Innate Immunity, and the Commensal Microbiota in Adaptive Intestinal Morphogenesis. *Nutrients*, *13*(7), 2198. https://doi.org/10.3390/nu13072198

- Bel, S., Pendse, M., Wang, Y., Li, Y., Ruhn, K. A., Hassell, B., Leal, T., Winter, S. E., Xavier, R. J., & Hooper, L. V. (2017). Paneth cells secrete lysozyme via secretory autophagy during bacterial infection of the intestine. *Science (New York, N.Y.)*, *357*(6355), 1047–1052. https://doi.org/10.1126/science.aal4677

- Bergström, J. H., Birchenough, G. M., Katona, G., Schroeder, B. O., Schütte, A., Ermund, A., Johansson, M. E., & Hansson, G. C. (2016). Gram-positive bacteria are held at a distance in the colon mucus by the lectin-like protein ZG16. *Proceedings of the National Academy of Sciences of the United States of America*, *113*(48), 13833–13838. https://doi.org/10.1073/pnas.1611400113

- Beumer, J., Artegiani, B., Post, Y., Reimann, F., Gribble, F., Nguyen, T. N., Zeng, H., Van den Born, M., Van Es, J. H., & Clevers, H. (2018). Enteroendocrine cells switch hormone expression along the crypt-to-villus BMP signalling gradient. *Nature cell biology*, *20*(8), 909–916. https://doi.org/10.1038/s41556-018-0143-y

- Beumer, J., Puschhof, J., Bauzá-Martinez, J., Martínez-Silgado, A., Elmentaite, R., James, K. R., Ross, A., Hendriks, D., Artegiani, B., Busslinger, G. A., Ponsioen, B., Andersson-Rolf, A., Saftien, A., Boot, C., Kretzschmar, K., Geurts, M. H., Bar-Ephraim, Y. E., Pleguezuelos-Manzano, C., Post, Y., Begthel, H., … Clevers, H. (2020a). High-Resolution mRNA and Secretome Atlas of Human Enteroendocrine Cells. *Cell*, *181*(6), 1291–1306.e19. https://doi.org/10.1016/j.cell.2020.04.036

- Beumer, J., Gehart, H., & Clevers, H. (2020b). Enteroendocrine Dynamics - New Tools Reveal Hormonal Plasticity in the Gut. *Endocrine reviews*, *41*(5), bnaa018. https://doi.org/10.1210/endrev/bnaa018

- Bezençon, C., Fürholz, A., Raymond, F., Mansourian, R., Métairon, S., Le Coutre, J., & Damak, S. (2008). Murine intestinal cells expressing Trpm5 are mostly brush cells and express markers of neuronal and inflammatory cells. *The Journal of comparative neurology*, *509*(5), 514–525. https://doi.org/10.1002/cne.21768

- Biyajima, K., Kakizaki, F., Shen, X., Mori, K., Sugai, M., Taketo, M. M., & Yokota, Y. (2015). Id2 deletion attenuates Apc-deficient ileal tumor formation. *Biology open*, *4*(8), 993–1001. https://doi.org/10.1242/bio.012252

- Bjerknes, M., & Cheng, H. (1981). The stem-cell zone of the small intestinal epithelium. III. Evidence from columnar, enteroendocrine, and mucous cells in the adult mouse. *The American journal of anatomy*, *160*(1), 77–91. https://doi.org/10.1002/aja.1001600107

- Bjerknes, M., & Cheng, H. (1999). Clonal analysis of mouse intestinal epithelial progenitors. *Gastroenterology*, *116*(1), 7–14. https://doi.org/10.1016/s0016-5085(99)70222-2

- Bjerknes, M., & Cheng, H. (2010). Cell Lineage metastability in Gfi1-deficient mouse intestinal epithelium. *Developmental biology*, *345*(1), 49–63. https://doi.org/10.1016/j.ydbio.2010.06.021

- Böttcher, G., Sjölund, K., Ekblad, E., Håkanson, R., Schwartz, T. W., & Sundler, F. (1984). Coexistence of peptide YY and glicentin immunoreactivity in endocrine cells of the gut. *Regulatory peptides*, *8*(4), 261–266. https://doi.org/10.1016/0167-0115(84)90034-x

- Casteleyn, C., Rekecki, A., Van der Aa, A., Simoens, P., & Van den Broeck, W. (2010). Surface area assessment of the murine intestinal tract as a prerequisite for oral dose translation from mouse to man. *Laboratory animals*, *44*(3), 176–183. https://doi.org/10.1258/la.2009.009112

- Cervantes, S., Yamaguchi, T. P., & Hebrok, M. (2009). Wnt5a is essential for intestinal elongation in mice. *Developmental biology*, *326*(2), 285–294. https://doi.org/10.1016/j.ydbio.2008.11.020

- Chang, L. Y., Mercer, R. R., & Crapo, J. D. (1986). Differential distribution of brush cells in the rat lung. *The Anatomical record*, *216*(1), 49–54. https://doi.org/10.1002/ar.1092160109

- Chen, J. J., Li, Z., Pan, H., Murphy, D. L., Tamir, H., Koepsell, H., & Gershon, M. D. (2001). Maintenance of serotonin in the intestinal mucosa and ganglia of mice that lack the high-affinity serotonin transporter: Abnormal intestinal motility and the expression of cation transporters. *The Journal of neuroscience : the official journal of the Society for Neuroscience*, *21*(16), 6348–6361. https://doi.org/10.1523/JNEUROSCI.21-16-06348.2001

- Cheng, H., & Leblond, C. P. (1974). Origin, differentiation and renewal of the four main epithelial cell types in the mouse small intestine. V. Unitarian Theory of the origin of the four epithelial cell types. *The American journal of anatomy*, *141*(4), 537–561. https://doi.org/10.1002/aja.1001410407

- Chin, A. M., Hill, D. R., Aurora, M., & Spence, J. R. (2017). Morphogenesis and maturation of the embryonic and postnatal intestine. *Seminars in cell & developmental biology*, *66*, 81–93. https://doi.org/10.1016/j.semcdb.2017.01.011

- Clevers, H., Loh, K. M., & Nusse, R. (2014). Stem cell signaling. An integral program for tissue renewal and regeneration: Wnt signaling and stem cell control. *Science (New York, N.Y.)*, *346*(6205), 1248012. https://doi.org/10.1126/science.1248012

- Coleman, N. S., Marciani, L., Blackshaw, E., Wright, J., Parker, M., Yano, T., Yamazaki, S., Chan, P. Q., Wilde, K., Gowland, P. A., Perkins, A. C., & Spiller, R. C. (2003). Effect of a novel 5-HT3 receptor agonist MKC-733 on upper gastrointestinal motility in humans. *Alimentary pharmacology & therapeutics*, *18*(10), 1039–1048. https://doi.org/10.1046/j.1365-2036.2003.01797.x

- Collins, J. T., Nguyen, A., & Badireddy, M. (2023). Anatomy, Abdomen and Pelvis, Small Intestine. In *StatPearls*. StatPearls Publishing.

- Cui, C., Wang, F., Zheng, Y., Wei, H., & Peng, J. (2023). From birth to death: The hardworking life of Paneth cell in the small intestine. *Frontiers in immunology*, *14*, 1122258. https://doi.org/10.3389/fimmu.2023.1122258

- Davis, H., Irshad, S., Bansal, M., Rafferty, H., Boitsova, T., Bardella, C., Jaeger, E., Lewis, A., Freeman-Mills, L., Giner, F. C., Rodenas-Cuadrado, P., Mallappa, S., Clark, S., Thomas, H., Jeffery, R., Poulsom, R., Rodriguez-Justo, M., Novelli, M., Chetty, R., Silver, A., … Leedham, S. J. (2015). Aberrant epithelial GREM1 expression initiates colonic tumorigenesis from cells outside the stem cell niche. *Nature medicine*, *21*(1), 62–70. https://doi.org/10.1038/nm.3750

- de Lau, W. B., Snel, B., & Clevers, H. C. (2012). The R-spondin protein family. *Genome biology*, *13*(3), 242. https://doi.org/10.1186/gb-2012-13-3-242

- de Lau, W., Barker, N., Low, T. Y., Koo, B. K., Li, V. S., Teunissen, H., Kujala, P., Haegebarth, A., Peters, P. J., van de Wetering, M., Stange, D. E., van Es, J. E., Guardavaccaro, D., Schasfoort, R. B., Mohri, Y., Nishimori, K., Mohammed, S., Heck,

A. J., & Clevers, H. (2011). Lgr5 homologues associate with Wnt receptors and mediate R-spondin signalling. *Nature*, *476*(7360), 293–297. https://doi.org/10.1038/nature10337

- de Lau, W., Peng, W. C., Gros, P., & Clevers, H. (2014). The R-spondin/Lgr5/Rnf43 module: regulator of Wnt signal strength. *Genes & development*, *28*(4), 305–316. https://doi.org/10.1101/gad.235473.113

- De Silva, A., & Bloom, S. R. (2012). Gut Hormones and Appetite Control: A Focus on PYY and GLP-1 as Therapeutic Targets in Obesity. *Gut and liver*, *6*(1), 10–20. https://doi.org/10.5009/gnl.2012.6.1.10

- del Álamo, D., Rouault, H., & Schweisguth, F. (2011). Mechanism and significance of cis-inhibition in Notch signalling. *Current biology : CB*, *21*(1), R40–R47. https://doi.org/10.1016/j.cub.2010.10.034

- Desai, S., Loomis, Z., Pugh-Bernard, A., Schrunk, J., Doyle, M. J., Minic, A., McCoy, E., & Sussel, L. (2008). Nkx2.2 regulates cell fate choice in the enteroendocrine cell lineages of the intestine. *Developmental biology*, *313*(1), 58–66. https://doi.org/10.1016/j.ydbio.2007.09.047

- Dharmsathaphorn K. (1985). Intestinal somatostatin function. *Advances in experimental medicine and biology*, *188*, 463–473. https://doi.org/10.1007/978-1-4615-7886-4_25

- Dornonville de la Cour, C., Lindström, E., Norlén, P., & Håkanson, R. (2004). Ghrelin stimulates gastric emptying but is without effect on acid secretion and gastric endocrine cells. *Regulatory peptides*, *120*(1-3), 23–32. https://doi.org/10.1016/j.regpep.2004.02.008

- Drucker D. J. (2013). Incretin action in the pancreas: potential promise, possible perils, and pathological pitfalls. *Diabetes*, *62*(10), 3316–3323. https://doi.org/10.2337/db13-0822

- Duffield, G. E., Watson, N. P., Mantani, A., Peirson, S. N., Robles-Murguia, M., Loros, J. J., Israel, M. A., & Dunlap, J. C. (2009). A role for Id2 in regulating photic entrainment of the mammalian circadian system. *Current biology : CB*, *19*(4), 297–304. https://doi.org/10.1016/j.cub.2008.12.052

- Dzama, M. M., Nigmatullina, L., Sayols, S., Kreim, N., & Soshnikova, N. (2017). Distinct populations of embryonic epithelial progenitors generate Lgr5^{+}intestinal stem cells. *Developmental biology*, *432*(2), 258–264. https://doi.org/10.1016/j.ydbio.2017.10.012

- Ewels, P. A., Peltzer, A., Fillinger, S., Patel, H., Alneberg, J., Wilm, A., Garcia, M. U., Di Tommaso, P., & Nahnsen, S. (2020). The nf-core framework for community-curated bioinformatics pipelines. *Nature biotechnology*, *38*(3), 276–278. https://doi.org/10.1038/s41587-020-0439-x

- Farin, H. F., Jordens, I., Mosa, M. H., Basak, O., Korving, J., Tauriello, D. V., de Punder, K., Angers, S., Peters, P. J., Maurice, M. M., & Clevers, H. (2016).

Visualization of a short-range Wnt gradient in the intestinal stem-cell niche. *Nature*, *530*(7590), 340–343. https://doi.org/10.1038/nature16937

- Fazio Coles, T. E., Fothergill, L. J., Hunne, B., Nikfarjam, M., Testro, A., Callaghan, B., McQuade, R. M., & Furness, J. B. (2020). Quantitation and chemical coding of enteroendocrine cell populations in the human jejunum. *Cell and tissue research*, *379*(1), 109–120. https://doi.org/10.1007/s00441-019-03099-3

- Fiedler, M., Mendoza-Topaz, C., Rutherford, T. J., Mieszczanek, J., & Bienz, M. (2011). Dishevelled interacts with the DIX domain polymerization interface of Axin to interfere with its function in down-regulating β-catenin. *Proceedings of the National Academy of Sciences of the United States of America*, *108*(5), 1937–1942. https://doi.org/10.1073/pnas.1017063108

- Fijneman, R. J., Anderson, R. A., Richards, E., Liu, J., Tijssen, M., Meijer, G. A., Anderson, J., Rod, A., O'Sullivan, M. G., Scott, P. M., & Cormier, R. T. (2012). Runx1 is a tumor suppressor gene in the mouse gastrointestinal tract. *Cancer science*, *103*(3), 593–599. https://doi.org/10.1111/j.1349-7006.2011.02189.x

- Flanagan, D. J., Pentinmikko, N., Luopajärvi, K., Willis, N. J., Gilroy, K., Raven, A. P., Mcgarry, L., Englund, J. I., Webb, A. T., Scharaw, S., Nasreddin, N., Hodder, M. C., Ridgway, R. A., Minnee, E., Sphyris, N., Gilchrist, E., Najumudeen, A. K., Romagnolo, B., Perret, C., Williams, A. C., … Sansom, O. J. (2021). NOTUM from Apc-mutant cells biases clonal competition to initiate cancer. *Nature*, *594*(7863), 430–435. https://doi.org/10.1038/s41586-021-03525-z

- Flanagan, D. J., Phesse, T. J., Barker, N., Schwab, R. H., Amin, N., Malaterre, J., Stange, D. E., Nowell, C. J., Currie, S. A., Saw, J. T., Beuchert, E., Ramsay, R. G., Sansom, O. J., Ernst, M., Clevers, H., & Vincan, E. (2015). Frizzled7 functions as a Wnt receptor in intestinal epithelial Lgr5(+) stem cells. *Stem cell reports*, *4*(5), 759–767. https://doi.org/10.1016/j.stemcr.2015.03.003

- Fre, S., Hannezo, E., Sale, S., Huyghe, M., Lafkas, D., Kissel, H., Louvi, A., Greve, J., Louvard, D., & Artavanis-Tsakonas, S. (2011). Notch lineages and activity in intestinal stem cells determined by a new set of knock-in mice. *PloS one*, *6*(10), e25785. https://doi.org/10.1371/journal.pone.0025785

- Fujimoto, S., Ikawa, T., Kina, T., & Yokota, Y. (2007). Forced expression of Id2 in fetal thymic T cell progenitors allows some of their progeny to adopt NK cell fate. *International immunology*, *19*(10), 1175–1182. https://doi.org/10.1093/intimm/dxm085

- Fukuma, M., Okita, H., Hata, J., & Umezawa, A. (2003). Upregulation of Id2, an oncogenic helix-loop-helix protein, is mediated by the chimeric EWS/ets protein in Ewing sarcoma. *Oncogene*, *22*(1), 1–9. https://doi.org/10.1038/sj.onc.1206055

- Ganz T. (2003). Defensins: antimicrobial peptides of innate immunity. *Nature reviews. Immunology*, *3*(9), 710–720. https://doi.org/10.1038/nri1180

- Gao, N., White, P., & Kaestner, K. H. (2009). Establishment of intestinal identity and epithelial-mesenchymal signaling by Cdx2. *Developmental cell*, *16*(4), 588–599. https://doi.org/10.1016/j.devcel.2009.02.010

- Garcia, M. I., Ghiani, M., Lefort, A., Libert, F., Strollo, S., & Vassart, G. (2009). LGR5 deficiency deregulates Wnt signaling and leads to precocious Paneth cell differentiation in the fetal intestine. *Developmental biology*, *331*(1), 58–67. https://doi.org/10.1016/j.ydbio.2009.04.020

- Gehart, H., & Clevers, H. (2019). Tales from the crypt: new insights into intestinal stem cells. *Nature reviews. Gastroenterology & hepatology*, *16*(1), 19–34. https://doi.org/10.1038/s41575-018-0081-y

- Gehart, H., van Es, J. H., Hamer, K., Beumer, J., Kretzschmar, K., Dekkers, J. F., Rios, A., & Clevers, H. (2019). Identification of Enteroendocrine Regulators by Real-Time Single-Cell Differentiation Mapping. *Cell*, *176*(5), 1158–1173.e16. https://doi.org/10.1016/j.cell.2018.12.029

- Gerbe, F., Sidot, E., Smyth, D. J., Ohmoto, M., Matsumoto, I., Dardalhon, V., Cesses, P., Garnier, L., Pouzolles, M., Brulin, B., Bruschi, M., Harcus, Y., Zimmermann, V. S., Taylor, N., Maizels, R. M., & Jay, P. (2016). Intestinal epithelial tuft cells initiate type 2 mucosal immunity to helminth parasites. *Nature*, *529*(7585), 226–230. https://doi.org/10.1038/nature16527

- Gerbe, F., van Es, J. H., Makrini, L., Brulin, B., Mellitzer, G., Robine, S., Romagnolo, B., Shroyer, N. F., Bourgaux, J. F., Pignodel, C., Clevers, H., & Jay, P. (2011). Distinct ATOH1 and Neurog3 requirements define tuft cells as a new secretory cell type in the intestinal epithelium. *The Journal of cell biology*, *192*(5), 767–780. https://doi.org/10.1083/jcb.201010127

- Ghil, S. H., Jeon, Y. J., & Suh-Kim, H. (2002). Inhibition of BETA2/NeuroD by Id2. *Experimental & molecular medicine*, *34*(5), 367–373. https://doi.org/10.1038/emm.2002.52

- Gracz, A. D., Samsa, L. A., Fordham, M. J., Trotier, D. C., Zwarycz, B., Lo, Y. H., Bao, K., Starmer, J., Raab, J. R., Shroyer, N. F., Reinhardt, R. L., & Magness, S. T. (2018). Sox4 Promotes Atoh1-Independent Intestinal Secretory Differentiation Toward Tuft and Enteroendocrine Fates. *Gastroenterology*, *155*(5), 1508–1523.e10. https://doi.org/10.1053/j.gastro.2018.07.023

- Grainger, S., Savory, J. G., & Lohnes, D. (2010). Cdx2 regulates patterning of the intestinal epithelium. *Developmental biology*, *339*(1), 155–165. https://doi.org/10.1016/j.ydbio.2009.12.025

- Guillemot, F., Nagy, A., Auerbach, A., Rossant, J., & Joyner, A. L. (1994). Essential role of Mash-2 in extraembryonic development. *Nature*, *371*(6495), 333–336. https://doi.org/10.1038/371333a0

- Gunawardene, A. R., Corfe, B. M., & Staton, C. A. (2011). Classification and functions of enteroendocrine cells of the lower gastrointestinal tract. *International*

journal of experimental pathology, *92*(4), 219–231. https://doi.org/10.1111/j.1365-2613.2011.00767.x

- Gustafsson, J. K., & Johansson, M. E. V. (2022). The role of goblet cells and mucus in intestinal homeostasis. *Nature reviews. Gastroenterology & hepatology*, *19*(12), 785–803. https://doi.org/10.1038/s41575-022-00675-x

- Gutierrez-Aguilar, R., & Woods, S. C. (2011). Nutrition and L and K-enteroendocrine cells. *Current opinion in endocrinology, diabetes, and obesity*, *18*(1), 35–41. https://doi.org/10.1097/MED.0b013e32834190b5

- Haber, A. L., Biton, M., Rogel, N., Herbst, R. H., Shekhar, K., Smillie, C., Burgin, G., Delorey, T. M., Howitt, M. R., Katz, Y., Tirosh, I., Beyaz, S., Dionne, D., Zhang, M., Raychowdhury, R., Garrett, W. S., Rozenblatt-Rosen, O., Shi, H. N., Yilmaz, O., Xavier, R. J., … Regev, A. (2017). A single-cell survey of the small intestinal epithelium. *Nature*, *551*(7680), 333–339. https://doi.org/10.1038/nature24489

- Haigis, K. M., Caya, J. G., Reichelderfer, M., & Dove, W. F. (2002). Intestinal adenomas can develop with a stable karyotype and stable microsatellites. *Proceedings of the National Academy of Sciences of the United States of America*, *99*(13), 8927–8931. https://doi.org/10.1073/pnas.132275099

- Hansen, G. H., Rasmussen, K., Niels-Christiansen, L. L., & Danielsen, E. M. (2009). Lipopolysaccharide-binding protein: localization in secretory granules of Paneth cells in the mouse small intestine. *Histochemistry and cell biology*, *131*(6), 727–732. https://doi.org/10.1007/s00418-009-0572-6

- Hao, H. X., Xie, Y., Zhang, Y., Charlat, O., Oster, E., Avello, M., Lei, H., Mickanin, C., Liu, D., Ruffner, H., Mao, X., Ma, Q., Zamponi, R., Bouwmeester, T., Finan, P. M., Kirschner, M. W., Porter, J. A., Serluca, F. C., & Cong, F. (2012). ZNRF3 promotes Wnt receptor turnover in an R-spondin-sensitive manner. *Nature*, *485*(7397), 195–200. https://doi.org/10.1038/nature11019

- Haramis, A. P., Begthel, H., van den Born, M., van Es, J., Jonkheer, S., Offerhaus, G. J., & Clevers, H. (2004). De novo crypt formation and juvenile polyposis on BMP inhibition in mouse intestine. *Science (New York, N.Y.)*, *303*(5664), 1684–1686. https://doi.org/10.1126/science.1093587

- Hardwick, J. C., Van Den Brink, G. R., Bleuming, S. A., Ballester, I., Van Den Brande, J. M., Keller, J. J., Offerhaus, G. J., Van Deventer, S. J., & Peppelenbosch, M. P. (2004). Bone morphogenetic protein 2 is expressed by, and acts upon, mature epithelial cells in the colon. *Gastroenterology*, *126*(1), 111–121. https://doi.org/10.1053/j.gastro.2003.10.067

- Harfe, B. D., Scherz, P. J., Nissim, S., Tian, H., McMahon, A. P., & Tabin, C. J. (2004). Evidence for an expansion-based temporal Shh gradient in specifying vertebrate digit identities. *Cell*, *118*(4), 517–528. https://doi.org/10.1016/j.cell.2004.07.024

- Hatzis, P., van der Flier, L. G., van Driel, M. A., Guryev, V., Nielsen, F., Denissov, S., Nijman, I. J., Koster, J., Santo, E. E., Welboren, W., Versteeg, R.,

Cuppen, E., van de Wetering, M., Clevers, H., & Stunnenberg, H. G. (2008). Genome-wide pattern of TCF7L2/TCF4 chromatin occupancy in colorectal cancer cells. *Molecular and cellular biology*, *28*(8), 2732–2744. https://doi.org/10.1128/MCB.02175-07

- Hayashi, M., Kaye, J. A., Douglas, E. R., Joshi, N. R., Gribble, F. M., Reimann, F., & Liberles, S. D. (2023). Enteroendocrine cell lineages that differentially control feeding and gut motility. *eLife*, *12*, e78512. https://doi.org/10.7554/eLife.78512

- He, X. C., Zhang, J., Tong, W. G., Tawfik, O., Ross, J., Scoville, D. H., Tian, Q., Zeng, X., He, X., Wiedemann, L. M., Mishina, Y., & Li, L. (2004). BMP signaling inhibits intestinal stem cell self-renewal through suppression of Wnt-beta-catenin signaling. *Nature genetics*, *36*(10), 1117–1121. https://doi.org/10.1038/ng1430

- Heino, S., Fang, S., Lähde, M., Högström, J., Nassiri, S., Campbell, A., Flanagan, D., Raven, A., Hodder, M., Nasreddin, N., Xue, H. H., Delorenzi, M., Leedham, S., Petrova, T. V., Sansom, O., & Alitalo, K. (2021). Lef1 restricts ectopic crypt formation and tumor cell growth in intestinal adenomas. *Science advances*, *7*(47), eabj0512. https://doi.org/10.1126/sciadv.abj0512

- Hendel, S. K., Kellermann, L., Hausmann, A., Bindslev, N., Jensen, K. B., & Nielsen, O. H. (2022). Tuft Cells and Their Role in Intestinal Diseases. *Frontiers in immunology*, *13*, 822867. https://doi.org/10.3389/fimmu.2022.822867

- Heredia, D. J., Dickson, E. J., Bayguinov, P. O., Hennig, G. W., & Smith, T. K. (2009). Localized release of serotonin (5-hydroxytryptamine) by a fecal pellet regulates migrating motor complexes in murine colon. *Gastroenterology*, *136*(4), 1328–1338. https://doi.org/10.1053/j.gastro.2008.12.010

- Hollnagel, A., Oehlmann, V., Heymer, J., Rüther, U., & Nordheim, A. (1999). Id genes are direct targets of bone morphogenetic protein induction in embryonic stem cells. *The Journal of biological chemistry*, *274*(28), 19838–19845. https://doi.org/10.1074/jbc.274.28.19838

- Houweling, A. C., Dildrop, R., Peters, T., Mummenhoff, J., Moorman, A. F., Rüther, U., & Christoffels, V. M. (2001). Gene and cluster-specific expression of the Iroquois family members during mouse development. *Mechanisms of development*, *107*(1-2), 169–174. https://doi.org/10.1016/s0925-4773(01)00451-8

- Hovanes, K., Li, T. W., Munguia, J. E., Truong, T., Milovanovic, T., Lawrence Marsh, J., Holcombe, R. F., & Waterman, M. L. (2001). Beta-catenin-sensitive isoforms of lymphoid enhancer factor-1 are selectively expressed in colon cancer. *Nature genetics*, *28*(1), 53–57. https://doi.org/10.1038/ng0501-53

- Howitt, M. R., Cao, Y. G., Gologorsky, M. B., Li, J. A., Haber, A. L., Biton, M., Lang, J., Michaud, M., Regev, A., & Garrett, W. S. (2020). The Taste Receptor TAS1R3 Regulates Small Intestinal Tuft Cell Homeostasis. *ImmunoHorizons*, *4*(1), 23–32. https://doi.org/10.4049/immunohorizons.1900099

- Howitt, M. R., Lavoie, S., Michaud, M., Blum, A. M., Tran, S. V., Weinstock, J. V., Gallini, C. A., Redding, K., Margolskee, R. F., Osborne, L. C., Artis, D., & Garrett,

W. S. (2016). Tuft cells, taste-chemosensory cells, orchestrate parasite type 2 immunity in the gut. *Science (New York, N.Y.)*, *351*(6279), 1329–1333. https://doi.org/10.1126/science.aaf1648

- Hrckulak, D., Kolar, M., Strnad, H., & Korinek, V. (2016). TCF/LEF Transcription Factors: An Update from the Internet Resources. *Cancers*, *8*(7), 70. https://doi.org/10.3390/cancers8070070

- Hua, H., Zhang, Y. Q., Dabernat, S., Kritzik, M., Dietz, D., Sterling, L., & Sarvetnick, N. (2006). BMP4 regulates pancreatic progenitor cell expansion through Id2. *The Journal of biological chemistry*, *281*(19), 13574–13580. https://doi.org/10.1074/jbc.M600526200

- Iqbal, A., Duitama, C., Metge, F., Rosskopp, D., Boucas, J. Flaski. (2021). doi:10.5281/zenodo.4849515

- Janda, C. Y., Waghray, D., Levin, A. M., Thomas, C., & Garcia, K. C. (2012). Structural basis of Wnt recognition by Frizzled. *Science (New York, N.Y.)*, *337*(6090), 59–64. https://doi.org/10.1126/science.1222879

- Jenny, M., Uhl, C., Roche, C., Duluc, I., Guillermin, V., Guillemot, F., Jensen, J., Kedinger, M., & Gradwohl, G. (2002). Neurogenin3 is differentially required for endocrine cell fate specification in the intestinal and gastric epithelium. *The EMBO journal*, *21*(23), 6338–6347. https://doi.org/10.1093/emboj/cdf649

- Jensen, J., Pedersen, E. E., Galante, P., Hald, J., Heller, R. S., Ishibashi, M., Kageyama, R., Guillemot, F., Serup, P., & Madsen, O. D. (2000). Control of endodermal endocrine development by Hes-1. *Nature genetics*, *24*(1), 36–44. https://doi.org/10.1038/71657

- Jiang, H., Zhang, Z., Yu, Y., Chu, H. Y., Yu, S., Yao, S., Zhang, G., & Zhang, B. T. (2022). Drug Discovery of DKK1 Inhibitors. *Frontiers in pharmacology*, *13*, 847387. https://doi.org/10.3389/fphar.2022.847387

- Johansson, M. E., Larsson, J. M., & Hansson, G. C. (2011). The two mucus layers of colon are organized by the MUC2 mucin, whereas the outer layer is a legislator of host-microbial interactions. *Proceedings of the National Academy of Sciences of the United States of America*, *108 Suppl 1*(Suppl 1), 4659–4665. https://doi.org/10.1073/pnas.1006451107

- Kageyama, R., Ohtsuka, T., & Tomita, K. (2000). The bHLH gene Hes1 regulates differentiation of multiple cell types. *Molecules and cells*, *10*(1), 1–7. https://doi.org/10.1007/s10059-000-0001-0

- Kakugawa, S., Langton, P. F., Zebisch, M., Howell, S., Chang, T. H., Liu, Y., Feizi, T., Bineva, G., O'Reilly, N., Snijders, A. P., Jones, E. Y., & Vincent, J. P. (2015). Notum deacylates Wnt proteins to suppress signalling activity. *Nature*, *519*(7542), 187–192. https://doi.org/10.1038/nature14259

- Kanai-Azuma, M., Kanai, Y., Gad, J. M., Tajima, Y., Taya, C., Kurohmaru, M., Sanai, Y., Yonekawa, H., Yazaki, K., Tam, P. P., & Hayashi, Y. (2002). Depletion of

definitive gut endoderm in Sox17-null mutant mice. *Development (Cambridge, England)*, *129*(10), 2367–2379. https://doi.org/10.1242/dev.129.10.2367

- Karlsson, L., Lindahl, P., Heath, J. K., & Betsholtz, C. (2000). Abnormal gastrointestinal development in PDGF-A and PDGFR-(alpha) deficient mice implicates a novel mesenchymal structure with putative instructive properties in villus morphogenesis. *Development (Cambridge, England)*, *127*(16), 3457–3466. https://doi.org/10.1242/dev.127.16.3457

- Katz, J. P., Perreault, N., Goldstein, B. G., Lee, C. S., Labosky, P. A., Yang, V. W., & Kaestner, K. H. (2002). The zinc-finger transcription factor Klf4 is required for terminal differentiation of goblet cells in the colon. *Development (Cambridge, England)*, *129*(11), 2619–2628. https://doi.org/10.1242/dev.129.11.2619

- Kayahara, T., Sawada, M., Takaishi, S., Fukui, H., Seno, H., Fukuzawa, H., Suzuki, K., Hiai, H., Kageyama, R., Okano, H., & Chiba, T. (2003). Candidate markers for stem and early progenitor cells, Musashi-1 and Hes1, are expressed in crypt base columnar cells of mouse small intestine. *FEBS letters*, *535*(1-3), 131–135. https://doi.org/10.1016/s0014-5793(02)03896-6

- Kazakevych, J., Sayols, S., Messner, B., Krienke, C., & Soshnikova, N. (2017). Dynamic changes in chromatin states during specification and differentiation of adult intestinal stem cells. *Nucleic acids research*, *45*(10), 5770–5784. https://doi.org/10.1093/nar/gkx167

- Kendig, D. M., & Grider, J. R. (2015). Serotonin and colonic motility. *Neurogastroenterology and motility*, *27*(7), 899–905. https://doi.org/10.1111/nmo.12617

- Kim, T. H., Escudero, S., & Shivdasani, R. A. (2012). Intact function of Lgr5 receptor-expressing intestinal stem cells in the absence of Paneth cells. *Proceedings of the National Academy of Sciences of the United States of America*, *109*(10), 3932–3937. https://doi.org/10.1073/pnas.1113890109

- Kim, T., Tao-Cheng, J. H., Eiden, L. E., & Loh, Y. P. (2001). Chromogranin A, an "on/off" switch controlling dense-core secretory granule biogenesis. *Cell*, *106*(4), 499–509. https://doi.org/10.1016/s0092-8674(01)00459-7

- Kohler, E. M., Derungs, A., Daum, G., Behrens, J., & Schneikert, J. (2008). Functional definition of the mutation cluster region of adenomatous polyposis coli in colorectal tumours. *Human molecular genetics*, *17*(13), 1978–1987. https://doi.org/10.1093/hmg/ddn095

- Kolev, H. M., & Kaestner, K. H. (2023). Mammalian Intestinal Development and Differentiation-The State of the Art. *Cellular and molecular gastroenterology and hepatology*, *16*(5), 809–821. https://doi.org/10.1016/j.jcmgh.2023.07.011

- Koo, B. K., Sasselli, V., & Clevers, H. (2013). Retroviral gene expression control in primary organoid cultures. *Current protocols in stem cell biology*, *27*, 5A.6.1–5A.6.8. https://doi.org/10.1002/9780470151808.sc05a06s27

- Koo, B. K., Spit, M., Jordens, I., Low, T. Y., Stange, D. E., van de Wetering, M., van Es, J. H., Mohammed, S., Heck, A. J., Maurice, M. M., & Clevers, H. (2012). Tumour suppressor RNF43 is a stem-cell E3 ligase that induces endocytosis of Wnt receptors. *Nature*, *488*(7413), 665–669. https://doi.org/10.1038/nature11308

- Kopan, R., & Ilagan, M. X. (2009). The canonical Notch signaling pathway: unfolding the activation mechanism. *Cell*, *137*(2), 216–233. https://doi.org/10.1016/j.cell.2009.03.045

- Korinek, V., Barker, N., Moerer, P., van Donselaar, E., Huls, G., Peters, P. J., & Clevers, H. (1998). Depletion of epithelial stem-cell compartments in the small intestine of mice lacking Tcf-4. *Nature genetics*, *19*(4), 379–383. https://doi.org/10.1038/1270

- Koshimizu, H., Kim, T., Cawley, N. X., & Loh, Y. P. (2010). Chromogranin A: a new proposal for trafficking, processing and induction of granule biogenesis. *Regulatory peptides*, *160*(1-3), 153–159. https://doi.org/10.1016/j.regpep.2009.12.007

- Kosinski, C., Li, V. S., Chan, A. S., Zhang, J., Ho, C., Tsui, W. Y., Chan, T. L., Mifflin, R. C., Powell, D. W., Yuen, S. T., Leung, S. Y., & Chen, X. (2007). Gene expression patterns of human colon tops and basal crypts and BMP antagonists as intestinal stem cell niche factors. *Proceedings of the National Academy of Sciences of the United States of America*, *104*(39), 15418–15423. https://doi.org/10.1073/pnas.0707210104

- Kuhre, R. E., Deacon, C. F., Holst, J. J., & Petersen, N. (2021). What Is an L-Cell and How Do We Study the Secretory Mechanisms of the L-Cell?. *Frontiers in endocrinology*, *12*, 694284. https://doi.org/10.3389/fendo.2021.694284

- Kuo, C. T., Morrisey, E. E., Anandappa, R., Sigrist, K., Lu, M. M., Parmacek, M. S., Soudais, C., & Leiden, J. M. (1997). GATA4 transcription factor is required for ventral morphogenesis and heart tube formation. *Genes & development*, *11*(8), 1048–1060. https://doi.org/10.1101/gad.11.8.1048

- Larsson, L. I., St-Onge, L., Hougaard, D. M., Sosa-Pineda, B., & Gruss, P. (1998). Pax 4 and 6 regulate gastrointestinal endocrine cell development. *Mechanisms of development*, *79*(1-2), 153–159. https://doi.org/10.1016/s0925-4773(98)00182-8

- Leis, O., Madrid, J. F., Ballesta, J., & Hernández, F. (1997). N- and O-linked oligosaccharides in the secretory granules of rat Paneth cells: an ultrastructural cytochemical study. *The journal of histochemistry and cytochemistry : official journal of the Histochemistry Society*, *45*(2), 285–293. https://doi.org/10.1177/002215549704500213

- Liddle R. A. (1997). Cholecystokinin cells. *Annual review of physiology*, *59*, 221–242. https://doi.org/10.1146/annurev.physiol.59.1.221

- Lim, K. J., Brandt, W. D., Heth, J. A., Muraszko, K. M., Fan, X., Bar, E. E., & Eberhart, C. G. (2015). Lateral inhibition of Notch signaling in neoplastic cells. *Oncotarget*, *6*(3), 1666–1677. https://doi.org/10.18632/oncotarget.2762

- Liman E. R. (2007). TRPM5 and taste transduction. *Handbook of experimental pharmacology*, (179), 287–298. https://doi.org/10.1007/978-3-540-34891-7_17

- Lin, P. W., Simon, P. O., Jr, Gewirtz, A. T., Neish, A. S., Ouellette, A. J., Madara, J. L., & Lencer, W. I. (2004). Paneth cell cryptdins act in vitro as apical paracrine regulators of the innate inflammatory response. *The Journal of biological chemistry*, *279*(19), 19902–19907. https://doi.org/10.1074/jbc.M311821200

- Liu, Q., Niu, X., Li, Y., Zhang, J. R., Zhu, S. J., Yang, Q. Y., Zhang, W., & Gong, L. (2022). Role of the mucin-like glycoprotein FCGBP in mucosal immunity and cancer. *Frontiers in immunology*, *13*, 863317. https://doi.org/10.3389/fimmu.2022.863317

- Liu, W., & Rodgers, G. P. (2016). Olfactomedin 4 expression and functions in innate immunity, inflammation, and cancer. *Cancer metastasis reviews*, *35*(2), 201–212. https://doi.org/10.1007/s10555-016-9624-2

- Liu, W., & Rodgers, G. P. (2022). Olfactomedin 4 Is Not a Precise Marker for Human Intestinal Stem Cells, But Is Involved in Intestinal Carcinogenesis. *Gastroenterology*, *162*(4), 1001–1004. https://doi.org/10.1053/j.gastro.2021.11.041

- Liu, W., Li, H., Hong, S. H., Piszczek, G. P., Chen, W., & Rodgers, G. P. (2016). Olfactomedin 4 deletion induces colon adenocarcinoma in $Apc^{Min/+}$ mice. *Oncogene*, *35*(40), 5237–5247. https://doi.org/10.1038/onc.2016.58

- Liu, W., Yan, M., Liu, Y., Wang, R., Li, C., Deng, C., Singh, A., Coleman, W. G., Jr, & Rodgers, G. P. (2010). Olfactomedin 4 down-regulates innate immunity against Helicobacter pylori infection. *Proceedings of the National Academy of Sciences of the United States of America*, *107*(24), 11056–11061. https://doi.org/10.1073/pnas.1001269107

- Liu, Y., & Chen, Y. G. (2020). Intestinal epithelial plasticity and regeneration via cell dedifferentiation. *Cell regeneration (London, England)*, *9*(1), 14. https://doi.org/10.1186/s13619-020-00053-5

- Lloyd, C., Yu, Q. C., Cheng, J., Turksen, K., Degenstein, L., Hutton, E., & Fuchs, E. (1995). The basal keratin network of stratified squamous epithelia: defining K15 function in the absence of K14. *The Journal of cell biology*, *129*(5), 1329–1344. https://doi.org/10.1083/jcb.129.5.1329

- Long, F., Shi, H., Li, P., Guo, S., Ma, Y., Wei, S., Li, Y., Gao, F., Gao, S., Wang, M., Duan, R., Wang, X., Yang, K., Sun, W., Li, X., Li, J., & Liu, Q. (2021). A SMOC2 variant inhibits BMP signaling by competitively binding to BMPR1B and causes growth plate defects. *Bone*, *142*, 115686. https://doi.org/10.1016/j.bone.2020.115686

- López-Díaz, L., Jain, R. N., Keeley, T. M., VanDussen, K. L., Brunkan, C. S., Gumucio, D. L., & Samuelson, L. C. (2007). Intestinal Neurogenin 3 directs differentiation of a bipotential secretory progenitor to endocrine cell rather than goblet cell fate. *Developmental biology*, *309*(2), 298–305. https://doi.org/10.1016/j.ydbio.2007.07.015

- Love, M. I., Huber, W., & Anders, S. (2014). Moderated estimation of fold change and dispersion for RNA-seq data with DESeq2. *Genome biology*, *15*(12), 550. https://doi.org/10.1186/s13059-014-0550-8

- Low M. J. (2004). Clinical endocrinology and metabolism. The somatostatin neuroendocrine system: physiology and clinical relevance in gastrointestinal and pancreatic disorders. *Best practice & research. Clinical endocrinology & metabolism*, *18*(4), 607–622. https://doi.org/10.1016/j.beem.2004.08.005

- Luo, X. C., Chen, Z. H., Xue, J. B., Zhao, D. X., Lu, C., Li, Y. H., Li, S. M., Du, Y. W., Liu, Q., Wang, P., Liu, M., & Huang, L. (2019). Infection by the parasitic helminth *Trichinella spiralis* activates a Tas2r-mediated signaling pathway in intestinal tuft cells. *Proceedings of the National Academy of Sciences of the United States of America*, *116*(12), 5564–5569. https://doi.org/10.1073/pnas.1812901116

- Luongo, C., Moser, A. R., Gledhill, S., & Dove, W. F. (1994). Loss of Apc+ in intestinal adenomas from Min mice. *Cancer research*, *54*(22), 5947–5952.

- Madison, B. B., Braunstein, K., Kuizon, E., Portman, K., Qiao, X. T., & Gumucio, D. L. (2005). Epithelial hedgehog signals pattern the intestinal crypt-villus axis. *Development (Cambridge, England)*, *132*(2), 279–289. https://doi.org/10.1242/dev.01576

- Mao, J., Kim, B. M., Rajurkar, M., Shivdasani, R. A., & McMahon, A. P. (2010). Hedgehog signaling controls mesenchymal growth in the developing mammalian digestive tract. *Development (Cambridge, England)*, *137*(10), 1721–1729. https://doi.org/10.1242/dev.044586

- Marathe, C. S., Rayner, C. K., Jones, K. L., & Horowitz, M. (2013). Glucagon-like peptides 1 and 2 in health and disease: a review. *Peptides*, *44*, 75–86. https://doi.org/10.1016/j.peptides.2013.01.014

- Markel, T. A., Crisostomo, P. R., Wang, M., Herring, C. M., Meldrum, K. K., Lillemoe, K. D., & Meldrum, D. R. (2007). The struggle for iron: gastrointestinal microbes modulate the host immune response during infection. *Journal of leukocyte biology*, *81*(2), 393–400. https://doi.org/10.1189/jlb.0906579

- Massagué J. (2012). TGFβ signalling in context. *Nature reviews. Molecular cell biology*, *13*(10), 616–630. https://doi.org/10.1038/nrm3434

- McCartney, B. M., & Näthke, I. S. (2008). Cell regulation by the Apc protein Apc as master regulator of epithelia. *Current opinion in cell biology*, *20*(2), 186–193. https://doi.org/10.1016/j.ceb.2008.02.001

- McDole, J. R., Wheeler, L. W., McDonald, K. G., Wang, B., Konjufca, V., Knoop, K. A., Newberry, R. D., & Miller, M. J. (2012). Goblet cells deliver luminal antigen to CD103+ dendritic cells in the small intestine. *Nature*, *483*(7389), 345–349. https://doi.org/10.1038/nature10863

- McKinley, E. T., Sui, Y., Al-Kofahi, Y., Millis, B. A., Tyska, M. J., Roland, J. T., Santamaria-Pang, A., Ohland, C. L., Jobin, C., Franklin, J. L., Lau, K. S., Gerdes, M. J., & Coffey, R. J. (2017). Optimized multiplex immunofluorescence single-cell analysis reveals tuft cell heterogeneity. *JCI insight*, *2*(11), e93487. https://doi.org/10.1172/jci.insight.93487

- McLin, V. A., Henning, S. J., & Jamrich, M. (2009). The role of the visceral mesoderm in the development of the gastrointestinal tract. *Gastroenterology*, *136*(7), 2074–2091. https://doi.org/10.1053/j.gastro.2009.03.001

- Modlin, I. M., Kidd, M., Pfragner, R., Eick, G. N., & Champaneria, M. C. (2006). The functional characterization of normal and neoplastic human enterochromaffin cells. *The Journal of clinical endocrinology and metabolism*, *91*(6), 2340–2348. https://doi.org/10.1210/jc.2006-0110

- Moloney, D. J., Panin, V. M., Johnston, S. H., Chen, J., Shao, L., Wilson, R., Wang, Y., Stanley, P., Irvine, K. D., Haltiwanger, R. S., & Vogt, T. F. (2000). Fringe is a glycosyltransferase that modifies Notch. *Nature*, *406*(6794), 369–375. https://doi.org/10.1038/35019000

- Mommaerts, H., Esguerra, C. V., Hartmann, U., Luyten, F. P., & Tylzanowski, P. (2014). Smoc2 modulates embryonic myelopoiesis during zebrafish development. *Developmental dynamics : an official publication of the American Association of Anatomists*, *243*(11), 1375–1390. https://doi.org/10.1002/dvdy.24164

- Monaghan, A. P., Kaestner, K. H., Grau, E., & Schütz, G. (1993). Postimplantation expression patterns indicate a role for the mouse forkhead/HNF-3 alpha, beta and gamma genes in determination of the definitive endoderm, chordamesoderm and neuroectoderm. *Development (Cambridge, England)*, *119*(3), 567–578. https://doi.org/10.1242/dev.119.3.567

- Montgomery, R. K., Carlone, D. L., Richmond, C. A., Farilla, L., Kranendonk, M. E., Henderson, D. E., Baffour-Awuah, N. Y., Ambruzs, D. M., Fogli, L. K., Algra, S., & Breault, D. T. (2011). Mouse telomerase reverse transcriptase (mTert) expression marks slowly cycling intestinal stem cells. *Proceedings of the National Academy of Sciences of the United States of America*, *108*(1), 179–184. https://doi.org/10.1073/pnas.1013004108

- Moon, R. T., Bowerman, B., Boutros, M., & Perrimon, N. (2002). The promise and perils of Wnt signaling through beta-catenin. *Science (New York, N.Y.)*, *296*(5573), 1644–1646. https://doi.org/10.1126/science.1071549

- Mootha, V. K., Lindgren, C. M., Eriksson, K. F., Subramanian, A., Sihag, S., Lehar, J., Puigserver, P., Carlsson, E., Ridderstråle, M., Laurila, E., Houstis, N., Daly, M. J., Patterson, N., Mesirov, J. P., Golub, T. R., Tamayo, P., Spiegelman, B., Lander, E. S., Hirschhorn, J. N., Altshuler, D., … Groop, L. C. (2003). PGC-1alpha-responsive

genes involved in oxidative phosphorylation are coordinately downregulated in human diabetes. *Nature genetics*, *34*(3), 267–273. https://doi.org/10.1038/ng1180

- Mori-Akiyama, Y., van den Born, M., van Es, J. H., Hamilton, S. R., Adams, H. P., Zhang, J., Clevers, H., & de Crombrugghe, B. (2007). SOX9 is required for the differentiation of paneth cells in the intestinal epithelium. *Gastroenterology*, *133*(2), 539–546. https://doi.org/10.1053/j.gastro.2007.05.020

- Mori, K., Nakamura, H., Kurooka, H., Miyachi, H., Tamada, K., Sugai, M., Takumi, T., & Yokota, Y. (2018). Id2 Determines Intestinal Identity through Repression of the Foregut Transcription Factor Irx5. *Molecular and cellular biology*, *38*(9), e00250-17. https://doi.org/10.1128/MCB.00250-17

- Mori, K., Tamada, K., Kurooka, H., Matsui, M., Takumi, T., & Yokota, Y. (2019). Gene expression profile data of the developing small intestine of *Id2*-deficient mice. *Data in brief*, *24*, 103717. https://doi.org/10.1016/j.dib.2019.103717

- Morita, H., Mazerbourg, S., Bouley, D. M., Luo, C. W., Kawamura, K., Kuwabara, Y., Baribault, H., Tian, H., & Hsueh, A. J. (2004). Neonatal lethality of LGR5 null mice is associated with ankyloglossia and gastrointestinal distension. *Molecular and cellular biology*, *24*(22), 9736–9743. https://doi.org/10.1128/MCB.24.22.9736-9743.2004

- Moser, A. R., Pitot, H. C., & Dove, W. F. (1990). A dominant mutation that predisposes to multiple intestinal neoplasia in the mouse. *Science (New York, N.Y.)*, *247*(4940), 322–324. https://doi.org/10.1126/science.2296722

- Mun, J., Hur, W., & Ku, N. O. (2022). Roles of Keratins in Intestine. *International journal of molecular sciences*, *23*(14), 8051. https://doi.org/10.3390/ijms23148051

- Muñoz, J., Stange, D. E., Schepers, A. G., van de Wetering, M., Koo, B. K., Itzkovitz, S., Volckmann, R., Kung, K. S., Koster, J., Radulescu, S., Myant, K., Versteeg, R., Sansom, O. J., van Es, J. H., Barker, N., van Oudenaarden, A., Mohammed, S., Heck, A. J., & Clevers, H. (2012). The Lgr5 intestinal stem cell signature: robust expression of proposed quiescent '+4' cell markers. *The EMBO journal*, *31*(14), 3079–3091. https://doi.org/10.1038/emboj.2012.166

- Nadjsombati, M. S., McGinty, J. W., Lyons-Cohen, M. R., Jaffe, J. B., DiPeso, L., Schneider, C., Miller, C. N., Pollack, J. L., Nagana Gowda, G. A., Fontana, M. F., Erle, D. J., Anderson, M. S., Locksley, R. M., Raftery, D., & von Moltke, J. (2018). Detection of Succinate by Intestinal Tuft Cells Triggers a Type 2 Innate Immune Circuit. *Immunity*, *49*(1), 33–41.e7. https://doi.org/10.1016/j.immuni.2018.06.016

- Nakamura, K., Yokoi, Y., Fukaya, R., Ohira, S., Shinozaki, R., Nishida, T., Kikuchi, M., & Ayabe, T. (2020). Expression and Localization of Paneth Cells and Their α-Defensins in the Small Intestine of Adult Mouse. *Frontiers in immunology*, *11*, 570296. https://doi.org/10.3389/fimmu.2020.570296

- Nawaz, N., Wen, S., Wang, F., Nawaz, S., Raza, J., Iftikhar, M., & Usman, M. (2022). Lysozyme and Its Application as Antibacterial Agent in Food

Industry. *Molecules (Basel, Switzerland)*, *27*(19), 6305. https://doi.org/10.3390/molecules27196305

- Niehrs C. (2012). The complex world of WNT receptor signalling. *Nature reviews. Molecular cell biology*, *13*(12), 767–779. https://doi.org/10.1038/nrm3470

- Nieuwenhuis, M. H., & Vasen, H. F. (2007). Correlations between mutation site in APC and phenotype of familial adenomatous polyposis (FAP): a review of the literature. *Critical reviews in oncology/hematology*, *61*(2), 153–161. https://doi.org/10.1016/j.critrevonc.2006.07.004

- Nigmatullina, L., Norkin, M., Dzama, M. M., Messner, B., Sayols, S., & Soshnikova, N. (2017). Id2 controls specification of Lgr5^{+} intestinal stem cell progenitors during gut development. *The EMBO journal*, *36*(7), 869–885. https://doi.org/10.15252/embj.201694959

- Niola, F., Zhao, X., Singh, D., Castano, A., Sullivan, R., Lauria, M., Nam, H. S., Zhuang, Y., Benezra, R., Di Bernardo, D., Iavarone, A., & Lasorella, A. (2012). Id proteins synchronize stemness and anchorage to the niche of neural stem cells. *Nature cell biology*, *14*(5), 477–487. https://doi.org/10.1038/ncb2490

- Nowotschin, S., Setty, M., Kuo, Y. Y., Liu, V., Garg, V., Sharma, R., Simon, C. S., Saiz, N., Gardner, R., Boutet, S. C., Church, D. M., Hoodless, P. A., Hadjantonakis, A. K., & Pe'er, D. (2019). The emergent landscape of the mouse gut endoderm at single-cell resolution. *Nature*, *569*(7756), 361–367. https://doi.org/10.1038/s41586-019-1127-1

- Nusse, R., & Clevers, H. (2017). Wnt/β-Catenin Signaling, Disease, and Emerging Therapeutic Modalities. *Cell*, *169*(6), 985–999. https://doi.org/10.1016/j.cell.2017.05.016

- Nyström, E. E. L., Birchenough, G. M. H., van der Post, S., Arike, L., Gruber, A. D., Hansson, G. C., & Johansson, M. E. V. (2018). Calcium-activated Chloride Channel Regulator 1 (CLCA1) Controls Mucus Expansion in Colon by Proteolytic Activity. *EBioMedicine*, *33*, 134–143. https://doi.org/10.1016/j.ebiom.2018.05.031

- O'Connor, T. M., O'Connell, J., O'Brien, D. I., Goode, T., Bredin, C. P., & Shanahan, F. (2004). The role of substance P in inflammatory disease. *Journal of cellular physiology*, *201*(2), 167–180. https://doi.org/10.1002/jcp.20061

- Oikarinen, S. I., Erlund, I., & Mutanen, M. (2007). Tumour formation in multiple intestinal neoplasia (*Apc*$^{Min/+}$) mice fed with filtered or unfiltered coffee. *Scandinavian Journal of Food & Nutrition*, *51*(4), 167–173. https://doi.org/10.1080/17482970701757119

- Okonechnikov, K., Golosova, O., Fursov, M., & UGENE team (2012). Unipro UGENE: a unified bioinformatics toolkit. *Bioinformatics (Oxford, England)*, *28*(8), 1166–1167. https://doi.org/10.1093/bioinformatics/bts091

- Ouellette A. J. (2010). Paneth cells and innate mucosal immunity. *Current opinion in gastroenterology*, *26*(6), 547–553. https://doi.org/10.1097/MOG.0b013e32833dccde

- Pacini, G., Thomaseth, K., & Ahrén, B. (2010). Dissociated effects of glucose-dependent insulinotropic polypeptide vs glucagon-like peptide-1 on beta-cell secretion and insulin clearance in mice. *Metabolism: clinical and experimental*, *59*(7), 988–992. https://doi.org/10.1016/j.metabol.2009.10.021

- Park, S. W., Zhen, G., Verhaeghe, C., Nakagami, Y., Nguyenvu, L. T., Barczak, A. J., Killeen, N., & Erle, D. J. (2009). The protein disulfide isomerase AGR2 is essential for production of intestinal mucus. *Proceedings of the National Academy of Sciences of the United States of America*, *106*(17), 6950–6955. https://doi.org/10.1073/pnas.0808722106

- Pellegrinet, L., Rodilla, V., Liu, Z., Chen, S., Koch, U., Espinosa, L., Kaestner, K. H., Kopan, R., Lewis, J., & Radtke, F. (2011). Dll1- and dll4-mediated notch signaling are required for homeostasis of intestinal stem cells. *Gastroenterology*, *140*(4), 1230–1240.e12407. https://doi.org/10.1053/j.gastro.2011.01.005

- Penman, E., Wass, J. A., Butler, M. G., Penny, E. S., Price, J., Wu, P., & Rees, L. H. (1983). Distribution and characterisation of immunoreactive somatostatin in human gastrointestinal tract. *Regulatory peptides*, *7*(1), 53–65. https://doi.org/10.1016/0167-0115(83)90281-1

- Polakis P. (2007). The many ways of Wnt in cancer. *Current opinion in genetics & development*, *17*(1), 45–51. https://doi.org/10.1016/j.gde.2006.12.007

- Potten, C. S., Hume, W. J., Reid, P., & Cairns, J. (1978). The segregation of DNA in epithelial stem cells. *Cell*, *15*(3), 899–906. https://doi.org/10.1016/0092-8674(78)90274-x

- Powell, A. E., Wang, Y., Li, Y., Poulin, E. J., Means, A. L., Washington, M. K., Higginbotham, J. N., Juchheim, A., Prasad, N., Levy, S. E., Guo, Y., Shyr, Y., Aronow, B. J., Haigis, K. M., Franklin, J. L., & Coffey, R. J. (2012). The pan-ErbB negative regulator Lrig1 is an intestinal stem cell marker that functions as a tumor suppressor. *Cell*, *149*(1), 146–158. https://doi.org/10.1016/j.cell.2012.02.042

- Raghoebir, L., Bakker, E. R., Mills, J. C., Swagemakers, S., Kempen, M. B., Munck, A. B., Driegen, S., Meijer, D., Grosveld, F., Tibboel, D., Smits, R., & Rottier, R. J. (2012). SOX2 redirects the developmental fate of the intestinal epithelium toward a premature gastric phenotype. *Journal of molecular cell biology*, *4*(6), 377–385. https://doi.org/10.1093/jmcb/mjs030

- Rainger, J., van Beusekom, E., Ramsay, J. K., McKie, L., Al-Gazali, L., Pallotta, R., Saponari, A., Branney, P., Fisher, M., Morrison, H., Bicknell, L., Gautier, P., Perry, P., Sokhi, K., Sexton, D., Bardakjian, T. M., Schneider, A. S., Elcioglu, N., Ozkinay, F., Koenig, R., … Fitzpatrick, D. R. (2011). Loss of the BMP antagonist, SMOC-1, causes Ophthalmo-acromelic (Waardenburg Anophthalmia) syndrome in humans and mice. *PLoS genetics*, *7*(7), e1002114. https://doi.org/10.1371/journal.pgen.1002114

- Ren, Q., Chen, J., & Liu, Y. (2021). LRP5 and LRP6 in Wnt Signaling: Similarity and Divergence. *Frontiers in cell and developmental biology*, *9*, 670960. https://doi.org/10.3389/fcell.2021.670960

- Reya, T., & Clevers, H. (2005). Wnt signalling in stem cells and cancer. *Nature*, *434*(7035), 843–850. https://doi.org/10.1038/nature03319

- Rezzani, R., Franco, C., Franceschetti, L., Gianò, M., & Favero, G. (2022). A Focus on Enterochromaffin Cells among the Enteroendocrine Cells: Localization, Morphology, and Role. *International journal of molecular sciences*, *23*(7), 3758. https://doi.org/10.3390/ijms23073758

- Riccio, O., van Gijn, M. E., Bezdek, A. C., Pellegrinet, L., van Es, J. H., Zimber-Strobl, U., Strobl, L. J., Honjo, T., Clevers, H., & Radtke, F. (2008). Loss of intestinal crypt progenitor cells owing to inactivation of both Notch1 and Notch2 is accompanied by derepression of CDK inhibitors p27Kip1 and p57Kip2. *EMBO reports*, *9*(4), 377–383. https://doi.org/10.1038/embor.2008.7

- Rock, S. A., Jiang, K., Wu, Y., Liu, Y., Li, J., Weiss, H. L., Wang, C., Jia, J., Gao, T., & Evers, B. M. (2022). Neurotensin Regulates Proliferation and Stem Cell Function in the Small Intestine in a Nutrient-Dependent Manner. *Cellular and molecular gastroenterology and hepatology*, *13*(2), 501–516. https://doi.org/10.1016/j.jcmgh.2021.09.006

- Rodríguez-Piñeiro, A. M., Bergström, J. H., Ermund, A., Gustafsson, J. K., Schütte, A., Johansson, M. E., & Hansson, G. C. (2013). Studies of mucus in mouse stomach, small intestine, and colon. II. Gastrointestinal mucus proteome reveals Muc2 and Muc5ac accompanied by a set of core proteins. *American journal of physiology. Gastrointestinal and liver physiology*, *305*(5), G348–G356. https://doi.org/10.1152/ajpgi.00047.2013

- Roschger, C., & Cabrele, C. (2017). The Id-protein family in developmental and cancer-associated pathways. *Cell communication and signaling : CCS*, *15*(1), 7. https://doi.org/10.1186/s12964-016-0161-y

- Rostène, W. H., & Alexander, M. J. (1997). Neurotensin and neuroendocrine regulation. *Frontiers in neuroendocrinology*, *18*(2), 115–173. https://doi.org/10.1006/frne.1996.0146

- Russell, R. G., Lasorella, A., Dettin, L. E., & Iavarone, A. (2004). Id2 drives differentiation and suppresses tumor formation in the intestinal epithelium. *Cancer research*, *64*(20), 7220–7225. https://doi.org/10.1158/0008-5472.CAN-04-2095

- Sakahara, M., Okamoto, T., Srivastava, U., Natsume, Y., Yamanaka, H., Suzuki, Y., Obama, K., Nagayama, S., & Yao, R. (2024). Paneth-like cells produced from $OLFM4^+$ stem cells support $OLFM4^+$ stem cell growth in advanced colorectal cancer. *Communications biology*, *7*(1), 27. https://doi.org/10.1038/s42003-023-05504-8

- Sakata, I., Nakamura, K., Yamazaki, M., Matsubara, M., Hayashi, Y., Kangawa, K., & Sakai, T. (2002). Ghrelin-producing cells exist as two types of cells, closed- and

opened-type cells, in the rat gastrointestinal tract. *Peptides*, *23*(3), 531–536. https://doi.org/10.1016/s0196-9781(01)00633-7

- Sanchez-Duffhues, G., Williams, E., Goumans, M. J., Heldin, C. H., & Ten Dijke, P. (2020). Bone morphogenetic protein receptors: Structure, function and targeting by selective small molecule kinase inhibitors. *Bone*, *138*, 115472. https://doi.org/10.1016/j.bone.2020.115472

- Sancho, R., Cremona, C. A., & Behrens, A. (2015). Stem cell and progenitor fate in the mammalian intestine: Notch and lateral inhibition in homeostasis and disease. *EMBO reports*, *16*(5), 571–581. https://doi.org/10.15252/embr.201540188

- Sangiorgi, E., & Capecchi, M. R. (2008). Bmi1 is expressed in vivo in intestinal stem cells. *Nature genetics*, *40*(7), 915–920. https://doi.org/10.1038/ng.165

- Sansom, O. J., Stark, L. A., Dunlop, M. G., & Clarke, A. R. (2001). Suppression of intestinal and mammary neoplasia by lifetime administration of aspirin in Apc(Min/+) and Apc(Min/+), Msh2(-/-) mice. *Cancer research*, *61*(19), 7060–7064.

- Saqui-Salces, M., Keeley, T. M., Grosse, A. S., Qiao, X. T., El-Zaatari, M., Gumucio, D. L., Samuelson, L. C., & Merchant, J. L. (2011). Gastric tuft cells express DCLK1 and are expanded in hyperplasia. *Histochemistry and cell biology*, *136*(2), 191–204. https://doi.org/10.1007/s00418-011-0831-1

- Saras, J., Grönberg, M., Stridsberg, M., Oberg, K. E., & Janson, E. T. (2007). Somatostatin induces rapid contraction of neuroendocrine cells. *FEBS letters*, *581*(10), 1957–1962. https://doi.org/10.1016/j.febslet.2007.04.019

- Sasaki, T., Mann, K., Miner, J. H., Miosge, N., & Timpl, R. (2002). Domain IV of mouse laminin beta1 and beta2 chains. *European journal of biochemistry*, *269*(2), 431–442. https://doi.org/10.1046/j.0014-2956.2001.02663.x

- Sato A. (2007). Tuft cells. *Anatomical science international*, *82*(4), 187–199. https://doi.org/10.1111/j.1447-073X.2007.00188.x

- Sato, T., van Es, J. H., Snippert, H. J., Stange, D. E., Vries, R. G., van den Born, M., Barker, N., Shroyer, N. F., van de Wetering, M., & Clevers, H. (2011a). Paneth cells constitute the niche for Lgr5 stem cells in intestinal crypts. *Nature*, *469*(7330), 415–418. https://doi.org/10.1038/nature09637

- Sato, T., Stange, D. E., Ferrante, M., Vries, R. G., Van Es, J. H., Van den Brink, S., Van Houdt, W. J., Pronk, A., Van Gorp, J., Siersema, P. D., & Clevers, H. (2011b). Long-term expansion of epithelial organoids from human colon, adenoma, adenocarcinoma, and Barrett's epithelium. *Gastroenterology*, *141*(5), 1762–1772. https://doi.org/10.1053/j.gastro.2011.07.050

- Sato, T., Vries, R. G., Snippert, H. J., van de Wetering, M., Barker, N., Stange, D. E., van Es, J. H., Abo, A., Kujala, P., Peters, P. J., & Clevers, H. (2009). Single Lgr5 stem cells build crypt-villus structures in vitro without a mesenchymal niche. *Nature*, *459*(7244), 262–265. https://doi.org/10.1038/nature07935

- Schuijers, J., Junker, J. P., Mokry, M., Hatzis, P., Koo, B. K., Sasselli, V., van der Flier, L. G., Cuppen, E., van Oudenaarden, A., & Clevers, H. (2015). Ascl2 acts as an R-spondin/Wnt-responsive switch to control stemness in intestinal crypts. *Cell stem cell*, *16*(2), 158–170. https://doi.org/10.1016/j.stem.2014.12.006

- Schwarz-Romond, T., Fiedler, M., Shibata, N., Butler, P. J., Kikuchi, A., Higuchi, Y., & Bienz, M. (2007). The DIX domain of Dishevelled confers Wnt signaling by dynamic polymerization. *Nature structural & molecular biology*, *14*(6), 484–492. https://doi.org/10.1038/nsmb1247

- Sherwood, R. I., Chen, T. Y., & Melton, D. A. (2009). Transcriptional dynamics of endodermal organ formation. *Developmental dynamics : an official publication of the American Association of Anatomists*, *238*(1), 29–42. https://doi.org/10.1002/dvdy.21810

- Shi, S., & Stanley, P. (2003). Protein O-fucosyltransferase 1 is an essential component of Notch signaling pathways. *Proceedings of the National Academy of Sciences of the United States of America*, *100*(9), 5234–5239. https://doi.org/10.1073/pnas.0831126100

- Shoemaker, A. R., Moser, A. R., & Dove, W. F. (1995). N-ethyl-N-nitrosourea treatment of multiple intestinal neoplasia (Min) mice: age-related effects on the formation of intestinal adenomas, cystic crypts, and epidermoid cysts. *Cancer research*, *55*(19), 4479–4485.

- Shroyer, N. F., Helmrath, M. A., Wang, V. Y., Antalffy, B., Henning, S. J., & Zoghbi, H. Y. (2007). Intestine-specific ablation of mouse atonal homolog 1 (Math1) reveals a role in cellular homeostasis. *Gastroenterology*, *132*(7), 2478–2488. https://doi.org/10.1053/j.gastro.2007.03.047

- Shroyer, N. F., Wallis, D., Venken, K. J., Bellen, H. J., & Zoghbi, H. Y. (2005). Gfi1 functions downstream of Math1 to control intestinal secretory cell subtype allocation and differentiation. *Genes & development*, *19*(20), 2412–2417. https://doi.org/10.1101/gad.1353905

- Silberg, D. G., Sullivan, J., Kang, E., Swain, G. P., Moffett, J., Sund, N. J., Sackett, S. D., & Kaestner, K. H. (2002). Cdx2 ectopic expression induces gastric intestinal metaplasia in transgenic mice. *Gastroenterology*, *122*(3), 689–696. https://doi.org/10.1053/gast.2002.31902

- Sosa-Pineda, B., Chowdhury, K., Torres, M., Oliver, G., & Gruss, P. (1997). The Pax4 gene is essential for differentiation of insulin-producing beta cells in the mammalian pancreas. *Nature*, *386*(6623), 399–402. https://doi.org/10.1038/386399a0

- Spence, J. R., Lauf, R., & Shroyer, N. F. (2011). Vertebrate intestinal endoderm development. *Developmental dynamics : an official publication of the American Association of Anatomists*, *240*(3), 501–520. https://doi.org/10.1002/dvdy.22540

- Spit, M., Koo, B. K., & Maurice, M. M. (2018). Tales from the crypt: intestinal niche signals in tissue renewal, plasticity and cancer. *Open biology*, *8*(9), 180120. https://doi.org/10.1098/rsob.180120

- St-Onge, L., Sosa-Pineda, B., Chowdhury, K., Mansouri, A., & Gruss, P. (1997). Pax6 is required for differentiation of glucagon-producing alpha-cells in mouse pancreas. *Nature*, *387*(6631), 406–409. https://doi.org/10.1038/387406a0

- Stamos, J. L., & Weis, W. I. (2013). The β-catenin destruction complex. *Cold Spring Harbor perspectives in biology*, *5*(1), a007898. https://doi.org/10.1101/cshperspect.a007898

- Sternini, C., Anselmi, L., & Rozengurt, E. (2008). Enteroendocrine cells: a site of 'taste' in gastrointestinal chemosensing. *Current opinion in endocrinology, diabetes, and obesity*, *15*(1), 73–78. https://doi.org/10.1097/MED.0b013e3282f43a73

- Stevenson, J. G., Sayegh, R., Pedicino, N., Pellitier, N. A., Wheeler, T., Bechard, M. E., ... & Zemper, A. E. (2022). Lrig3 restricts the size of the colon stem cell compartment. *bioRxiv*, 2022-03.

- Su, L. K., Kinzler, K. W., Vogelstein, B., Preisinger, A. C., Moser, A. R., Luongo, C., Gould, K. A., & Dove, W. F. (1992). Multiple intestinal neoplasia caused by a mutation in the murine homolog of the APC gene. *Science (New York, N.Y.)*, *256*(5057), 668–670. https://doi.org/10.1126/science.1350108

- Subramanian, A., Tamayo, P., Mootha, V. K., Mukherjee, S., Ebert, B. L., Gillette, M. A., Paulovich, A., Pomeroy, S. L., Golub, T. R., Lander, E. S., & Mesirov, J. P. (2005). Gene set enrichment analysis: a knowledge-based approach for interpreting genome-wide expression profiles. *Proceedings of the National Academy of Sciences of the United States of America*, *102*(43), 15545–15550. https://doi.org/10.1073/pnas.0506580102

- Sussel, L., Kalamaras, J., Hartigan-O'Connor, D. J., Meneses, J. J., Pedersen, R. A., Rubenstein, J. L., & German, M. S. (1998). Mice lacking the homeodomain transcription factor Nkx2.2 have diabetes due to arrested differentiation of pancreatic beta cells. *Development (Cambridge, England)*, *125*(12), 2213–2221. https://doi.org/10.1242/dev.125.12.2213

- Tack, J., Depoortere, I., Bisschops, R., Delporte, C., Coulie, B., Meulemans, A., Janssens, J., & Peeters, T. (2006). Influence of ghrelin on interdigestive gastrointestinal motility in humans. *Gut*, *55*(3), 327–333. https://doi.org/10.1136/gut.2004.060426

- Takeda, N., Jain, R., LeBoeuf, M. R., Wang, Q., Lu, M. M., & Epstein, J. A. (2011). Interconversion between intestinal stem cell populations in distinct niches. *Science (New York, N.Y.)*, *334*(6061), 1420–1424. https://doi.org/10.1126/science.1213214

- Terry, N. A., Walp, E. R., Lee, R. A., Kaestner, K. H., & May, C. L. (2014). Impaired enteroendocrine development in intestinal-specific Islet1 mouse mutants causes impaired glucose homeostasis. *American journal of physiology.*

Gastrointestinal and liver physiology, *307*(10), G979–G991. https://doi.org/10.1152/ajpgi.00390.2013

- Thomas, J. T., Canelos, P., Luyten, F. P., & Moos, M., Jr (2009). Xenopus SMOC-1 Inhibits bone morphogenetic protein signaling downstream of receptor binding and is essential for postgastrulation development in Xenopus. *The Journal of biological chemistry*, *284*(28), 18994–19005. https://doi.org/10.1074/jbc.M807759200

- Tsai, Y. H., VanDussen, K. L., Sawey, E. T., Wade, A. W., Kasper, C., Rakshit, S., Bhatt, R. G., Stoeck, A., Maillard, I., Crawford, H. C., Samuelson, L. C., & Dempsey, P. J. (2014). ADAM10 regulates Notch function in intestinal stem cells of mice. *Gastroenterology*, *147*(4), 822–834.e13. https://doi.org/10.1053/j.gastro.2014.07.003

- Tsai, Y. H., Wu, A., Wu, J. H., Capeling, M. M., Holloway, E. M., Huang, S., Czerwinkski, M., Glass, I., Higgins, P. D. R., & Spence, J. R. (2022). Acquisition of NOTCH dependence is a hallmark of human intestinal stem cell maturation. *Stem cell reports*, *17*(5), 1138–1153. https://doi.org/10.1016/j.stemcr.2022.03.007

- Tschöp, M., Smiley, D. L., & Heiman, M. L. (2000). Ghrelin induces adiposity in rodents. *Nature*, *407*(6806), 908–913. https://doi.org/10.1038/35038090

- Tucker, J. D., Dhanvantari, S., & Brubaker, P. L. (1996). Proglucagon processing in islet and intestinal cell lines. *Regulatory peptides*, *62*(1), 29–35. https://doi.org/10.1016/0167-0115(95)00167-0

- Ueo, T., Imayoshi, I., Kobayashi, T., Ohtsuka, T., Seno, H., Nakase, H., Chiba, T., & Kageyama, R. (2012). The role of Hes genes in intestinal development, homeostasis and tumor formation. *Development (Cambridge, England)*, *139*(6), 1071–1082. https://doi.org/10.1242/dev.069070

- Valenta, T., Degirmenci, B., Moor, A. E., Herr, P., Zimmerli, D., Moor, M. B., Hausmann, G., Cantù, C., Aguet, M., & Basler, K. (2016). Wnt Ligands Secreted by Subepithelial Mesenchymal Cells Are Essential for the Survival of Intestinal Stem Cells and Gut Homeostasis. *Cell reports*, *15*(5), 911–918. https://doi.org/10.1016/j.celrep.2016.03.088

- van der Flier, L. G., Sabates-Bellver, J., Oving, I., Haegebarth, A., De Palo, M., Anti, M., Van Gijn, M. E., Suijkerbuijk, S., Van de Wetering, M., Marra, G., & Clevers, H. (2007). The Intestinal Wnt/TCF Signature. *Gastroenterology*, *132*(2), 628–632. https://doi.org/10.1053/j.gastro.2006.08.039

- van der Flier, L. G., van Gijn, M. E., Hatzis, P., Kujala, P., Haegebarth, A., Stange, D. E., Begthel, H., van den Born, M., Guryev, V., Oving, I., van Es, J. H., Barker, N., Peters, P. J., van de Wetering, M., & Clevers, H. (2009). Transcription factor achaete scute-like 2 controls intestinal stem cell fate. *Cell*, *136*(5), 903–912. https://doi.org/10.1016/j.cell.2009.01.031

- van Es, J. H., de Geest, N., van de Born, M., Clevers, H., & Hassan, B. A. (2010). Intestinal stem cells lacking the Math1 tumour suppressor are refractory to

Notch inhibitors. *Nature communications*, *1*(2), 18. https://doi.org/10.1038/ncomms1017

- van Lidth de Jeude, J. F., Vermeulen, J. L., Montenegro-Miranda, P. S., Van den Brink, G. R., & Heijmans, J. (2015). A protocol for lentiviral transduction and downstream analysis of intestinal organoids. *Journal of visualized experiments : JoVE*, (98), 52531. https://doi.org/10.3791/52531

- van Neerven, S. M., de Groot, N. E., Nijman, L. E., Scicluna, B. P., van Driel, M. S., Lecca, M. C., Warmerdam, D. O., Kakkar, V., Moreno, L. F., Vieira Braga, F. A., Sanches, D. R., Ramesh, P., Ten Hoorn, S., Aelvoet, A. S., van Boxel, M. F., Koens, L., Krawczyk, P. M., Koster, J., Dekker, E., Medema, J. P., … Vermeulen, L. (2021). Apc-mutant cells act as supercompetitors in intestinal tumour initiation. *Nature*, *594*(7863), 436–441. https://doi.org/10.1038/s41586-021-03558-4

- Vandeputte, D. A., Troost, D., Leenstra, S., Ijlst-Keizers, H., Ramkema, M., Bosch, D. A., Baas, F., Das, N. K., & Aronica, E. (2002). Expression and distribution of id helix-loop-helix proteins in human astrocytic tumors. *Glia*, *38*(4), 329–338. https://doi.org/10.1002/glia.10076

- VanDussen, K. L., Carulli, A. J., Keeley, T. M., Patel, S. R., Puthoff, B. J., Magness, S. T., Tran, I. T., Maillard, I., Siebel, C., Kolterud, Å., Grosse, A. S., Gumucio, D. L., Ernst, S. A., Tsai, Y. H., Dempsey, P. J., & Samuelson, L. C. (2012). Notch signaling modulates proliferation and differentiation of intestinal crypt base columnar stem cells. *Development (Cambridge, England)*, *139*(3), 488–497. https://doi.org/10.1242/dev.070763

- Velcich, A., Yang, W., Heyer, J., Fragale, A., Nicholas, C., Viani, S., Kucherlapati, R., Lipkin, M., Yang, K., & Augenlicht, L. (2002). Colorectal cancer in mice genetically deficient in the mucin Muc2. *Science (New York, N.Y.)*, *295*(5560), 1726–1729. https://doi.org/10.1126/science.1069094

- Villar, H. V., Fender, H. R., Rayford, P. L., Bloom, S. R., Ramus, N. I., & Thompson, J. C. (1976). Suppression of gastrin release and gastric secretion by gastric inhibitory polypeptide (GIP) and vasoactive intestinal polypeptide (VIP). *Annals of surgery*, *184*(1), 97–102. https://doi.org/10.1097/00000658-197607000-00016

- Vincent, J. P., Mazella, J., & Kitabgi, P. (1999). Neurotensin and neurotensin receptors. *Trends in pharmacological sciences*, *20*(7), 302–309. https://doi.org/10.1016/s0165-6147(99)01357-7

- Visel, A., Thaller, C., & Eichele, G. (2004). GenePaint.org: an atlas of gene expression patterns in the mouse embryo. *Nucleic acids research*, *32*(Database issue), D552–D556. https://doi.org/10.1093/nar/gkh029

- Wallaeys, C., Garcia-Gonzalez, N., & Libert, C. (2023). Paneth cells as the cornerstones of intestinal and organismal health: a primer. *EMBO molecular medicine*, *15*(2), e16427. https://doi.org/10.15252/emmm.202216427

- Walton, K. D., Kolterud, A., Czerwinski, M. J., Bell, M. J., Prakash, A., Kushwaha, J., Grosse, A. S., Schnell, S., & Gumucio, D. L. (2012). Hedgehog-

responsive mesenchymal clusters direct patterning and emergence of intestinal villi. *Proceedings of the National Academy of Sciences of the United States of America*, *109*(39), 15817–15822. https://doi.org/10.1073/pnas.1205669109

- Wang, P., Jin, J. M., Liang, X. H., Yu, M. Z., Yang, C., Huang, F., Wu, H., Zhang, B. B., Fei, X. Y., Wang, Z. T., Xu, R., Shi, H. L., & Wu, X. J. (2022). Helichrysetin inhibits gastric cancer growth by targeting c-Myc/PDHK1 axis-mediated energy metabolism reprogramming. *Acta pharmacologica Sinica*, *43*(6), 1581–1593. https://doi.org/10.1038/s41401-021-00750-0

- Wang, S., & Chen, Y. G. (2018). BMP signaling in homeostasis, transformation and inflammatory response of intestinal epithelium. *Science China. Life sciences*, *61*(7), 800–807. https://doi.org/10.1007/s11427-018-9310-7

- Wang, S., Qu, Y., Xia, P., Chen, Y., Zhu, X., Zhang, J., Wang, G., Tian, Y., Ying, J., & Fan, Z. (2020). Transdifferentiation of tumor infiltrating innate lymphoid cells during progression of colorectal cancer. *Cell research*, *30*(7), 610–622. https://doi.org/10.1038/s41422-020-0312-y

- Wang, Y., Chang, H., Rattner, A., & Nathans, J. (2016). Frizzled Receptors in Development and Disease. *Current topics in developmental biology*, *117*, 113–139. https://doi.org/10.1016/bs.ctdb.2015.11.028

- Wang, Y., Sims, C. E., & Allbritton, N. L. (2020). Enterochromaffin Cell-Enriched Monolayer Platform for Assaying Serotonin Release from Human Primary Intestinal Cells. *Analytical chemistry*, *92*(18), 12330–12337. https://doi.org/10.1021/acs.analchem.0c02016

- Wei, L., Singh, R., & Ghoshal, U. C. (2022). Enterochromaffin Cells-Gut Microbiota Crosstalk: Underpinning the Symptoms, Pathogenesis, and Pharmacotherapy in Disorders of Gut-Brain Interaction. *Journal of neurogastroenterology and motility*, *28*(3), 357–375. https://doi.org/10.5056/jnm22008

- Wells, J. M., & Melton, D. A. (2000). Early mouse endoderm is patterned by soluble factors from adjacent germ layers. *Development (Cambridge, England)*, *127*(8), 1563–1572. https://doi.org/10.1242/dev.127.8.1563

- Whalley, N. M., Pritchard, L. E., Smith, D. M., & White, A. (2011). Processing of proglucagon to GLP-1 in pancreatic α-cells: is this a paracrine mechanism enabling GLP-1 to act on β-cells?. *The Journal of endocrinology*, *211*(1), 99–106. https://doi.org/10.1530/JOE-11-0094

- White, B. D., Chien, A. J., & Dawson, D. W. (2012). Dysregulation of Wnt/β-catenin signaling in gastrointestinal cancers. *Gastroenterology*, *142*(2), 219–232. https://doi.org/10.1053/j.gastro.2011.12.001

- Wierup, N., Björkqvist, M., Weström, B., Pierzynowski, S., Sundler, F., & Sjölund, K. (2007). Ghrelin and motilin are cosecreted from a prominent endocrine cell population in the small intestine. *The Journal of clinical endocrinology and metabolism*, *92*(9), 3573–3581. https://doi.org/10.1210/jc.2006-2756

- Wong, V. W., Stange, D. E., Page, M. E., Buczacki, S., Wabik, A., Itami, S., van de Wetering, M., Poulsom, R., Wright, N. A., Trotter, M. W., Watt, F. M., Winton, D. J., Clevers, H., & Jensen, K. B. (2012). Lrig1 controls intestinal stem-cell homeostasis by negative regulation of ErbB signalling. *Nature cell biology*, *14*(4), 401–408. https://doi.org/10.1038/ncb2464

- Wu, Y., Cain-Hom, C., Choy, L., Hagenbeek, T. J., de Leon, G. P., Chen, Y., Finkle, D., Venook, R., Wu, X., Ridgway, J., Schahin-Reed, D., Dow, G. J., Shelton, A., Stawicki, S., Watts, R. J., Zhang, J., Choy, R., Howard, P., Kadyk, L., Yan, M., … Siebel, C. W. (2010). Therapeutic antibody targeting of individual Notch receptors. *Nature*, *464*(7291), 1052–1057. https://doi.org/10.1038/nature08878

- Xiong, X., Shao, W., & Jin, T. (2012). New insight into the mechanisms underlying the function of the incretin hormone glucagon-like peptide-1 in pancreatic β-cells: the involvement of the Wnt signaling pathway effector β-catenin. *Islets*, *4*(6), 359–365. https://doi.org/10.4161/isl.23345

- Yagi, R., Zhong, C., Northrup, D. L., Yu, F., Bouladoux, N., Spencer, S., Hu, G., Barron, L., Sharma, S., Nakayama, T., Belkaid, Y., Zhao, K., & Zhu, J. (2014). The transcription factor GATA3 is critical for the development of all IL-7Rα-expressing innate lymphoid cells. *Immunity*, *40*(3), 378–388. https://doi.org/10.1016/j.immuni.2014.01.012

- Yamashita, J., Ohmoto, M., Yamaguchi, T., Matsumoto, I., & Hirota, J. (2017). Skn-1a/Pou2f3 functions as a master regulator to generate Trpm5-expressing chemosensory cells in mice. *PloS one*, *12*(12), e0189340. https://doi.org/10.1371/journal.pone.0189340

- Yan, K. S., Chia, L. A., Li, X., Ootani, A., Su, J., Lee, J. Y., Su, N., Luo, Y., Heilshorn, S. C., Amieva, M. R., Sangiorgi, E., Capecchi, M. R., & Kuo, C. J. (2012). The intestinal stem cell markers Bmi1 and Lgr5 identify two functionally distinct populations. *Proceedings of the National Academy of Sciences of the United States of America*, *109*(2), 466–471. https://doi.org/10.1073/pnas.1118857109

- Yang, J., Wang, P., Liu, T., Lin, L., Li, L., Kou, G., Zhou, R., Li, P., & Li, Y. (2021). Involvement of mucosal flora and enterochromaffin cells of the caecum and descending colon in diarrhoea-predominant irritable bowel syndrome. *BMC microbiology*, *21*(1), 316. https://doi.org/10.1186/s12866-021-02380-2

- Yang, Q., Bermingham, N. A., Finegold, M. J., & Zoghbi, H. Y. (2001). Requirement of Math1 for secretory cell lineage commitment in the mouse intestine. *Science (New York, N.Y.)*, *294*(5549), 2155–2158. https://doi.org/10.1126/science.1065718

- Yokota, Y., Mansouri, A., Mori, S., Sugawara, S., Adachi, S., Nishikawa, S., & Gruss, P. (1999). Development of peripheral lymphoid organs and natural killer cells depends on the helix-loop-helix inhibitor Id2. *Nature*, *397*(6721), 702–706. https://doi.org/10.1038/17812

- Yu, S., Balasubramanian, I., Laubitz, D., Tong, K., Bandyopadhyay, S., Lin, X., Flores, J., Singh, R., Liu, Y., Macazana, C., Zhao, Y., Béguet-Crespel, F., Patil, K.,

Midura-Kiela, M. T., Wang, D., Yap, G. S., Ferraris, R. P., Wei, Z., Bonder, E. M., Häggblom, M. M., … Gao, N. (2020). Paneth Cell-Derived Lysozyme Defines the Composition of Mucolytic Microbiota and the Inflammatory Tone of the Intestine. *Immunity*, *53*(2), 398–416.e8. https://doi.org/10.1016/j.immuni.2020.07.010

- Zeineldin, M., & Neufeld, K. L. (2013). Understanding phenotypic variation in rodent models with germline Apc mutations. *Cancer research*, *73*(8), 2389–2399. https://doi.org/10.1158/0008-5472.CAN-12-4607

- Zhao, L., Song, W., & Chen, Y. G. (2022). Mesenchymal-epithelial interaction regulates gastrointestinal tract development in mouse embryos. *Cell reports*, *40*(2), 111053. https://doi.org/10.1016/j.celrep.2022.111053

- Zhou, B., Lin, W., Long, Y., Yang, Y., Zhang, H., Wu, K., & Chu, Q. (2022). Notch signaling pathway: architecture, disease, and therapeutics. *Signal transduction and targeted therapy*, *7*(1), 95. https://doi.org/10.1038/s41392-022-00934-y

- Zinina, V. V., Ruehle, F., Winkler, P., Rebmann, L., Lukas, H., Möckel, S., Diefenbach, A., Mendez-Lago, M., & Soshnikova, N. (2022). ID2 controls differentiation of enteroendocrine cells in mouse small intestine. *Acta physiologica (Oxford, England)*, *234*(2), e13773. https://doi.org/10.1111/apha.13773

6. CONTRIBUTIONS

Artemiy Golden performed the DESeq analysis on samples from *Id2*-deficient and control embryos. For all other bulk transcriptome analyses, Dr. rer. Nat. Matthias Klein processed the raw fastq files using QIAGEN CLC Genomics Workbench 24 to generate raw unnormalized gene counts. I conducted all remaining experiments and analyses.